A Coordinated Voltage Management Method Utilizing Battery Energy Storage Systems and Smart PV Inverters in Distribution Networks with High PV and Wind Penetrations

Musaed O Alrashidi

Dissertation submitted to the faculty of the Virginia Polytechnic Institute and State University in partial fulfillment of the requirements for the degree of

DOCTOR OF PHILOSOPHY

in

Electrical Engineering

Saifur Rahman

Manisa Pipattanasomporn

Virgilio A. Centeno

Mazen H. Farhood

A. Lynn Abbott

July 15, 2021

Blacksburg, Virginia

Keywords: Renewable Distributed Generations, Battery Energy Storage, Smart PV Inverters, Voltage Control, Bi-level Optimization, Solar PV Forecasting

A Coordinated Voltage Management Method Utilizing Battery Energy Storage Systems and Smart PV Inverters in Distribution Networks with High PV and Wind Penetrations

Musaed O Alrashidi

Abstract

Electrical distribution networks face many operational challenges as various renewable distributed generation (DG), such as solar photovoltaic (PV) systems and wind, become part of their structure. Unlike conventional distribution systems, where the only unpredictable aspect is the load level, the intermittent nature of DG poses additional uncertainty levels for distribution system operators (DSO). The voltage quality problem considers the most restrictive issue that hinders high DG integration into distribution grids. Voltage deviates from the nominal grid voltage limits due to the excess power from the DG. DSOs are accustomed to improving the voltage profile by optimal adjustments of the on-load tap changers, voltage regulator taps and capacitor banks. Nevertheless, due to the frequent variability of the output energy from DG, these devices may fail in doing the needful.

Battery energy storage systems (BESS) and smart PV inverter functionalities are regarded as promising solutions to promote the seamless integration of renewable resources into distribution networks. BESS are utilized to store the surplus energy during the high penetration of renewable DG that causes high voltage levels and discharge the stored energy when the distribution grid is heavily loaded, which leads to the low voltage levels. Smart PV inverters regulate the network voltage by controlling the reactive power injection or absorption at the inverter end. This dissertation proposes a management strategy that coordinates BESS and smart PV inverter reactive power capability to improve voltage quality in the distribution systems with high PV and wind penetrations.

The proposed management method is based on a bi-level optimization algorithm consisting of upper and lower optimization levels. The proposed method determines the optimal location, capacity, numbers and BESS charging and discharging rates to support the distribution system

voltage and to ensure optimal deployment of BESS. Case studies are conducted to evaluate the proposed voltage control method. The large size PV system and wind turbine impacts are studied and simulated on the modified IEEE-34 bus test feeder. In addition, the proposed method is applied to the modified IEEE low voltage test feeder to investigate the effectiveness of installing residential rooftop PV systems on the distribution system's voltage. Experimental results show promising outcomes of the proposed method in controlling the distribution networks' voltage.

In addition, a day-ahead forecast of PV power output is developed in this dissertation to assist the DSOs to accurately predict the future amounts of PV energy available and reinforcing the decision-making process of batteries operation. Hybrid forecasting models are proposed based on machine learning algorithms, which utilize support vector regression and backpropagation neural network, optimized with three metaheuristic optimization algorithms, namely Social Spider Optimization (SSO), Particle Swarm Optimization (PSO) and Cuckoo Search Optimization (CSO). These algorithms are used to improve the predictive efficacy of the selected algorithms, where the optimal selection of their hyperparameters and architectures plays a significant role in yielding precise forecasting outcomes.

A Coordinated Voltage Management Method Utilizing Battery Energy Storage Systems and Smart PV Inverters in Distribution Networks with High PV and Wind Penetrations

Musaed O Alrashidi

General Audience Abstract

The need for more renewable energy has grown significantly, and many countries are embracing these technologies. However, the integration of distributed generation (DG), such as PV systems and wind turbines, poses several operational problems to the distribution system. The voltage problem represents the most significant issue that needs to be addressed. The traditional voltage control equipment may not cope with the rapid fluctuation and may impact their service life.

The continuous developments in the battery energy storage systems (BESS) and the smart PV inverter technologies result in increasing the hosting capacity of DG. BESS can store the excess power from the distributed generators and supply this energy to the grid for different operational objectives. On the other hand, the advanced PV inverter's reactive power capability can be exploited from which the grid can attain many benefits. This dissertation aims at providing a reliable control method to the voltage profile in distribution networks embedded with high PV and wind energy by optimal coordination between the operation of the BESS and the smart PV inverter.

In addition, the solar forecasting can mitigate the uncertainty associated with PV system generation. In this dissertation, the PV power forecasting application is applied in the distribution system to control the voltage. Through utilizing PV power forecasting, the decision-making for battery operation can be upheld and reinforced. The BESS can store the surplus energy from the PV system as needed and supply it back in low PV power incidents.

Experimental results indicate that proper coordination between the BESS and smart PV inverter is beneficial for distribution system operation that can seamlessly integrate PV and wind energy.

Acknowledgments

I would like to express my sincere gratitude to all individuals who supported me during my Ph.D. journey and provided me with valuable support and effort that assisted in completing this dissertation.

First and foremost, I am immensely grateful to my advisor, Prof. Saifur Rahman, for providing me the opportunity to work closely with him and in his research group. His encouragement and guidance taught me how to be an independent researcher. Professor Saifur Rahman always embraces critical thinking and looks at any issue in a broader image, which has encouraged me in my academic research and personal life. I admire his immense knowledge and plentiful experience that I have personally benefited from. I appreciate him for the continuous support during the course of my Ph.D. degree work.

My thanks to Dr. Manisa Pipattanasomporn for her help in different aspects of my research work as a member of my Ph.D. committee. I would like to thank her for her patience and the effort she has put for my research since I joined the Virginia Tech Advance Research Institute (VT-ARI). My thanks also go to my friends at ARI for the fruitful conversations, support and encouragement. I would like to especially mention Yonael, Gana, Abdullah, Ashraf, Dr. Manef, Nazmul, Zejia, Xiangyu, Mengmeng and Sneha.

I would like to take this opportunity to thank other members of my Ph.D. committee Dr. Virgilio A. Centeno, Dr. Mazen Farhood and Dr. A. Lynn Abbott for their willingness to be on the committee and for providing valuable feedback on my dissertation.

In addition, I would like to acknowledge my sponsor, Qassim University in Saudi Arabia, for the financial support in the form of funded educational scholarships during my graduate studies.

My special thanks of gratitude to my brother, Massoud, for his support during my graduate studies journey. Last but not least, I am deeply indebted to my family. The love and the unwavering support I receive from my mother, brothers and sisters gave me the strength and motivation to overcome the challenges and to complete this work.

To my father and wonderful family …

Table of Contents

List of Figures

List of Tables

Abbreviations

DG	Distributed Generation
PV	Photovoltaics
DSO	Distribution Network Operators
OLTC	On-Load Tap Changer
VR	Voltage Regulator
CB	Capacitor Banks
BESS	Battery Energy Storage Systems
PCC	Point of Common Coupling
POI	Point of Interconnection
LP	Linear Programming
LV	Low Voltage
MV	Medium Voltage
SSO	Social Spider Optimization
PSO	Particle Swarm Optimization
CSO	Cuckoo Search Optimization
ANN	Artificial Neural networks
SVR	Support Vector Regression
MPP	Maximum Power Point
OPF	Optimal Power Flow
APC	Active Power Curtailment
RB	Radial Basis
SOCb	State Of Charge of Battery
BPNN	Backpropagation Neural Network
RMSE	Root Mean Square Error
nRMSE	normalized Root Mean Square Error
MAE	Mean Absolute Error
nMAE	normalized Mean Absolute Error
KACST	King Abdelaziz City for Science and Technology
SEC	Saudi Electricity Company
K.A.CARE	King Abdulla City for Atomic and Renewable Energy
VT-ARI	Virginia Tech-Advance Research Institute

Chapter 1: Introduction

1.1 Background

The increasing global demand for renewable distributed generation (DG), such as solar photovoltaic systems (PV) and wind, has expedited the pace of integrating these resources with electrical power grids. These resources are eco-friendly, inexhaustible and sustainable. Renewable energy resources have a significant impact on lowering electricity demand from fossil fuels globally; thus, many countries started to exploit these sources to cover their domestic loads at least partially. Since 2014 and for five consecutive years, the net annual addition power from renewable energy resources exceeds the net addition power from fossil fuel and nuclear power capacity combined, making such resources count for 27.3% of the global electricity generation, see Figure 1.1 [1].

More than 200 GW was added in the power sector in 2019 from different renewable energy technologies increasing the global total to 2588 GW [1]. Figure 1.2 illustrates the annual addition contribution of renewable power capacity by each technology between 2013-2019. Figure 1.2 shows that 115 GW of new PV capacity was added in 2019. This is 57% of the total capacity added that year. This technology is the leader in the new generation capacity. Wind power considered the second leading technology with around 60 GW or 30%, followed by hydropower with 16 GW or 8%. The remaining 5% of the additional annual power came from bio-power, geothermal power and concentrating solar thermal power (CSP).

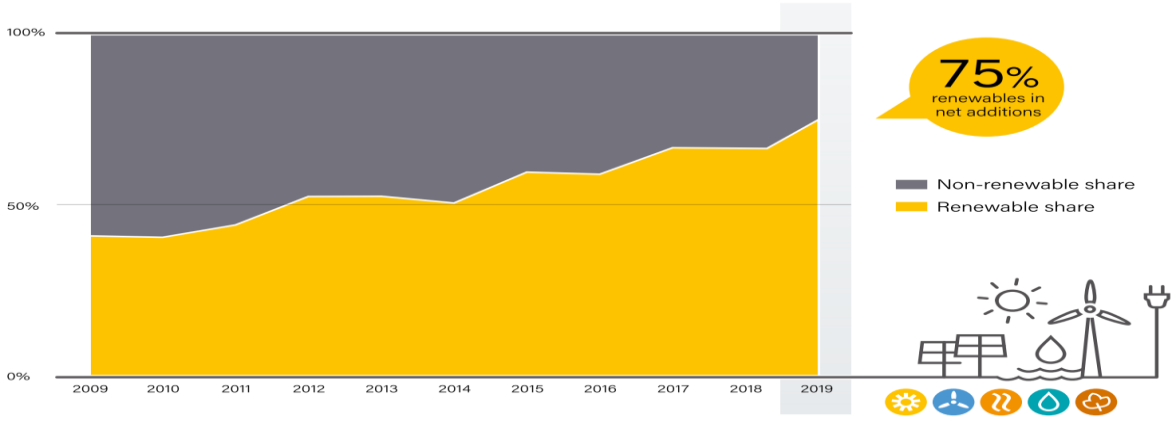

Figure 1. 1 The net annual addition in power capacity from renewable energy resources and non-renewable energy sources, 2009-2019 [1]

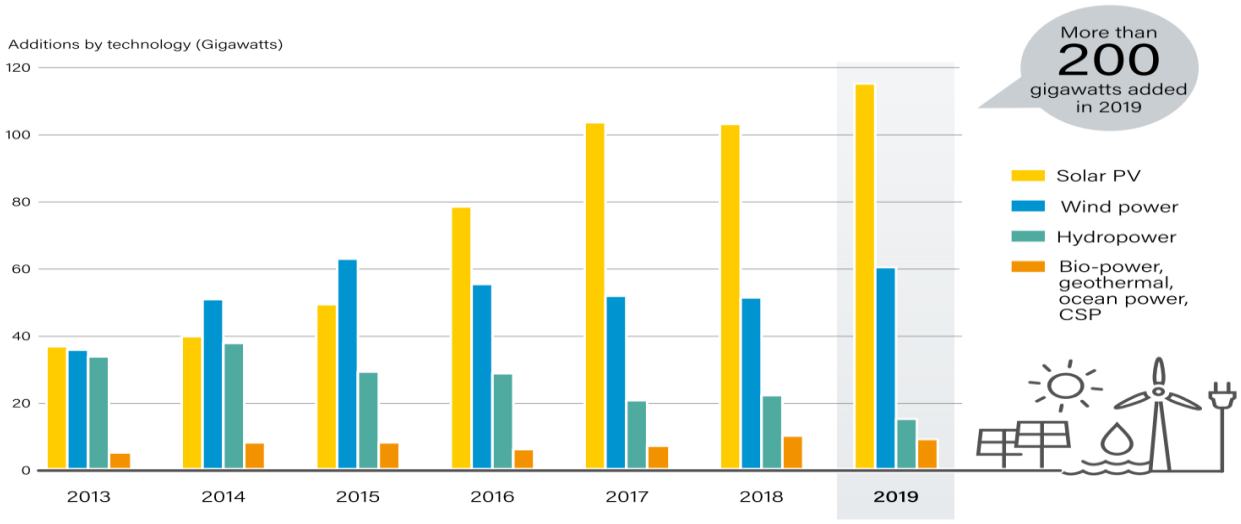

Figure 1. 2 The annual addition power capacity from different renewable energy technology between 2013-2019 [1]

Solar PV and wind technology are considered the fastest in growth compared to all other renewable resources. Solar PV can be installed as large-scale centralized PV plants or distributed, such as rooftop PV systems. Whereas wind is usually in the form of a centralized onshore or offshore wind farm consists of groups of wind turbines. In 2019, one-fifth of the global renewable capacity was in the form of small to medium size solar PV panels deployed on residential or commercial building rooftops [2]. The installation of residential rooftop PV in the electrical distribution systems, for example, has been increasing globally driven by falling prices and government incentives [3]. The rooftop PV systems can assist not only in deferring the need for distribution network reinforcement but also in providing various ancillary services. Figure 1.3 shows the distribution system with DG.

Nevertheless, several operational challenges encounter the distribution network operators (DSO) when different DG units become part of its structure. This primarily is due to the uncertain nature of such resources that leads to variation in their power generation.

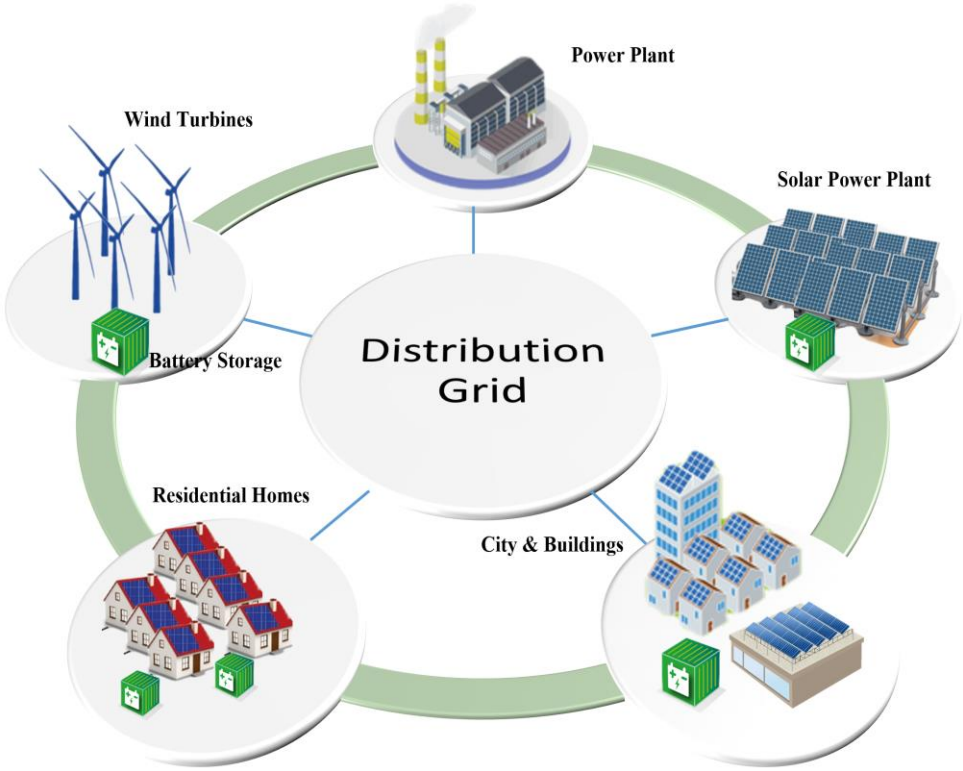

Figure 1. 3 Smart distribution network

1.2 Technical issues with increased penetration of DG

The presence of the PV systems and wind, for instance, in the distribution networks brings about several shortcomings in voltage, frequency and protection system controls [4]. Some of the technical issues related to the DG penetration are as follows:

- **Reverse power**

In the conventional distribution network, the power flows in a unidirectional manner from the main feeder toward the end of the feeder lines and circuits and to the load. However, with the appearance of DG generation, the power flow direction may get reversed when the amount of DG energy production is higher than the load, causing acute operational problems in the distribution systems [5]. This new situation may affect the devices that are used to operate under unidirectional flow. To overcome the reverse power problem, these devices must be replaced by their bidirectional counterparts, which presents a financial burden.

- **Protection**

The protection scheme is primarily affected by this bidirectional flow of power. The impacts on the protection in the distribution network appear in several forms, such as changing the distribution network short circuit current, changing the fault current level and changing the characteristic of the fault current [6]. For example, the fault protection relays cannot function properly in a radial distribution network when the bidirectional flow of power occurs [7].

- **Voltage issue**

The voltage violation issue (rise/dip) is considered one of the crucial issues associated with DG generation fluctuation when they are present in the distribution network. When the power coming from PV is higher than the customer load, this situation increases bus voltage. The voltage violation is not only a function in the PV generation but also is a function of the PV panel location and the network configuration. The straightforward solution is to upgrade the distribution network components with larger conductors and transformers [8]. However, this solution is costly.

- **System losses**

The installation of the PV systems and wind turbines in the distribution systems is to feed the network load and reduce the dependency on power supplied from the main feeder, which eventually minimizes the overall system losses. However, this situation changes with high penetration levels, where power starts to reverse and line current becomes higher than normal (without PV). This may cause an increase in network losses without proper controls [9].

1.3 Motivation

Among the above technical issues, the voltage quality problem is considered the most severe obstacle to the DSOs. According to [10,11], the voltage problem represents the most significant issue that must be controlled for efficient operation of the distribution systems with high DG penetrations. Unlike traditional passive distribution systems where load level is the only unpredictable element, DG integration poses additional uncertainty levels for the DSOs and utilities. Traditionally, DSOs are accustomed to bringing the voltage at every node in the system back to its acceptable limit by an optimal adjustment of on-load tap changers (OLTC), voltage

regulator (VR) taps and capacitor banks (CB). However, because of the DG's intermittent nature, these devices cannot react as fast as required. Hence, exploiting the DG integration in distribution systems without compromising the voltage stability of distribution systems is necessary to be investigated.

Battery energy storage systems (BESS) and smart PV inverters are two potential solutions for controlling the voltage in distribution systems. The pace of embracing these technologies is growing, which motivates using them as voltage control devices. Combined Heat and Power (CHP), also known as a cogeneration system, is an energy technology that generates electricity and captures the produced heat. CHP is typically located close to the point of consumption where the need for electricity and thermal energy is high. CHP has been used efficiently for different applications, such as industrial, commercial and institutional, and may not be as efficient if employed outside these applications [12]. The feeder used in this dissertation is a residential feeder where only battery and PV units can be installed; thus, CHP is not an option in this model. If in the future any other researcher wants to include commercial buildings in the model, CHP may be an option to consider.

Furthermore, as the distribution systems become more dynamic with the ongoing modifications in their structure, it becomes essential to reconsider the controlling strategies and analysis tools. The analysis of power systems with conventional approaches becomes challenging due to the complexity and the large amount of data to handle. In the past decade, intelligent algorithms have seen noticeable improvements in various aspects, including optimizations, machine learning, game theory, etc. The development of such contemporary techniques is to address engineering problems more effectively. Different engineering applications have been adapted with such algorithms. This provides a motivation to apply such modern approaches in this study to enhance the operation of distribution systems connected with DG.

1.4 Dissertation objectives

Therefore, the main objective of this dissertation is to mitigate the problem of voltage deviation in distribution systems with high penetrations of renewable resources, namely solar PV and wind. The proposed model is called the open architecture model, meaning that other sources can be added

if the user wants. In this dissertation, the voltage control is accomplished by developing a voltage management approach that coordinates the battery energy storage systems (BESS) and the smart PV inverter's reactive power capability. By utilizing the management strategy, this research aims at providing a reliable control method to the voltage profile in LV distribution networks embedded with high residential rooftop PV systems. In addition, this control algorithm would regulate the voltage in distribution systems where centralized large-size PV systems and wind turbines are connected. Considering the uncertainty associated with solar and wind generation, this study incorporates the day-ahead (24-hours in 1-hour intervals) solar PV forecast in the management process to prevent voltage problems in the distribution networks. Hence, the dissertation objectives are outlined as follows:

Objective 1: Improving the voltage profile in a distribution system using battery energy storage systems

In the LV-distribution network, for example, the PV active power affects the voltage profile more than the reactive power due to the higher resistance-to-reactance ratio (R/X). Limiting the active power to overcome the voltage problem may not be a feasible option. Instead, distributed BESS has a promising future in distribution systems. The incidence of high voltage levels usually occurs in the midday (off-peak period) when the active power from PVs exceeds the residential demand. In contrast, low voltage instants happen at night when the electricity demand is high compared to the PV power output. Therefore, the first objective is to use the BESS to improve the LV distribution networks' voltage at the point of common coupling (PCC) with residential rooftop PV systems. Another objective is to use the BESS to improve the voltage in the MV distribution system with large PV systems and wind turbines.

Objective 2: Developing a coordinated voltage control method between battery energy storage systems and the smart PV inverter's reactive power capability

In the distribution systems, the reactive power provided by the smart PV inverters can be employed as a controlling approach for the voltage profile. The smart PV inverters can be used when BESS cannot yield to the desired voltage regulation. The current distribution systems operation codes in many countries permit controlling the PV inverters outcomes that facilitate their roles as dynamic devices. Thus, the second objective is to coordinate the PV inverter's reactive power injection or

absorption with BESS to manage the system voltage at the point of interconnections (POI) in the MV distribution systems. The study considers the BESS as the only controlling equipment in the LV distribution network, and the smart PV inverter functionality is not employed.

Objective 3: Optimal daily charge/discharge of BESS

Appropriate modeling of BESS is essential for attaining the required services from installing batteries in distribution systems. This dissertation's goal is to mitigate the voltage problem in the distribution systems. Thus, the third objective is to develop an optimization problem to dispatch the charging and discharging rates of each BESS, taking into consideration the BESS specifications. This objective is attained when the BESS store the excess energy from the DG at the incidence of high voltage magnitudes and supply the stored energy at the incidence of low voltage magnitudes. The 24-hours of BESS scheduling is solved by the linear programming (LP) optimization to attain the appropriate charging/discharging rates in response to the distribution system's daily voltage signals.

Objective 4: Determining the BESS characteristics

The planning strategy of BESS depends mainly on their characteristics. They are significant to acquire the intended goals and justify the deployment of BESS in a distribution network. In addition, BESS characteristics are crucial for reliable operation of the distribution network; hence, obtaining the optimal capacity, number and site of each battery storage unit in the grid is the fourth objective of this study. The goal here is to analyze these factors and exhibit their influence on the grid, which is accomplished by developing the voltage management approach.

Objective 5: Developing an optimal management approach to control voltage in distribution systems

Reliable operations of distribution systems are guaranteed by the optimal coordination of the connected DG and the regulation devices. Therefore, the fifth objective is to develop a management strategy to control the voltage in the distribution systems by considering all distribution system elements. The modern artificial intelligence optimization algorithms facilitate many engineering problems due to their powerful capability in dealing with sophisticated scenarios. In this dissertation, a hybrid optimization algorithm is used to obtain the optimal sizing,

numbers, locations and daily (24-hours) charging/discharging scheduling of each BESS to control the grid's voltage. This goal is acquired by developing a bi-level optimization algorithm where LP is embedded within the metaheuristic optimization algorithm. This research studies the performance of three optimization algorithms, namely Social Spider Optimization (SSO), Particle Swarm Optimization (PSO) and Cuckoo Search Optimization (CSO). The power flow is conducted by the Open Distribution System Simulator (OpenDSS), where the distribution systems are modeled.

Objective 6: Developing hybrid forecasting models for solar PV

Since the voltage level depends mainly on the amount of the unpredictable PV power outputs, such quantities are required to be forecasted and amalgamated with the proposed voltage mitigation approach. The operations of the voltage mitigation devices considered in this study, namely BESS and smart PV inverters, are scheduled a day ahead (24-hours in 1-hour intervals). Hence, the sixth objective is to develop a day-ahead hybrid forecasting model based on machine learning techniques. Artificial Neural networks (ANN) and Support Vector Regression (SVR) are used in this research work. To accomplish this objective, the historical PV power and weather data are used in the area in question: Riyadh city in Saudi Arabia. The data of the PV power is obtained from a PV unit placed at the rooftop of a mosque located in Riyadh city. The distribution systems load data are from a distribution system located in Riyadh city. Hence, the only data utilized from the mosque is the PV data without considering the load data of the mosque.

1.5 Tasks

Based on the objectives above, the following main tasks are highlighted and identified to be conducted in this study:

Task 1: Develop a day-ahead solar PV forecasting model using hybrid forecasting methods

- Collect real-time metrological weather data at the sites in question and apply the data preparation processes and the normalization technique.
- Collect real-time PV power output at the sites in question and apply the data preparation processes and the normalization technique.

- Build the day ahead hybrid forecasting models SVR and backpropagation neural network ($BPNN$) optimized by SSO ($SSO-SVR$)/($SSO-BPNN$), PSO ($PSO-SVR$)/($PSO-BPNN$) and by CSO ($CSO-SVR$)/ ($CSO-BPNN$).
- Evaluate the accuracy of each of the forecasting models.
- Evaluate the performance of the metaheuristic optimization algorithms.
- Compare the performance of the developed forecasting models and select the best model.

Task 2: Formulate the BESS charging/discharging optimization problem.

- Formulate a minimization optimization problem using LP to represent the behavior of the battery in response to the day-ahead distribution system voltage signal. The LP represents the lower-level optimization of the main algorithm.

Task 3: Develop the test-bed systems to simulate the behavior of the distribution systems.

- Develop the modified IEEE-34-bus systems and the modified Low Voltage Test Feeder using the OpenDSS.
- Exchange the decision variables through the component object model (COM) interface between OpenDSS and MATLAB software.

Task 4: Develop the proposed voltage regulation strategy consisting of bi-level optimization algorithms.

- Develop the metaheuristic optimization algorithms, Social Spider Optimization (SSO), Particle Swarm Optimization (PSO) and Cuckoo Search Optimization (CSO). These algorithms represent the upper-level optimization of the main algorithm.
- Identify the decision variables to be optimized.
- Incorporate the forecasting model, charging/discharging optimization problem and the test-bed systems within the upper-level optimization.
- Attain the results from the management algorithm.
- Evaluate the performance of the metaheuristic optimization algorithms.

Task 5: Evaluate the proposed algorithm through comprehensive case studies using the test-bed systems.

- Compare the distribution system voltage profile under PV and wind power penetrations.
- Compare the distribution system voltage profile under different numbers of available BESS.
- Show the effect of BESS locations on the battery sizes, scheduling and grid's voltage.
- Analyze the impact of hybrid generation systems (PV and wind) on the distribution grid.
- Show the effect of the smart PV inverter reactive power output and the BESS on the distribution systems voltage profile.

1.6 Dissertation organization

The rest of the dissertation is organized as follows: in Chapter 2, a comprehensive literature review about the proposed voltage mitigation approaches and strategies together with the PV power output forecasting techniques. Chapter 3 discusses the study management approach. In Chapter 4, the results of the hybrid forecasting methods based on machine learning algorithms are presented. Chapter 5 contains the results of the first case study, which is based on the medium voltage distribution network with high PV and wind integration. Chapter 6 shows the second case study, where the LV distribution network is considered with the residential rooftop of PV units. The dissertation's summary, conclusions and future work are provided in Chapter 7.

Chapter 2: Literature Review

This chapter contains a comprehensive literature review of the state-of-art works discussing themes relevant to the developed models and the proposed methodology utilized in this dissertation. The literature review chapter is divided into six sections. Section 2.1 shows the voltage problem in the distribution systems with DG integration. Section 2.2 discusses the voltage mitigation approaches and strategies investigated by researchers with high PV and wind penetration. Section 2.3 discusses the battery energy storage systems method as a voltage mitigation approach. Section 2.4 reviews the works that have been conducted related to the PV power output forecast. Finally, Section 2.5 discusses the metaheuristics optimization algorithms. Section 2.6 presents the knowledge of gaps and limitations acquired from the literature and how this dissertation addressed them.

2.1 Distribution systems with distributed generation

Voltage regulation is considered the fundamental operation challenge in the LV and MV distribution grids with high integration of distributed generation (DG), such as PV system and wind [6,13]. This problem is caused by the reverse power flow in the network that alters the distribution networks' operation behavior. The distribution system operators (DSO) require that the system voltage be within acceptable higher and lower limits. According to the Saudi Arabian distribution code, for instance, under steady-state and normal operation conditions, the service voltages in an LV distribution network should be within $\pm 5\%$ of the nominal voltage [14].

In Figure 2.1, a simple network structure of the conventional distribution system is displayed. It can be seen from Figure 2.1 that there are two buses such that V_s represents the sending end voltage and V_r is the receiving end voltage. R and X denote the resistance and the reactance of the distribution system. $SubTrans$ stands for the substation transformer that connects the distribution system to the main grid, MG. The P and Q are the active and reactive power flowing in the feeder, respectively. P_l and Q_l are the consumed active and reactive power by the load, respectively. In Figure 2.2, the distribution system structure is changed when DG is connected to the feeder. The power flow from the feeder has changed, causing a voltage rise at the receiving end, V_g. The active and reactive power produced by DG are donated as P_g and Q_g, respectively.

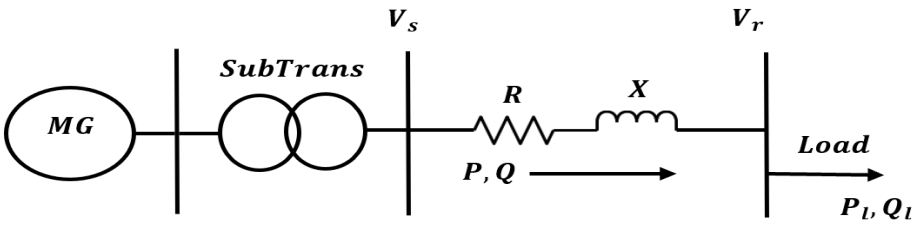

Figure 2. 1 Distribution system structure without DG

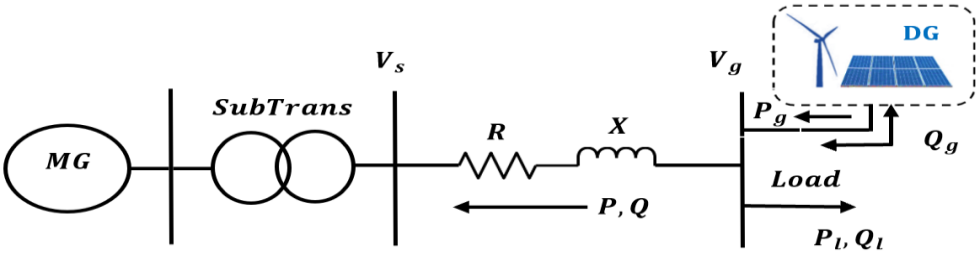

Figure 2. 2 Distribution system structure with DG

From Figure 2.2, the DG bus voltage can be expressed as follows [15]:

$$V_g = V_s + I(R + jX) \tag{2-1}$$

Where, I is the current flowing through the distribution feeder, while the power flowing in the distribution network is expressed as $P + jQ = V_g.I^*$; hence, the current flowing in the feeder is equal to $I = \frac{P-jQ}{V_g^*}$. So, Eq. (2-1) can be rewritten as:

$$V_g = V_s + \frac{P - jQ}{V_g^*}(R + jX) = V_s + \frac{RP + XQ}{V_g^*} + j\frac{XP - RQ}{V_g^*} \tag{2-2}$$

Since the angle between V_g and V_s is very small, the voltage droop can be roughly equal to the real part of the voltage drop. If we assumed that V_g is the reference bus, the angle of DG bus voltage is zero. Therefore, Eq. (2-2) can be approximated as follows:

$$\Delta V \approx V_g - V_s \approx \frac{RP + XQ}{V_g} \tag{2-3}$$

Where, ΔV is the voltage drop in the feeder.

Assuming also that the DG voltage bus is the base voltage, we can set $V_g = 1$. So, Eq. (2-3) can be expressed as follows:

$$\Delta V \approx V_g - V_s \approx RP + XQ \tag{2-4}$$

Such that, $P = P_g - P_l$ and $Q = \pm Q_g - Q_l$. Thus, the Eq. (2-4) is rewritten as,

$$Vg \approx V_s + R\left(P_g - P_l\right) + X(\pm Q_g - Q_l) \tag{2-5}$$

From Eq. (2-5) and by considering the unity factor of the DG units, two worst seniors are arising:

(I) Overvoltage: maximum generation minimum load ($P_g = P_{gmax}, P_l = 0, Q_l = 0$)

(II) Undervoltage: minimum generation maximum load $\left(P_g = 0, Q_g = 0, P_l = P_{lmax}\right)$.

When high active power coming from the DG unit exceeds the demand, the voltage tends to rise. On the other hand, when the low DG production coincided with high load, the voltage drop occurs along the feeder [16]. Therefore, controlling the voltage in the distribution system is very important with the appearance of DG sources.

Furthermore, by derivative of Eq. (2-3) with respect to the power, we get the following equation:

$$|\Delta V| = \frac{\partial|\Delta V|}{\partial P}dP + \frac{\partial|\Delta V|}{\partial Q}dQ = \frac{R}{V_g}dP + \frac{X}{V_g}dQ \tag{2-6}$$

From Eq. (2-6), we can see that the active or reactive power can regulate the DG bus's voltage. The voltage V_g increases or decreases with decreasing or increasing the amount of active power, respectively. Whereas by applying negative reactive power (absorbing) or by positive reactive power (injection), the voltage V_g decreases or increases, respectively.

2.2 Voltage mitigation methods with DG integration

Many works in the literature have proposed to keep the distribution system voltage within the operating limits with the appearance of PV systems. Such methods include feeder enhancement, traditional devices (OLTC, VR) [17–21], active power curtailment [22–24], smart PV inverter's reactive power capability [25–27] and battery energy storage systems [28–30]. In the following, smart PV inverter reactive power capability, active power curtailment, and battery energy storage system are reviewed as they represent the most effective voltage control approaches.

2.2.1 Smart PV-inverter reactive power capability

Smart PV inverter reactive power capability can efficiently regulate the distribution network voltage by injecting or absorbing reactive power into or from the grid. This feature incentivizes many countries to demand reactive power as a controlling method and include it in their regulation codes. For example, in 2003, the IEEE 1547 standard, which is a guideline for interconnecting distributed resources with electric power systems, prevents PV invert from being utilized to regulate the voltage at the point of common coupling (PCC) [31]. However, the IEEE 1547 standard has been modified and turned the passive inverters into active elements for voltage control in power system applications [32]. In the literature, there are three reactive power control approaches for voltage mitigation purposes, namely fixed power factor type control (FPF), power factor in term of injected active power control (PF(P)) and reactive power-voltage dependent control or droop control (Q(V)).

In the FPF method, the PV system sustains a constant power factor (PF) aiming to control the system voltage. In the moment of high active power generation from PV systems, the amount of active power will be high, and the overvoltage events are high, as represented in Figure 3.2 (a). Nevertheless, with low active production from the PV systems, the probability of voltage rise is negligible. Therefore, reactive power injection will increase system losses. This drawback is solved by employing PF(P), as shown in Figure 3.2 (b). In PF(P), the amount of reactive power is a function of the active power production from the PV system. The droop characteristics are selected in this approach to eliminate any reactive power absorption by the PV inverter during low active power flow from PV systems.

The FPF and PF(P) methods regulate the voltage through active power. Also, these methods assume that distribution networks voltage is influenced merely by the amount of power produced by PV system without considering the load variation. Yet, when the actual demand is higher than the PV production, the voltage rise problem may not occur. This issue is solved by Q(V) or the Volt-VAR control method. In the Q(V), the local voltage magnitude of the PV inverter at PCC, which reflects the power generation and consumption, is utilized to determine the required amount of reactive power. Figure 3.2 (c) shows that as the voltage deviates from the nominal values, the higher reactive power magnitudes are needed.

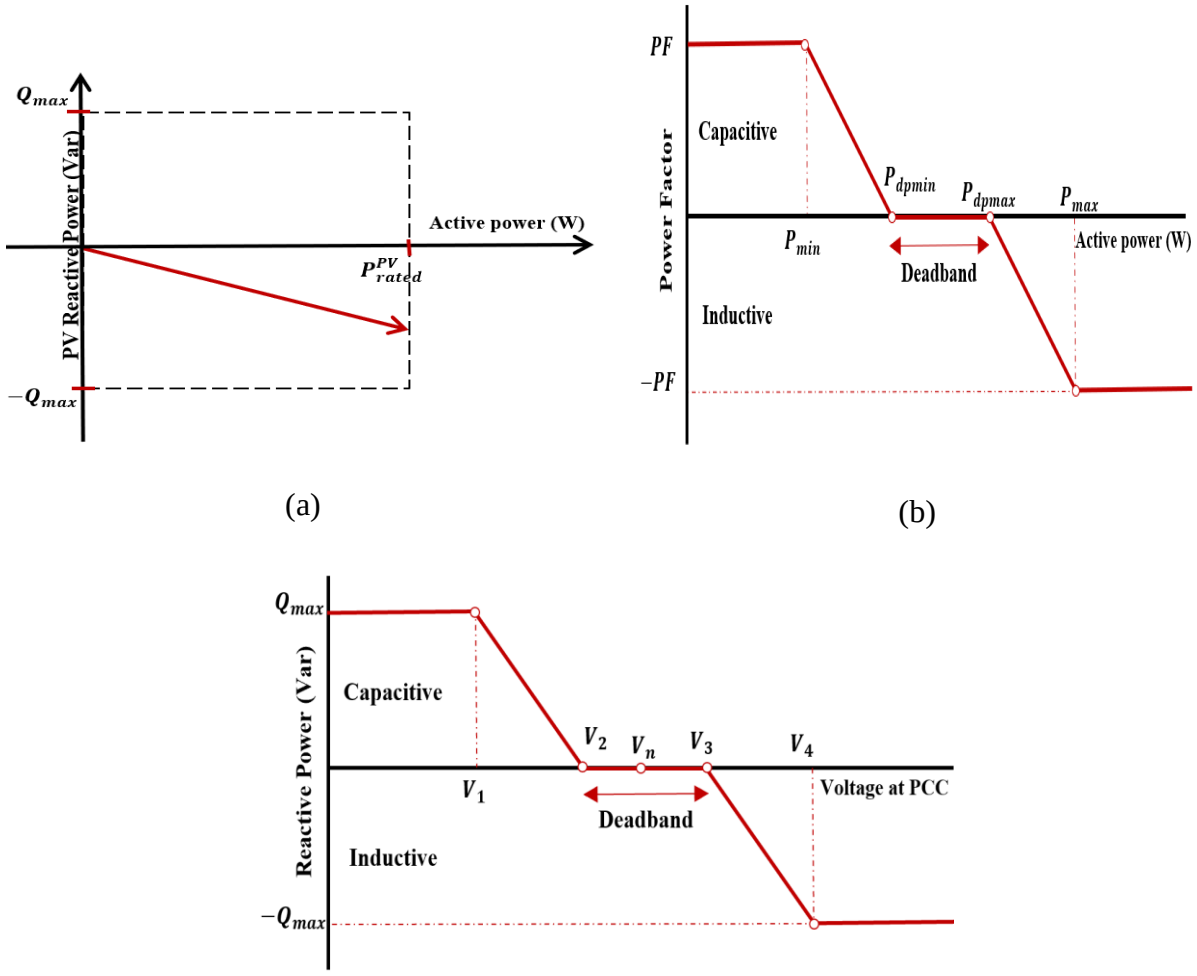

Figure 2. 3 Different types of reactive power control (a) FPF, (b) FP(P), and (c) Q(V)/Volt-VAR

In the literature, there are different regulation strategies proposed by researchers. The work in [33] utilizes the PV inverter reactive power capability to increase PV penetration in LV networks. The authors propose a method that does not require a communication infrastructure, called PF (P, V). This method is a combination of both PF(P) and Q(V). Their method is based on voltage sensitivity analysis using the system Jacobian matrix obtained from load power flow using the Newton-Raphson algorithm. The proposed method is also compared with all reactive power methods, namely FPF, PF(P) and Q(V). Results show that the proposed method effectively reduces the critical bus voltage. Also, their method leads to less reactive power consumption than PF(P) but more compared to Q(V). Besides, the proposed method increases the hosting capacity of PV in the LV network in the equation.

Reference [34] also use the voltage sensitivity matrix to solve the problem of voltage deviation locally. The proposed approach, which is active power dependent (APD), controls the magnitude of the PV inverters' reactive power determined by the local active power production of each PV system. Another study [35] dealt with the same problem but this time by formulating a multi-objective optimization problem to alter the parameters of the Q(V) characteristic with the voltage-sensitive analysis. The optimization problem is compared with an equal reactive power-sharing approach in terms of voltage regulation, minimizing the reactive power consumption and line losses. The comparison is validated with a test feeder. Results show that both methods might control the system voltage, and the multi-objective optimization problem has the superiority in reducing the reactive power from the inverters.

The authors in [36] set the V(Q) mode for the PV inverter to control the voltage level in a field distribution network in Kihei, on the island of Maui, Hawaii. The study uses different V(Q) curves and proved their efficiency in controlling the voltage. In this study, a central controller sends the set points of the PV inverters through communication channels. Furthermore, the study showed how oversizing the PV inverter could assist in dispatching the reactive power without threatening the real power output produced from the PV system. In [37], an optimal APD curve is proposed and compared with the standard APD curve to locally control network voltage. The proposed APD curve efficiently preserved the voltage profile within the predefined limit with a noticeable reduction in grid losses and less reactive power than the standard APD.

2.2.2 Active power curtailment

In order to provide reactive power without losing any amount of active power, the apparent power of the PV inverter is required to be exploited. As we have discussed previously, controlling the reactive power in LV distribution networks, which have more resistive line characteristics, may increase the losses and current and lower the input feeder's power factor. Therefore, active power curtailment could be considered a possible solution to overcome the overvoltage problem due to the appearance of PV systems. It is suggested that this method is utilized to solve the problem of overvoltage in LV networks because it concerns limiting the output of PV systems at the incidence of high PV power [38]. In this mitigation approach, the active power output of the PV inverter is controlled by controlling the maximum power point (MPP) tracker to an optimal limit.

In [39], the authors propose a centralized coordination approach of the PV inverters droop control to mitigate the overvoltage problem in LV distribution networks. The problem is formulated as an optimal power flow (OPF) optimization problem by incorporating the droop control into the OPF formulation by exploiting the sensitivity theory. The objective of this optimization is to minimize the active power curtailment of the installed PV systems uniformly. In their case studies, a radial LV network consists of 14 load buses and 10 PV units with different rated power and consumption is considered. Results show that the proposed control strategy and the active power curtailment approach effectively assist in maintaining the network voltage within prespecified limits.

In [8], the main objective of this paper is to use the droop-based active power curtailment method for overvoltage mitigation in radial LV feeders equipped with residential rooftop PV systems. Two types of droop designs were considered, which are based on the voltage sensitivity matrix obtained by running a Newton-Raphson load flow. The first type is assumed to have the same droop coefficients for all houses/PV inverters, while the other type is considered to have different droop coefficients. A 240 V/75 kVA suburban radial distribution feeder is used. This feeder consists of 12 houses, each with rooftop PV systems rated at 8.4kWp. The study outcomes exhibit that the houses located at the end of the feeder inject less power than those close to the transformer, which minimizes their PV revenues. The authors conclude that if the objective is to maximize the PV generation in the network, the unequal share of APC among PV systems should be employed (same droop coefficients). On the other hand, if the desire is to implement equal revenue sharing, equal APC should be used, even though that will increase feeder energy losses.

Unlike [8,39], which utilized merely the APC method, the work in [40] merges both the droop-based reactive power compensation and APC capability of the PV inverter for a local overvoltage regulation with high PV penetrations. Their technique augmented with very short-term PV power forecasts (15 seconds). A modified IEEE 34-node test feeder is modeled with real load and PV power data. Results display that the PV size and location have the major influence on the voltage profile and the amount of the active power curtailment. In other words, the PV systems located at the end of the feeder encounters higher curtailment and dominates the voltage profile.

Similarly, the study in [41] uses the reactive power and APC of single-phase inverter to prevent voltage problems in unbalanced four-wire LV distribution networks in the Perth Solar City trial, Australia. However, their strategy is formulated as a multi-objective OPF problem and solved by

the global Sequential Quadratic Programming. The optimization objectives are to improve the voltage values and balance profiles, minimize the network losses and minimize the generation profile. Results indicate that in the case of high load and low PV generation (undervoltage), the reactive power injection would improve the network voltage, and no power is curtailed. However, when the power coming from PV systems is greater than the load, APC is used with the reactive power to control the overvoltage.

2.3 Battery energy storage systems

2.3.1 Background

In the early 20th century, the history of BESS started when the Lead-Acid battery was utilized to supply power for residual load in a DC electricity network [42]. After that, BESS applications have been increasing in the power system field, particularly after PV and wind systems penetrations into distribution systems. This integration, however, significantly changes the way the distribution network operates. These operational obstacles could be mitigated by incorporating BESS to provide various services, such as voltage support, frequency regulation, load shifting, load leveling, peak shaving, network expansion deferral and greenhouse gas reduction [42]. Therefore, many countries are embracing the development of BESS and facilitating the deployment of BESS in their national programs [43].

In the distribution network with the appearance of DG, the BESS converts electrical energy from the grid or the excess power from the PV system/wind into a form that can be stored. After that, it discharges the energy back to the grid or load when required with almost zero emission. This operation principle permits the integration of these intermittent resources not only for smoothing their production but also to provide ancillary services, such as voltage control. The voltage problem represents the most operational challenge for DSOs that needs to be addressed.

The primary concern with BESS is the associated high initial cost. However, with the continuous developments in the batteries field, the BESS prices have been decreasing noticeably over time. Such developments permit their deployment in the distribution systems to regulate the voltage. However, improper usage, misallocating or non-optimal operation of the BESS in distribution networks may affect the reliability and degrade the power quality. Therefore, the successful

implementation of BESS depends mainly on the planning strategy where location, size and operational characteristics should be considered.

The voltage control in the distribution system by utilizing BESS has been studied by researchers in the past decade. Some studies use BESS to improve distribution network load [44,45], while others discuss the BESS applications for peak load shaving [46,47]. In the following, voltage mitigation in the distribution system through BESS with/without other voltage control approaches, such as PV inverter reactive power control or OLTC, is discussed from the viewpoints of objectives to be accomplished, controlling strategies, algorithms and test feeders.

2.3.2 BESS without other controlling methods

The work in [48] proposes a mitigation strategy for voltage rise or drop in LV distribution networks with the installation of solar PV using battery energy storage. The authors assume that each of the rooftop PV systems is equipped with battery storage. For battery operation protocol, an iterative method was employed for dispatching the battery charging/discharging, which is based on local information. Two practical LV-distribution feeders located in Western Sydney, New South Wales, Australia, have been studied with rooftop residential PV systems with rated capacities of 2-4 kW. The authors conclude that a proper selection of the charging/discharging rate is required for effective daily utilization of the battery storage devices. Reference [49] uses Fourier Series description based on a day-ahead energy forecast for optimal daily charging/discharging of batteries to minimize battery losses, cyclic battery cost and the network voltage profile. A total of 26 batteries are randomly placed along three phases LV distribution feeder. In this study, the management of batteries is accomplished by the Data Management System using hierarchical bi-directional communication infrastructures. The analysis reveals that the size and charging/discharging rates are significantly impacted by BESS locations and the number of controlled BESS. While [49] considered only a LV network, the same strategy is applied in [44] for optimal siting of BESS in MV and LV distribution networks. The MV distribution network, the IEEE 33-test system, has two wind distributed generation (DG) with a rate of 1 MW and seven PV DG; three of the PV have a rate of 400 kVA and four with the rate of 500 kVA. In this study, the optimal placement of BESS is based on centralized batteries in both MV and LV networks. Results reflect that the tradeoffs between desired services, including voltage regulation, loss reduction and battery parameters, are greatly influenced by the battery storage location.

The optimal siting, sizing and operation of BESS in distribution grids with renewable integration have a crucial impact on their overall efficiency and performance. Also, the distributed BESS brings about better benefits to distribution networks if allocated in a distributed manner than centralized ones [42]. Many studies have been conducted to tackle the ideal allocation and capacity of BESS. Reference [50], for instance, discusses the optimal allocation and sizing problem of 25 BESS in a distribution system. The goal of this study is to minimize voltage deviation and network losses while also addressing the capital and operation lifetime of BESS. The objective function is tackled by Genetic Algorithm (GA) based on multilayer objective optimization. For battery operation, linear programming (LP) is utilized to minimize the daily non-coincident peak demand. Their study reveals a distinct relation between the BESS capacity and location decisions and the voltage improvement. Furthermore, the researchers in [51] propose a controlling strategy to identify the optimal location, capacity and operational characteristics of different BESS in a distribution system with PV generation. The latter objectives are achieved by maximizing the total net present value (NPV). In this study, the GA is utilized to maximize the NPV, while battery charging/discharging was managed by an iterative and analytical method. By determining the optimal location, size and operation of BESS, results demonstrate that several economic benefits can be obtained, including energy arbitrage, peaking power generation, energy loss reduction, system upgrade deferral, a reduction in CO_2 emissions and VAR support. The study assumed that PV units are placed at all system busses to represent rooftop solar PV with a total annual PV generation of 28.62%. On the other hand, the authors in [52] perform a two-steps optimization approach to find the optimal size and location of PV and BESS. The first step is to identify the optimal placement of the PV systems that lead to minimum loss, cost and voltage deviation in the distribution system. The second step is to determine the optimal sites for BESS that result in minimizing the previous objectives. In this study, the optimization problem was solved by GA. For the charging and discharging rates, an analytical method is used through peak load checking. Results indicate that by installing 20 batteries of Lithium-Ion Power Pack Battery System manufactured by Tesla Company (assumed to be the battery technology), the peak power losses in significantly minimized and the network voltage is enhanced.

2.3.3 BESS with other controlling methods

The coordination of BESS with other voltage mitigation approaches, such as the smart PV inverters or OLTC and SVR, has been studied recently in the literature due to its positive impact on enhancing the distribution systems voltage profile and reducing BESS costs. The authors in [53] examine such a hybrid approach by proposing a coordination technique between PV inverters and battery energy storage systems to solve the voltage rise and dip. The control approach is evaluated on LV rural and urban scenarios, which have different R/X ratios. This study shows that in the case of the urban scenario (low R/X ratio), the reactive compensation utilizing the PV inverters is enough to keep the voltage within the acceptable voltage limits. However, for the rural scenario (high R/X ratio), the coordination between PV inverters and BESS is required. The authors in [54] present a distributed control algorithm that coordinates BESS with PV inverters to maintain voltage within save operation limits. A LV distribution system is modeled with the appearance of PV systems. The study conducted without affecting the benefits of BESS to owners. The study considers such coordination at the overvoltage instants when BESS fails to regulate the voltage. The proposed strategy proved its efficiency. Initially, BESS starts to control the overvoltage locally, while the central controller interferes through managing the PV-inverter reactive power output if the voltage problem still exists. Moreover, the coordination between BESS, PV inverters reactive power capability and step voltage regulators (VR) is examined by authors in [55]. Their case study is based on real PV and load data with a 1-second resolution. The study found that BESS and PV inverters managed to control the fast fluctuation of PV power output. At the same time, VR was able to regulate voltage variation caused by load changes.

2.4 Forecasting techniques

The tendency toward embracing emission-free energy from different renewable energy technologies, such as solar PV, has resulted in necessary changes in the distribution system operation. These operational obstacles are due to the intermittency nature of the power coming from the sun, which requires additional ancillary services to control the variability in the PV system generations [56]. However, these services are economically unfeasible, and adopting them may discourage installing the PV systems in the distribution networks [57]. Therefore, an accurate prediction of the amount of energy from the PV system would facilitate mitigating the technical issues of these PV systems [58]. There are various forecasting topics in electrical power systems,

such as load, wind, solar and electricity market forecasts [58]. In this study, the solar PV power forecast is of focus.

2.4.1 Forecasting power output of PV system

PV power output is highly correlated with the meteorological variables, such as solar irradiance, wind speed, humidity and temperature. These variables depend mainly on the geographical location and the climate condition at the site in question. In term of the PV power forecasting horizon, four main categories are considered: very short-term forecasting (1second - < 1hour), short-term forecasting (1hour-24hours), medium-term forecasting (1week-1month), and long-term forecasting (1month-1year). According to [59,60], the PV output prediction horizon should be identified before choosing the forecasting technique because the forecasting accuracy decreases as the forecasting time increases. Furthermore, the choice of the forecasting time depends on the desired application. For instance, the very short-term forecasting can be applied for power smoothing, real-time dispatch and control and regulation services, while short-term is primarily focused on load-following and zone-control purposes [61]. For medium-term forecasting, it is useful for persevering the power system planning and maintenance schedule, whereas long-term forecast assists in generation planning, energy bidding and security operation [59].

With respect to the forecasting techniques, physical, statistical and hybrid-based prediction models can be employed for PV power production. Physical approaches are mathematical models that use weather forecast data attained from numerical weather prediction (NWP), while the statistical methods utilize historical data to predict future behavior without prior knowledge about the system state [62]. The hybrid method combines two independent forecasting methods to overcome each other drawbacks and strengthen the advantages by adding some optimization algorithms [63]. For the statistical methods, they are divided into (i) time series models, i.e., autoregressive (AR), autoregressive moving average (ARMA) and autoregressive integrated moving average (ARIMA), and (ii) machine learning methods, i.e., artificial neural network (ANN), support vector regression (SVR) and extreme learning machine (ELM).

A systematic literature review about PV power production forecast can be found in [64]. The authors in [65] conduct a comparison between statistical approaches, namely ARMA, ARIMA and seasonal ARIMA (SARIMA), with six different neural networks (NN) to forecast the output power

of a PV plant. Eight-time delays of the power production from a PV plant are used as the input variables to generate the forecasting results. The analysis shows that NNs have better performance than time series models with less computation time. In [66], the PV power forecasting model is created based on backpropagation neural network (BPNN) model to perform a 24-hours ahead PV output forecast in Ashland, Oregon. Results show good accuracy results for forecasting the power output of photovoltaic systems with low Mean Absolute Percentage Errors.

In [67], a support vector regression (SVR) model using six weather variables, including normalized temperature, relative humidity, low-level cloudiness, mid-level cloudiness and upper-level cloudiness, is built to predict the power generated from a 1-MW photovoltaic plant in Kitakyushu, Japan. The results of this study indicate that SVR with the cloudiness factor led to better accuracy. Furthermore, a short-term solar irradiance is proposed by [68], where two different SVR models based on clearness index were used. In [69], the authors formulate solar generation forecasting models using linear least square regression and SVR with the radial basis function. The outputs of this study exhibit that the SVR model with seven weather metrics is 27% more precise compared to other forecasting models that use only sky conditions for predictions. The study in [70] predicts the power output of two wind farms and two PV power plants using different forecasting techniques. Machine learning-based forecasting models proved to be the most effective models in dealing with the non-linear relationship between weather parameters and wind/PV power production.

From the above literature, machine learning algorithms proved to capture and deal with the nonlinearity in forecasting problems compared to other forecasting methods. However, the main drawback of applying these algorithms is that they are sensitive to specific parameters. For instance, SVR depends highly on Kernel function hyperparameters, namely the error penalty parameter (C) and the width (γ). Also, ANN performance is influenced by the number of hidden layers and neurons at each hidden layer. Therefore, the hybrid models have been investigated by the literature recently to overcome the overmentioned disadvantages of SVR and ANN. Metaheuristic optimization techniques, such as genetic algorithm (GA), simulated annealing (SA), immune algorithm (IA) and particle swarm optimization (PSO), have also been used aiming at selecting the appropriate parameters. For instance, authors in [71] use GA to optimize SVM model parameters for electricity price forecasting. Furthermore, IA and SA are used in [72] and [73],

respectively, to determine the best parameters to forecast Taiwan's annual electric load. The study in [72] show that the proposed models superior to other models, such as ANN models. For the PV power generation forecast, a hybrid model is created in [74] between Genetic Algorithm and SVR (GASVR) to optimize Kernel function parameters. Study results demonstrate that GASVR is more accurate than the conventional SVR, with improvements in Root Mean Square Error value of 669.624, and 98.7648% in the Mean Absolute Percentage Error.

2.5 Metaheuristics optimization algorithms

2.5.1 Background

Optimization is an approach to attain the best solution for maximizing or minimizing a certain problem. To solve an optimization problem, an efficient optimization algorithm is required to be utilized. There are many optimization algorithms that can be used, and the selection depends highly on the focus and the characteristic of the problem. Figure 2.4 shows the classification of the optimization algorithms. If the exact methods cannot assist in tackling a particular optimization problem, the modern optimization method can be used to solve the complex issue.

2.5.2 Metaheuristics optimization techniques

Metaheuristics optimization algorithms prove their ability to solve complex optimization problems [75][76]. The Metaheuristics optimization algorithms are divided into trajectory and population-based algorithms. Unlike the trajectory-baes algorithms, which have a single agent tracking out a single path, the population-based algorithms employ multiple agents tracking out multiple paths. Figure 2.4 shows the classifications of the optimization algorithms.

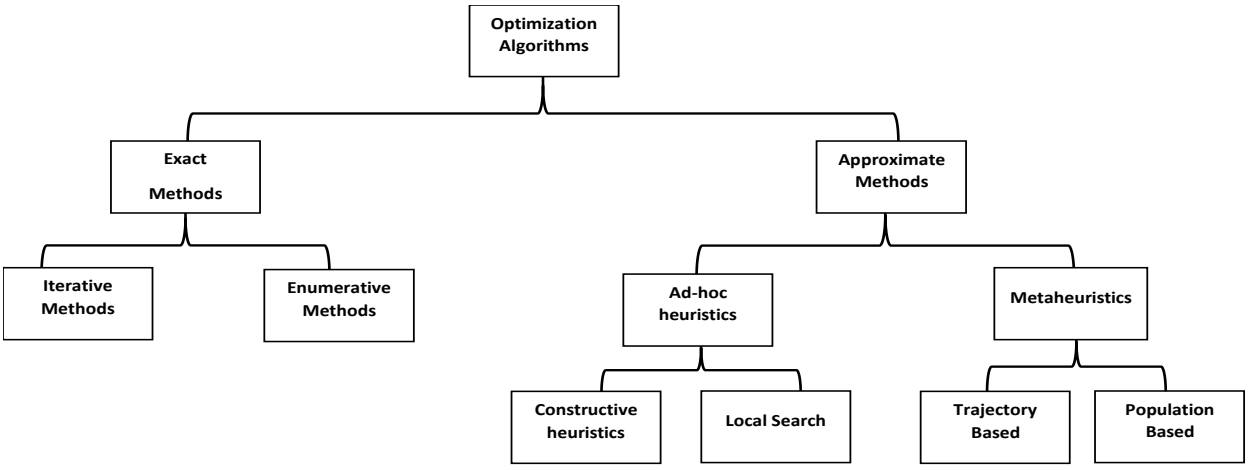

Figure 2. 4 Optimization algorithms classification [77]

Metaheuristics population-based algorithms inspired many researchers from different fields to incorporate these algorithms to solve varieties of problems. In this work, metaheuristic optimization techniques are used for the following reasons:

- In the electrical power system, issues related to the operation, planning, control, forecasting and demand management have widely used such algorithms [76,78]. Therefore, metaheuristics optimization algorithms could be used to enhance the operation of distribution systems connected with renewable resources.

- Furthermore, the electrical distribution systems become more dynamic with the ongoing modifications of their structure. The analysis of power systems with conventional approaches becomes challenging due to the complexity and the large amount of data to handle. Thus, it becomes essential to reconsider the controlling strategies and analysis tools.

- ***The applications of metaheuristic optimization techniques in this dissertation***

In this dissertation, two applications in which the metaheuristics optimization algorithms are applied. The applications are as follows:

- First, these algorithms are applied in the bi-level optimization of the proposed management approach for the sake of controlling the voltage in distribution systems through the optimal operation of BESS. The metaheuristics optimization algorithms represent the upper level optimization of the main algorithm. For this application, Social Spider Optimization (SSO),

Particle Swarm Optimization (PSO) and Cuckoo Search Optimization (CSO) are utilized. In addition, a comparison is conducted based on their performance and convergence rate to attain the optimal values.

- Second, the day-ahead PV power forecast is developed using hybrid forecasting models based on machine learning techniques, artificial Neural networks (ANN), and Support Vector Regression (SVR). The metaheuristic optimization techniques are used to improve the performance of the forecasting models through optimal tuning to the learning algorithms' parameters. The SVR and BPNN's parameters are optimized by three metaheuristics optimization algorithms, namely Social Spider Optimization (SSO), Particle Swarm Optimization (PSO) and Cuckoo Search Optimization (CSO).

- ***Drawback of the metaheuristic optimization techniques***

The main obstacle in such algorithms is the guarantee of obtaining the global optimum. This depends significantly on an algorithm's operators that modify individuals' positions to overcome local minimum. According to [79], the most aspect regarding the metaheuristics optimization algorithms is in their exploitation and exploration capability. Exploration means the ability to explore all the points in the search space, while exploitation means the ability to use previous knowledge from the solution that was already obtained to drive the search to the local region. Metaheuristics optimization algorithms prove their ability in obtaining the global optimum solutions.

2.6 Knowledge gaps

After reviewing the literature and state of the art studies related to the voltage problems in distribution systems and the forecasting algorithms mentioned above, the knowledge gaps are summarized as follows:

- **Voltage control strategy using BESS and smart PV inverters**

In the literature, several mitigation approaches have been proposed to regulate the voltage with PV systems and wind integrations. Some researchers employ the reactive power capability of the smart PV inverters, generation/consumption. Others suggest curtailment strategies of the PV system's active power whenever the terminal voltage exceeds predefined limits. Battery energy storage

systems (BESS) have proved their efficiency in providing various services to the distribution systems. Despite the effectiveness of different voltage mitigation strategies using BESS, these studies lack the following:

Most of the controlling strategies are based on local information and they did not provide a system-level optimality guarantee. That is, the optimum amount of active power to be stored by each installed battery in the network is absent. This opens a space to study and analyze the need for a network-level optimization for BESS operation in distribution networks with high level of PV and wind penetrations.

In addition, studies that use BESS as controlling voltage equipment in grids connected with PV systems are utilizing only the active power control without considering the functionality of the smart PV inverters. BESS may not always be able to improve the voltage. For that purpose, it is better to investigate the smart PV inverters capability to regulate the voltage through controlling their reactive power output. Thus, more studies need to be performed to explore the impact of such coordination.

- **Optimal operation of BESS for over/under voltage**

The integration of BESS with PV systems and wind into distribution systems makes controlling the charging/discharging rates significant. BESS stores the surplus energy coming from the PV system and supplies it back at low load time. The missing aspects in the literature regarding the optimal operation of BESS are:

Most of the studies use analytical approaches and local information to control the operation of the batteries. This creates a gap to come up with new charging/discharging strategies, taking into consideration all batteries in the distribution system to improve the voltage profile.

In addition, different daily charging/discharging strategies have been proposed in the literature. Some of them proposed a load following control method, while others utilized a drop-based method. Therefore, another controlling objective needs to be examined. To the best of the author's knowledge, no paper has used the daily voltage signal to control the battery operation for voltage regulation purposes, which is used in this research.

- **Optimal BESS characteristics**

BESS size plays a significant role in the reliable operation of distribution networks. Randomly selecting BESS size can increase cost, network losses and may not improve the network efficiency. Hence, selecting the optimal number of BESS, sizing each battery storage unit appropriately and optimally placing and operating them collectively in a distributed system level required to be studied thoroughly. In the literature, however:

Most papers have assumed predetermined sizes, numbers and BESS locations in the distribution network. Their assumption may not be ideal since considering different sizes, numbers or locations could result in better operation scenarios. In addition, different PV and wind penetration levels have been considered in various studies. However, some of them ignore the hybrid connection between PV systems and wind. Such operation scenarios need to be investigated.

- **Incorporating solar PV output forecast with the voltage management approach**

The uncertainty associated with the solar PV generation significantly impacts the scheduling of the regulation devices in distribution networks. The author in [80] points out that the next day forecast of PV output is important in the decision process of battery operation. In fact, BESS size and dispatching the next day charging and discharging limit depends on the amount of available power from sun, wind and load. Hence, to operate BESS appropriately, an efficient forecasting model of the solar PV output is needed. Thus, incorporating solar PV forecast in the voltage management strategy is required to be studied.

Furthermore, the hybrid forecasting methods have been showing a good forecasting performance compared to other methods. Different metaheuristic optimization algorithms methods have been applied in the literature to improve the SVR and ANN predication performance. The primary objective of such optimization algorithms is to determine the optimal parameters of SVR and ANN. However, there is still no persistent conclusion to select a particular algorithm to estimate these parameters. Therefore, considering the need for more advanced optimization algorithms, using recent metaheuristic optimization methods is required. In addition, conducting a comparison between their performance is to be explored.

Chapter 3: Voltage Management Strategy

This Chapter describes the overall voltage management strategy proposed in this study. The proposed approach is a coordination algorithm consisting of two controlling stages aiming to control the voltage in distribution networks connected with solar PV and wind. The first stage is accomplished by optimal planning of the BESS through a network-level optimization. The second stage is accomplished by controlling the reactive power of the smart solar PV inverters. The primary objective of BESS planning is to determine the optimal numbers, sites, sizes and operation characteristics of each BESS to regulate the voltage in the distribution systems with high PV and wind penetration over a specified planning horizon and interval.

In this study, there are two case studies in which the proposed voltage mitigation method is applied. The first case study (Chapter 5) considers a medium voltage distribution system with high PV and wind energy, penetrations, where the overvoltage problem is the main issue. In this case study, the coordination between the BESS and smart PV inverters is applied. In the first case study, the locations of the BESS are assumed to be fixed and installed at the distributed generation sites. On the other hand, the second case study (Chapter 6) studies the overvoltage and undervoltage problems in a LV distribution network. Unlike the first case study, the functionality of the smart PV inverter in this case study is absent, and the main voltage mitigation equipment is the BESS. Also, the size, capacity, number and optimal daily operation scheduling of batteries are obtained.

BESS plays a significant role in mitigating the negative impact of the installed solar PV and wind turbines in distribution systems. In this research, therefore, the first step to improve the voltage profile is by using BESS, especially when PV production is higher or lesser than the load. BESS charge when the available power from the PV and wind is more than the load and discharge when demand is at the peak. The storage units may not improve the voltage in the distribution system. For that purpose, the smart PV inverters interfere as the secondary voltage regulation equipment through controlling their reactive power (VAR) output. The Volt-VAR mode is set for the PV inverters. In this mode, the PV inverter injects or absorbs the reactive power based on the local information of the voltage.

3.1 Voltage management strategy

Figure 3.1 illustrates the framework of the coordination management strategy proposed in this dissertation. For BESS planning, a hybrid optimization algorithm is used to obtain the optimal sizing, location, number and daily (24-hours) charging/discharging scheduling of batteries to enhance the voltage of the distribution network. The proposed management is a bi-level optimization algorithm. It consists of two optimization levels, namely the upper-level optimization and the lower-level optimization. In the upper-level optimization, three metaheuristic optimization algorithms are used, namely Social Spider Optimization (SSO), Particle Swarm Optimization (PSO) and Cuckoo Search Optimization (CSO). In this study, the performance comparison between these algorithms is conducted based on performance and convergence experiments to analyze their searching capability. On the other hand, linear programming (LP) is utilized to represent the lower-level optimization.

Initially, the day-ahead forecasting of PV power output, wind power data, load data and prespecified available BESS are fed as input data to the algorithm. The predicted data of the PV power output are obtained from the best forecasting model proposed in Chapter 4. Second, the SSO, PSO and CSO generate the initial values of the population for the optimization problem. Each of these metaheuristic optimization algorithms has a searching mechanism. The explanation of these algorithms is presented in Sections 3.4-3.6. For instance, the SSO female and male spiders are formulated as a vector containing battery sizes in kWh (W_{max}) and kW ($S_{\max}$) and location of each BESS. That is, the dimension of the vectors is three times the number of BESS installed in the network. Considering N number of BESS deployed in the distribution network, the decision variables vectors can be expressed as follows:

$$v = [\, S^1_{\max} S^2_{max} \dots S^N_{max} \;\; W^1_{\max} W^2_{max} \dots W^N_{max} \;\; L^1 L^2 \dots L^N] \tag{3-1}$$

Where $S^1_{\max}$, $W^1_{\max}$ and L^1 are BESS capacity in kW, BESS capacity in kWh and the location of the first BESS, respectively.

After that, the optimal scheduling of BESS for the next day is optimized using the LP method (lower-level optimization), which is solved in MATLAB (see Section 3.2). Therefore, optimal location and daily charge/discharge of BESS are determined and fed to OpenDSS [81], where the distribution system is modeled. Then, the objective function, Eq. (3-2), that minimizes the voltage

deviation is obtained by 3 phase load flow in OpenDSS. This process is repeated for several iterations. Finally, in case the BESS were not able to improve the voltage, the reactive power output by the smart PV inverters is applied.

$$\varepsilon rror(v_i) = \frac{1}{2}\left(\sum_{i=1}^{N}\sum_{t=1}^{24}\left(1.05 - \mathrm{V}_{i,t}\right)^2 + \left(0.95 - \mathrm{V}_{i,t}\right)^2\right) \quad (3\text{-}2)$$

Where N is the wind and PV systems buses in the distribution network. $\mathrm{V}_{i,t}$ is the voltage magnitude at bus i at time t.

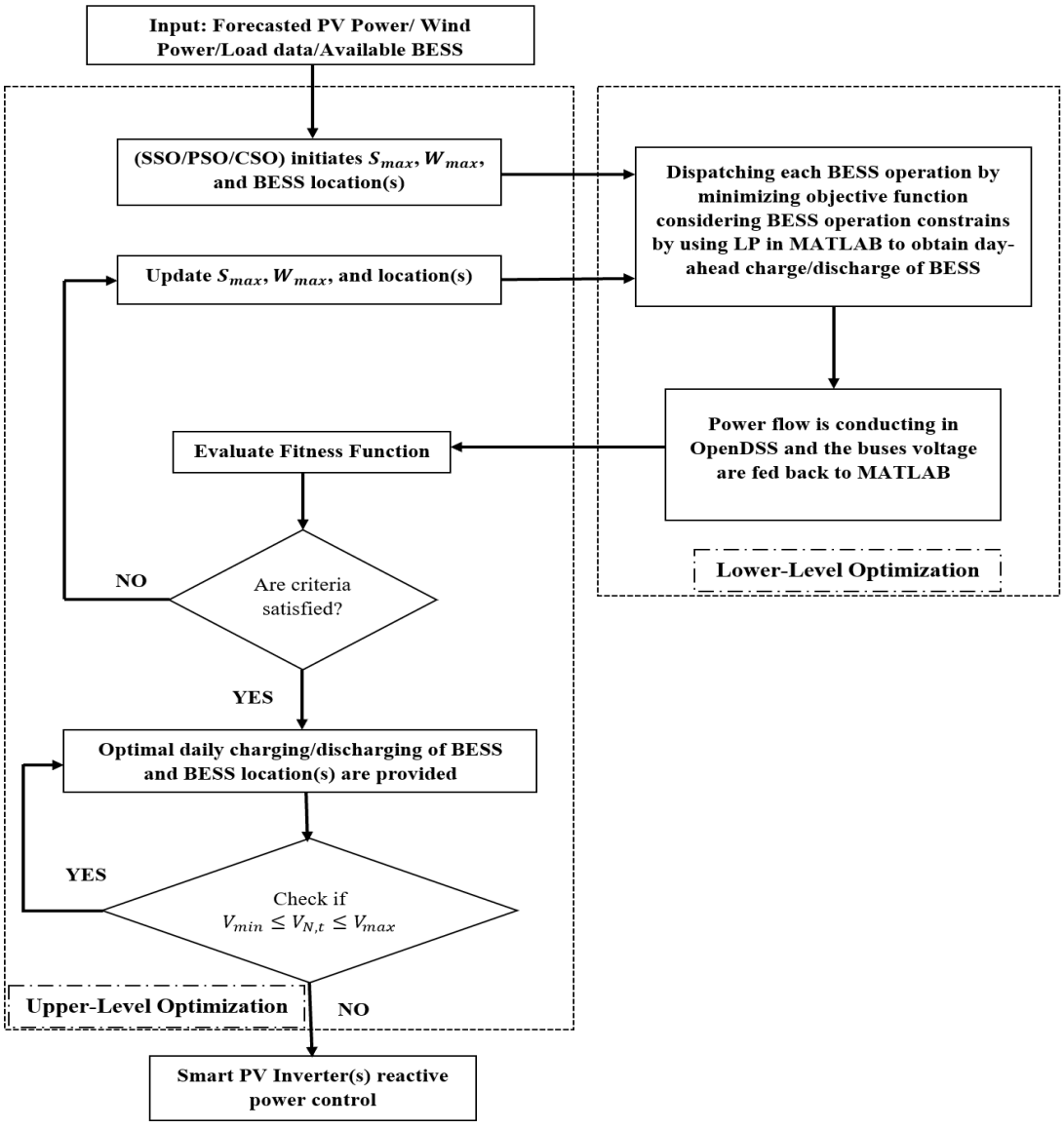

Figure 3. 1 Framework of the study voltage management strategy

3.2 Battery modeling

The applications of battery energy storage systems (BESS) have been increasing in the distribution systems. Therefore, appropriate modeling of BESS operation is crucial for providing the desired ancillary services and supporting the ongoing expansion of renewable energy resources, such as solar PV and wind. Figure 3.2 shows a configuration of the distribution grid connected with a residential rooftop PV system and a BESS at the PCC. The PV system is connected to the PCC through a solar inverter that converts the DC power to AC power. The BESS is connected through a power converter parallel with the load, grid and PV system.

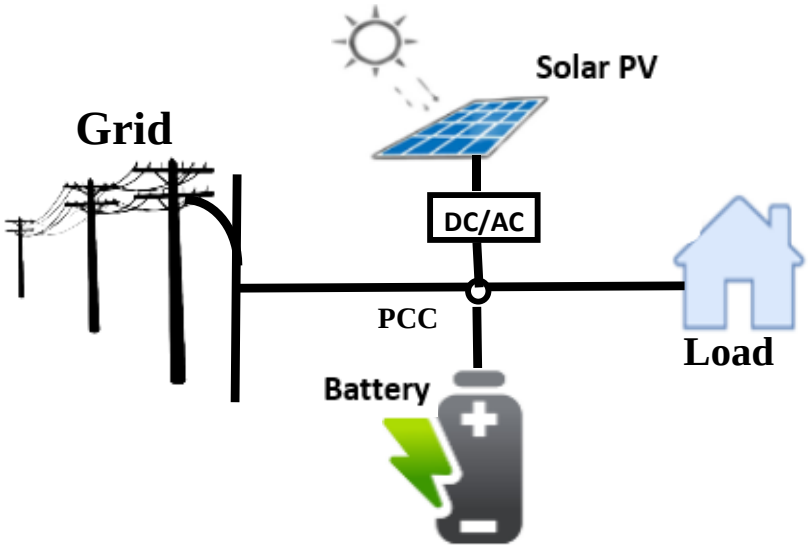

Figure 3. 2 System configuration of home-connected PV and BESS

Overvoltage usually occurs when the amount of real power coming from PV is more than the local demand, while the undervoltage happens when low PV power coincides with the heavy load. Hence, if BESS could store this excess power produced from the PV systems and use it later to supply the load, the voltage profile of the distribution system could be enhanced. This requires an optimal operation of the BESS units installed in the network.

Tesla Powerwall 2 is one of the BESS technologies that can be used as a home energy storage. The Powerwall 2 is an AC battery, meaning that it has lithium battery cells and an integrated AC-DC inverter/charger in one compact unit. Therefore, to operate this battery with a rooftop solar system, a PV inverter is required. In Tesla Powerwall 2 system, the DC power from the PV system is converted to AC by the PV inverter to supply the home. If there is surplus energy, the

switchboard lets the solar AC power be converted to DC to charge the battery and then back to AC to supply the load when needed. Similarly, the Tesla Powerpack represents large-scale energy storage. This battery is also a lithium-ion and an AC-connected BESS. For modeling and characterizing such batteries' operation, some requiring inputs and specifications are needed—these include BESS capacity, roundtrip efficiency and BESS state of charge. Table 3.1 lists the information and specifications of different technologies of the Tesla Powerwall 2 and Powerpack [82,83]. According to Table 3.1, the factors to be considered are:

- **BESS capacity**

BESS performance can be defined by battery output and energy density. A single Tesla Powerwall 2 pack, for example, has a usable capacity (energy) of 13.5 kWh, which is the total energy that can be stored in the battery and used by the battery owner. The BESS is also defined by its power capability, reflecting the amount of output power in kW drawn from or stored in the battery. In Tesla Powerwall 2, a 7kW peak or a 5kW continuous rate is the power capabilities of this type of BESS. On the other hand, the Powerpack has different energy and power capacities, 130kW/160kWh, 109 kW, 174kWh, 108kW/215kWh, or 130kW/228kWh.

- **Round trip efficiency**

Round trip efficiency considers the losses from the power conversion associated with the operating of the BESS. The BESS is either charging or discharging. The efficiency is the ratio of the total amount of energy discharged to the total amount of energy charged over all timesteps. For example, Tesla Powerwall 2 has 90% efficiency. That means, 10% of the power sent into or discharged from the battery is lost. The Powerpack has 84.5%, 86%, 86.5%, or 90% round-trip efficiencies depending on its capacity.

- **State of charge**

The state of charge (SOC) measures how much energy is available in BESS at a specific time step. The BESS is either in charging, discharging, or idle mode. The BESS should adhere to the prespecified maximum and minimum state of charge.

Table 3. 1 The specification of the battery energy storage system

Specification		Powerwall 2	Powerpack
AC voltage	AC	120/240 V	380-480 3-phase
Usable Energy	W_{max}	13.5 kWh	160, 174, 215, or 228 kWh
Maximum charging/discharging power	S_{max}	5 kW	130, 109, 108, 57, or 130 kW
Minimum charging/discharging power	S_{min}	0 kW	0 kW
Maximum State of Charge	SOC_{max}	100%	100%
Minimum State of Charge	SOC_{min}	10%	10%
Round trip efficiency	η	90%	84.5%, 86%, 86.5%, or 90%

3.2.1 Modeling BESS operational characteristics

In this study, the BESS operation is modeled as an optimization problem. This research work assumes that the battery technologies are lithium-ion Powerpack for case study 1 (see Chapter 5) and Powerwall 2 for study 2 (see Chapter 6). The BESS performance specifications are listed in Table 3.1. For this purpose, BESS optimal planning and operation need to be obtained based on a cost function to obtain the desired objective from the BESS installation. In this dissertation, the main goal of using the BESS is to control the voltage in the distribution network. In the Case study 2 presented in Chapter 6, the BESS operation is based on the following assumptions:

During the day:

- The PV system extracts the available power from the sun and produces solar energy.
- See if the produced energy can be utilized to supply the demand.
- Any excess energy is considered as the available energy to charge the BESS.
- If the BESS is completely charged, the surplus energy is exported to the main grid.

At night:

- The PV system generates little amounts of no solar energy.
- The BESS initially supplies the demand.
- If the load is completely supplied by BESS, the remaining energy in BESS is exported to the main grid.
- If the BESS is fully discharged, the load is supplied from the main grid.

The maximum benefits from BESS are accomplished when BESS charges at the incidence of high PV generations and low demand and discharges when the electricity demand is high. This is reflected by the voltage profile of the system on each bus. Hence, the optimal daily charge/discharge of BESS is determined by minimizing the following function, Eq. (3-3), that uses the daily voltage signals determined a day ahead to control each BESS operation, taking into consideration the operation assumptions above and the BESS specifications:

$$Minimize \qquad \sum_{t=1}^{24}\left(\left(P_t^{B,dich} - P_t^{B,ch}\right) \times \left(Volatge_{signal}\right)\right) \tag{3-3}$$

$$Subject\ to \qquad \sum_{t=1}^{24}\left(\left(\eta_{disch} P_t^{B,dich} - \eta_{ch} P_t^{B,ch}\right) = 0 \tag{3-4}$$

$$\sum_{t=1}^{24} P_t^{B,dich} \leq \alpha_t S_{max} \tag{3-5}$$

$$0 \leq P_t^{B,dich} \leq S_{max} \tag{3-6}$$

$$0 \leq P_t^{B,ch} \leq S_{max} \tag{3-7}$$

$$0 \leq P_t^{B,ch} \leq \beta_t (PV_t/Wind_t) \tag{3-8}$$

$$SOC_1 = \frac{\eta_{disch} P_1^{B,dich} - \eta_{ch} P_1^{B,ch}}{W_{max}} + SOC_{int}, \quad For\ t = 1 \tag{3-9}$$

$$SOC_{t+1} = \frac{\eta_{disch} P_{t+1}^{B,dich} - \eta_{ch} P_{t+1}^{B,ch}}{W_{max}} + SOC_{t-1}, \quad \forall\, t > 1 \tag{3-10}$$

$$SOC_{max} \leq SOC_t \leq SOC_{min} \tag{3-11}$$

$$\alpha_t + \beta_t = 1 \tag{3-12}$$

Where $P_t^{B,dich}$ and $P_t^{B,ch}$ are the discharge and charge rates of BESS in t^{th} hour. The η_{disch} and η_{ch} are the BESS discharging and charging efficiency, respectively. The sum of the discharging and charging efficiency is equal to the round-trip efficiency of the BESS technology. $Volatge_{signal}$ is the daily voltage signal of the network at each load bus. $PV_t/Wind_t$ are the available power from the PV system or wind turbine at time t. W_{max} is the maximum energy capacity of BESS in kWh, while S_{max} is the maximum rated power of BESS in kW. SOC_1 is the state of charge of the 1^{st} hour of the day that depends on the initial state of charge of the BESS, SOC_{int}. In this research, 10% is assumed in both case studies. SOC_{t+1} is the BESS's state of charge for the next 23 hours, while

SOC_{max} and SOC_{min} are the maximum and minimum state of charge, respectively. α_t is the discharging status of BESS at time t, and β_t is the charging status of BESS at time t. Both α_t and β_t are either 1 if discharging/charging or 0 otherwise.

From Eq. (3-3), the goal is to minimize the amount of charging and discharging that is triggered by the daily network voltage signal. In other words, the goal is to maximize renewable energy exploitation while controlling the voltage levels. Eq. (3-4) indicates that the battery is a daily refill, and the daily final state of charge is similar to the initial state of charge. The charging and discharging powers are limited to the rated kW capacity of the BESS technology and the available power from the PV system/wind turbine, as shown in Eq. (3-5)-Eq. (3-8). The state of the charge is limited to the maximum and minimum permitted state of charge, considering the kWh capacity of BESS, displayed in Eq. (3-9)-Eq. (3-11). Finally, Eq. (3-12) ensures that BESS is either charging, discharging or in idle mode.

3.3 Volt-VAR control

The Volt-VAR control approach manages the PV inverter reactive power output based on the local voltage values at the inverter terminal. The Volt-VAR controller operates by absorbing reactive power when the voltage exceeds a specific voltage limit or injecting reactive power when voltage lies below a prespecified threshold. Figure 3.3 exhibits Volt-VAR curve that is defined by determining the three modes, namely capacitive, inductive or deadband mode. This curve is used as the Volt-VAR mode in Case study 1 in Chapter 5. It can be seen from Figure 3.3 that when the voltage is less than $0.9\ p.u$ the inverter works in a capacitive mode by injecting the maximum available reactive power aiming to increase the voltage to the nominal voltage, $1\ p.u$. When the voltage lies between $0.9\ p.u$ and $0.95\ p.u$, the inverter injects reactive power based on a slop to maintain the nominal voltage. If the voltage is between $0.95\ p.u$ and $1.05\ p.u$, the inverter does not contribute since the voltage is within the network operation limits. On the other hand, when the voltage increases to be between $1.05\ p.u$ and $1.1\ p.u$, the inverter absorbs reactive power to move the voltage toward the nominal values. When the voltage is greater than $1.1\ p.u$, the maximum reactive power from the inverter is absorbed. In general, the settings of Volt-VAR

curves are usually provided by the inverter vendors. Table 3.2 lists the parameters of the Smart PV inverters for the Volt-VAR mode.

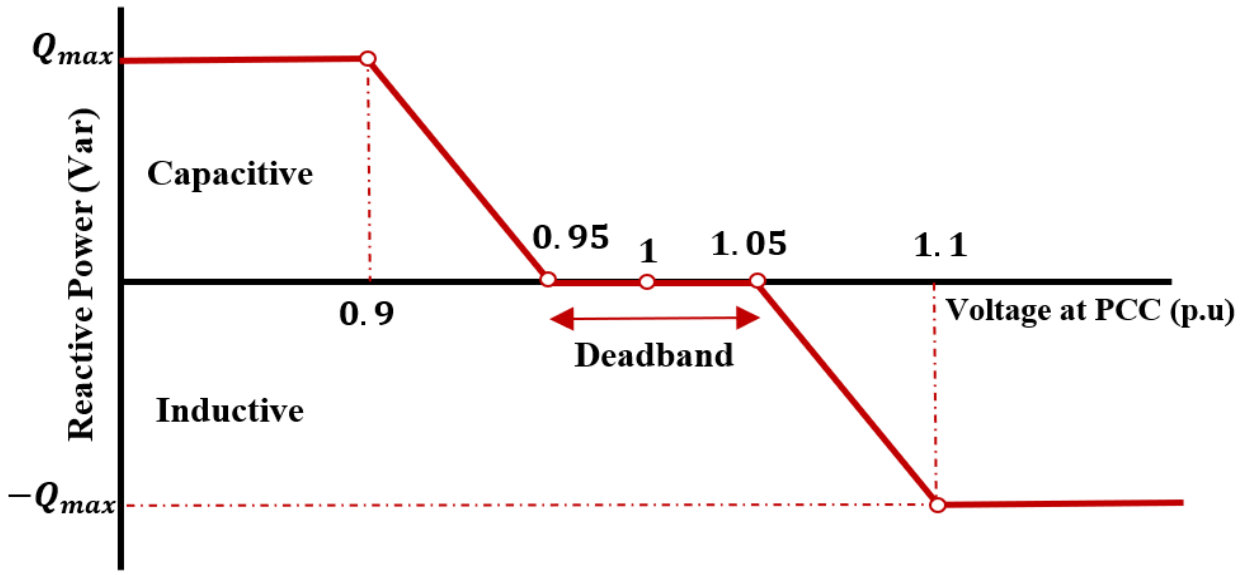

Figure 3. 3 Volt-VAR control curve

Table 3. 2 Smart PV inverter Volt-VAR parameters

Voltage Setpoint	Voltage Value	Reactive Setpoint	Reactive Value	Operation
V1	90%	Q1	Q_{max}	Reactive Power Injection
V2	0.95%	Q2	0	Unity Power Factor
V3	105%	Q3	0	Unity Power Factor
V4	110%	Q4	$-Q_{max}$	Reactive Power Absorption

3.4 Social Spider Optimization Algorithm

Social Spider Optimization (SSO) is a swarm intelligence algorithm introduced in 2013 by Cuevas et al. [84]. SSO mimics the cooperative style of social spiders, where male and female are the two searching agents considered in this algorithm. Usually, in the spider colonies, female spiders outnumber male spiders. Roughly 65-90% of the whole colony population N is female.

According to the SSO algorithm introduced in [84], the mathematical steps are as follows:

Step 1: Determine the female and male spiders' numbers in the search space. The number of female spiders N_f is generated randomly between 65-90% using the following equation:

$$N_f = floor[0.9 - rand \times 0.25].N] \tag{3-13}$$

Where $rand$ is a random number within the range [0,1]. The male spiders' number is then: $N_m = N - N_f$.

As a result, the population S contains N elements and is divided into two sub-groups: female spider ($F = \{f_1, f_2, \dots., f_{N_f}\}$) and male spiders ($M = \{m_1, m_2, \dots., m_{N_m}\}$), where $S = F \cup M$ ($S = \{s_1, s_2, \dots., s_N\}$), such that $S = \{s_1 = f_1, s_2 = f_2, \dots., s_{N_f} = f_{N_f}, s_{N_f+1} = m_1, s_{N_f+2} = m_2, \dots, s_N = m_{N_m}\}$.

Step 2: Assign weight w_i for each spider implying the solution quality of the spider i in the population S. The weight of each one is calculated by the following expression:

$$w_i = \frac{J(s_i) - worst_s}{best_s - worst_s} \tag{3-14}$$

Where $J(s_i)$ is the fitness value of spider evaluated by the objective value $J(.)$ of the spider position s_i. In this study, Eq. (3-2) is considered. $worst_s$ and $best_s$ are corresponding to the worst and best individual in the population, respectively, and are defined as follows:

$$best_s = max_{k\in\{1,2,\dots N\}}\left(J(S_k)\right) \quad and \quad worst_s = min_{k\in\{1,2,\dots N\}}\left(J(S_k)\right) \tag{3-15}$$

Step 3: Identify the vibration process. If, for example, a spider i perceives a vibration sent from a spider j, this vibration process can be written as:

$$VIB_{i,j} = w_j \times exp\,(-d_{i,j}^2) \tag{3-16}$$

Where $d_{i,j}$ is the Euclidian distance between spiders i and j, such that $d_{i,j} = \|S_i - S_j\|$. Each spider, i.e., i, in the population receives either of these three types of vibration as follows:

I. Closest spider, c, that has the highest fitness value ($VIB_{i,c} = w_c \times exp\,(-d_{i,c}^2)$);

II. Spider, b, that has the best fitness value in the entire population ($VIB_{i,b} = w_b \times exp\,(-d_{i,b}^2)$);

III. Closest female spider, f, to the male, i, $\left(VIB_{i,f} = w_f \times exp\,(-d_{i,f}^2)\right)$.

Step 4: Initialize the population S with N spider position. The positions' coordination for each spider, f_i or m_i, is an n-dimensional vector determined by the number of parameters to be optimized. The values of these parameters are randomly generated within the predefined upper, p_j^{high}, and lower, p_j^{low}, bounds. This is described by the following equations:

$$\begin{cases} \mathrm{f}_{\mathrm{i,j}}^0 = p_j^{low} + \mathrm{rand}(0,1).\left(p_j^{high} - p_j^{low}\right) \quad i = 1,2,\dots,N_f; j = 1,2,\dots,n \\ m_{k,\mathrm{j}}^0 = p_j^{low} + \mathrm{rand}(0,1).\left(p_j^{high} - p_j^{low}\right) \quad k = 1,2,\dots,N_m; j = 1,2,\dots,n \end{cases} \tag{3-17}$$

Where j *and* i are the parameter indexes, whereas k is the spider index. Zero indicates the initial population. $\mathrm{rand}(0,1)$ is a random number generated between 0 and 1, and $f_{i,j}$ is the ith female individual position that has jth parameter.

Step 5: The cooperative interaction behavior within the colony individuals is based on the spider gender. To imitate the cooperative behavior of the female spider, the following mathematical equation is defined that explains the change in position of the female spider, i, in each iteration:

$$f(D,C) = \sum_{i=1}^{n} min\{\|d_i - c_k\| \mid k = 1,2,\dots K\} \tag{3-18}$$

Where, D is the dataset, and C is the clustering center vector.

Based on other spiders' vibrations transmitted over the colony web, the movement of attraction or dislike can be modeled as follows:

$$f_i(k+1) = \begin{cases} f_i(k) + \alpha\,.VIB_{i,c}\,.\left(s_c - f_i(k)\right) + \beta\,.VIB_{i,b}\,.\left(s_b - f_i(k)\right) + \delta\,.\left(rand - \frac{1}{2}\right) < PF \\ f_i(k) - \alpha\,.VIB_{i,c}\,.\left(s_c - f_i(k)\right) - \beta\,.VIB_{i,b}\,.\left(s_b - f_i(k)\right) + \delta\,.\left(rand - \frac{1}{2}\right) \geq PF \end{cases} \tag{3-19}$$

Where α, β, δ and $rand$ are random numbers in the range of 0 and 1; k is the number of iterations, which is set to be 250 in the case studies in Chapter 5; PF is the threshold value; $s_c \; and \; s_b$ are the nearest best spider to the spider i and the best spider in the entire population S according to the fitness value, respectively.

Step 6: Define the male cooperative behavior. In the spider population, there are dominant and non-dominant male spiders. The dominant ones have high-quality fitness values and better chances to attract the closed female spiders. Non-dominant male spiders, in contrast, tend to gather in the male population center to exploit resources lost by dominant ones:

$$m_i(k+1) = \begin{cases} m_i(k) + \alpha \,.\, VIB_{i,\mathrm{f}} \,.\, \left(S_f - m_i(k)\right) + \delta \,.\, \left(rand - \frac{1}{2}\right) & if \; w_{N_{f+i}} > \; w_{N_{f+m}} \\ m_i(k) + \alpha \,.\, \left(\frac{\sum_{h=1}^{N_m} m_h(k).\, w_{N_{f+h}}}{\sum_{h=1}^{N_m} w_{N_{f+h}}} - m_i(k) \right) & if \; w_{N_{f+i}} > \; w_{N_{f+m}} \end{cases} \tag{3-20}$$

Where, S_f is the nearest female spider to the male spider i and the term $\left(\frac{\sum_{h=1}^{N_m} m_h(k).w_{N_{f+h}}}{\sum_{h=1}^{N_m} w_{N_{f+h}}} \right)$ represents the mean value of the male spiders M in the population S.

Step 7: Select the best spiders to represent the next spider generation. Within a certain radius calculated using Eq. (3-21), the dominant male and female spiders are matings resulting in new spiders. After that, the fitness of newly produced spiders is evaluated and compared with their parents. If new spiders have better quality than the parents, the new spiders continue, and the parents are eliminated.

$$r = \frac{\sum_{j=1}^{n} (p_j^{high} - p_j^{low})}{2 \,.\, n} \tag{3-21}$$

Where n represents the problem dimension, and $p_j^{high} and \; p_j^{low}$ are the upper and lower bounds, respectively.

3.5 Particle Swarm Optimization

Particle Swarm Optimization (PSO) was proposed by Kennedy and Eberhart in 1995 by observing the movement behavior of species, such as birds and fish swarms [85]. In PSO, a group of particles evolves in the search space aiming to obtain the optimal solution. In a D-dimensional searching space, each of these particles is assigned with the position vector $X_i = [x_{i1}, x_{i2}, \dots., x_{iN}]$ and the velocity vector $V_i = [v_{i1}, v_{i2}, \dots, v_{iN}]$. In each of the algorithm iterations, the fitness values of each particle is evaluated based on the objective function, see Eq. (3-2), and the best position $P_i = [p_{i1}, p_{i2}, \dots, p_{iN}]$ is recorded. The coordinate of the best particle fitness of the swarm is assigned as the global best position $P_g = [p_{g1}, p_{g2}, \dots, p_{gN}]$. Until the stopping criteria are satisfied, the position and the velocity of ith particle is updated in each iteration based on the following equations:

$$V_i^{k+1} = \omega \times V_i + c_\mathrm{s} \times rand() \times \left(P_i^k - X_i^k\right) + c_\mathrm{g} \times rand() \times \left(Pg^k - X_i^k\right) \quad (3\text{-}22)$$

$$X_i^{k+1} = X_i^k + V_i^{k+1} \quad (3\text{-}23)$$

Where ω is the inertia weight. c_s and c_g are social and cognitive parameters, respectively. $rand()$ is a random number selected in the range [0, 1].

In this study, the PSO algorithm was initiated with 250 maximum iterations ($iter_{max}$), and 50 particles as random populations. The inertia weight (ω), the social parameter (c_s) and the cognitive parameter (c_g) are updated nonlinearly at each iteration (j) using Eq. (3-24)-(3-26) [86]:

$$\omega(j) = \left(1 - \frac{j}{iter_{max}}\right)^{\alpha} (\omega_{max} - \omega_{min}) + \omega_{min} \quad (3\text{-}24)$$

$$c_\mathrm{s}(j) = \left(1 - \frac{j}{iter_{max}}\right)^{\beta} \left(c_{\mathrm{s},max} - c_{1min}\right) + c_{\mathrm{s},min} \quad (3\text{-}25)$$

$$c_\mathrm{g}(j) = \left(1 - \frac{j}{iter_{max}}\right)^{\gamma} \left(c_{\mathrm{g},min} - c_{2max}\right) + c_{\mathrm{g},max} \quad (3\text{-}26)$$

Where $\omega_{max}\ and\ \omega_{min}$ are the inertia weight maximum and minimum values, which are 0.9 and 0.4, respectively. $c_{\mathrm{s},max}\ and\ c_{\mathrm{s},min}$ are the maximum and minimum values of the social parameters, which are 2.5 and 0, respectively. The maximum and minimum values of the cognitive

parameters $c_{g,max}\ and\ c_{g,min}$ are set to 2.5 and 0, respectively. The power coefficients $\alpha, \beta\ and\ \gamma$ are set to 0.5, 1.5 and 1, respectively.

3.6 Cuckoo Search Optimization

Cuckoo search optimization (CSO) is a meta-heuristic optimization algorithm stimulated by observing the lifestyle of cuckoo birds in their survival strategy along with the behavior of Lévy flight. Cuckoos laid their eggs in other birds' nests called host birds. If host birds discover cuckoo eggs, they may throw cuckoo eggs out or abandon their nests and live in a new location [87]. In the CSO algorithm, the egg in a certain nest represents a solution to the algorithm, while a new solution is represented by each cuckoo egg. A set of solutions can be represented by a nest that has many eggs.

The CSO algorithm is mainly idealized based on the following three assumptions [88]:

1) One egg is laid by each Cuckoo at a time, and the nest to hatch is selected randomly.
2) The nests with high-quality eggs (solutions) continue to be the next Cuckoo generation.
3) The available host nests are set to be fixed, and the host bird probability of detecting the Cuckoo egg is $p \in [0,1]$. In this case, the egg can be thrown by the host bird, or the host bird leaves the entire nest and rebuilds a new nest somewhere else.

The Cuckoos' location is updated based on the Lévy flight, by using the following formula:

$$x_i^{(t+1)} = x_i^{(t)} + \partial \oplus levy(\beta) \tag{3-27}$$

Where $\partial > 0$ is the scale factor on which the direction and the step size depend. $\partial = 1$ is used frequently. $\oplus$ means entry-wise multiplication. Lévy flight is a random walk, and the levy distribution is used to generate the random steps:

$$levy{\sim}\mu = t^{(-1-\beta)} \quad , (0 \le \beta \le 2) \tag{3-28}$$

The main steps of the CSO algorithm are as follows [88]:

Step 1: Initialize the algorithm parameters: host nest (h), problem dimension (D), discovery probability by the host nest (p), number of iterations $(Iter)$, minimum and maximum step sizes

of the random walk and the boundary of search space, lower (low) and upper (up) bound. In this study: h= 20, p=0.25, and 250 is the number of iterations.

Step 2: Evaluate the fitness of each Cuckoo by using the objective function. Eq. (3-2) is the objective function to be minimized in this study.

Step 3: A new position is generated for each Cuckoo in the next generation using Lévy flight (Eq. 3-28).

Step 4: Compare the locations of the new Cuckoos' generation with their parents. If the fitness of the new generation $f(x_i^{(t+1)})$ is better than the previous generation $f(x_i^{(t)})$, the new Cuckoo $x_i^{(t+1)}$ is selected; otherwise, the parent, $x_i^{(t)}$, would retain.

Step 5: Compare the probability of discovery, p, with a new number (u) generated uniformly from [0,1]. In case $u > p$, the new nests are created, and the worst nests are abandoned. These new nest locations should be evaluated and compared with the solution attained in *Step 4*. The optimal nest locations are selected accordingly.

Step 6: Check if the stopping conditions are satisfied; otherwise, the algorithm should return to *step 2*.

Step 7: The optimum nest position represents the optimal solution to the problem.

Chapter 4: Hybrid Forecasting Algorithms for PV Generation

This chapter presents the proposed hybrid forecasting techniques and other forecasting algorithms used in this study to predict the PV power output. The proposed forecasting methods include a hybrid method between support vector regression (SVR) and backpropagation neural network (PBNN) with three metaheuristic optimization algorithms. These algorithms are Social Spider Optimization (SSO), Particle Swarm Optimization (PSO) and Cuckoo Search Optimization (CSO). Initially, the forecasting framework is highlighted. After that, the fundamental of the BPNN and SVR are explained together with SSO, PSO and CSO. Finally, the criteria to evaluate the forecasting models' accuracy are described.

4.1 Framework of the proposed forecasting models

In order to enhance the accuracy of the prediction, twelve hybrid models and three default models have been proposed. In this study, therefore, the forecasting approaches used are as follows:

- Hybrid Model 1: SVR based on RB function with SSO ($SSO - SVR_{RB}$).
- Hybrid Model 2: SVR based on RB function with PSO ($PSO - SVR_{RB}$).
- Hybrid Model 3: SVR based on RB function with CSO ($CSO - SVR_{RB}$).
- Hybrid Model 4: SVR based on linear function with SSO ($SSO - SVR_{linear}$).
- Hybrid Model 5: SVR based on linear function with PSO ($PSO - SVR_{linear}$).
- Hybrid Model 6: SVR based on linear function with CSO ($CSO - SVR_{linear}$).
- Hybrid Model 7: BPNN model with one hidden layer with SSO ($SSO - BPNN^1$).
- Hybrid Model 8: BPNN model with one hidden layer with PSO ($PSO - BPNN^1$).
- Hybrid Model 9: BPNN model with one hidden layer with CSO ($CSO - BPNN^1$).
- Hybrid Model 10: BPNN model with two hidden layers with SSO ($SSO - BPNN^2$).
- Hybrid Model 11: BPNN model with two hidden layers with PSO ($PSO - BPNN^2$).
- Hybrid Model 12: BPNN model with two hidden layers with CSO ($CSO - BPNN^2$).

- Model 13: Default SVR model based on RB function (SVR_{RB}^{D}).
- Model 14: Default SVR model based on linear function $\left(SVR_{linear}^{D}\right)$.
- Model 15: Default BPNN model ($BPNN^{D}$).

SVR-based kernel functions and BPNN are implemented in this study employing MATLAB R2020a and LIBSVM tools [89]. The framework that explains the proposed PV power output forecast is depicted in Figure 4.1. This framework can be used for any forecasting objective in other countries. The process is described as follows:

Step 1: Data preparation: input data are initially checked, cleaned and normalized to minimize the numerical difficulties during the training phase by the forecasting algorithms and the searching process of the parameters.

Step 2: Data splitting: the input data are divided into training and testing datasets. The training data are used to train the forecasting algorithms, while testing data are used to test the forecasting models' performance. In this study, 10-fold cross-validation is used. The cross-validation process is described in Subsection 4.5.2.

Step 3: Parameters tuning: SSO, PSO and CSO algorithms are applied to determine the SVR models' best hyperparameters and BPNN best network configurations for all the considered feature combinations. SVR parameters are the error penalty parameter (C) and the width (γ) for RB function, and the (C) for the linear function. BPNN parameters are the number of neurons at each hidden layer. In this study, one and two hidden layers are assumed. During the algorithms, these parameters are evolved, and their values are generated until the lowest normalized Mean Square Error $(nRMSE)$ values (Eq. 4-7) are attained. For parameter tuning, 10-fold cross-validation is used. The cross-validation process is described in Subsection 4.5.2.

Step 4: Building models: by using the best parameters mentioned in *Step 3*, twelve hybrid models are generated for each of the considered feature combinations, namely SSO-SVR_{RB}, $PSO-SVR_{RB}$, $CSO-SVR_{RB}$, SSO-SVR_{linear}, PSO-SVR_{linear}, CSO-SVR_{linear}, $SSO-BPNN^{1}$, $PSO-BPNN^{1}$, $CSO-BPNN^{1}$, $SSO-BPNN^{2}$, $PSO-BPNN^{2}$ and $CSO-BPNN^{2}$.

Step 5: Generating results: the hybrid forecasting models created in *Step 4* are tested under the testing dataset determined in *Step 2*. Their output is the prediction results.

Step 6: Results comparison: the forecasting models are then compared with the actual values of the PV power output utilizing Root Mean Square Error ($RMSE$), normalized Mean Square Error ($nRMSE$), Mean Absolute Error (MAE) and normalized Mean Absolute Error ($nMAE$). The results are compared and then analyzed. The best forecasting model is used with the voltage management approach mentioned in Chapter 3.

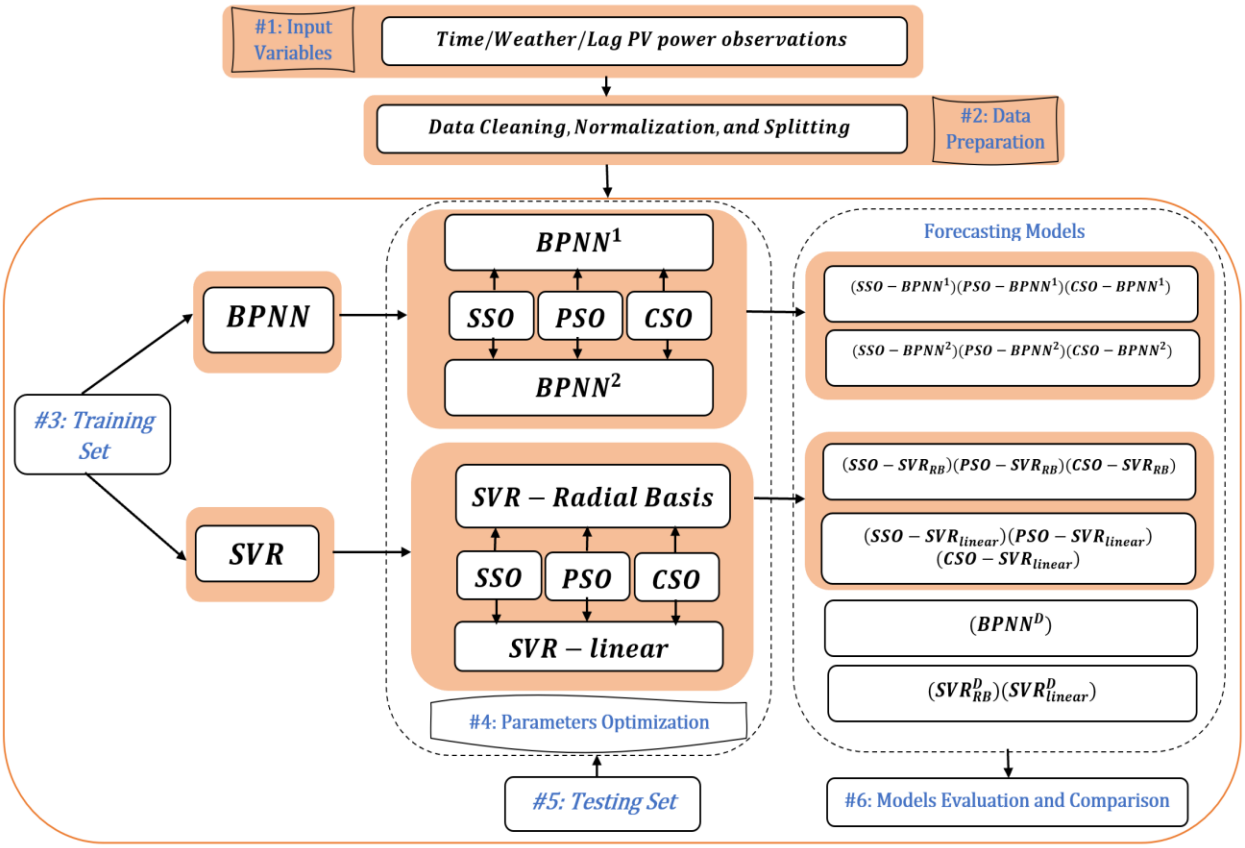

Figure 4. 1 Framework of the study proposed forecasting models.

Each process is discussed in detail in the sections below.

4.2 Backpropagation Neural Network

The artificial neural network (ANN) has been used in a variety of forecasting applications. ANN is an information computing system. ANN mimics approaches that human brain analyzes information [90]. ANN is created similar to the human brain, where a huge number of neuron nodes are interconnected to tackle problems that represent the uniqueness of this network. Backpropagation is one of the most popular ANN methods utilized in the learning process. Figure 4.2 shows a multilayer feed-forward neural network.

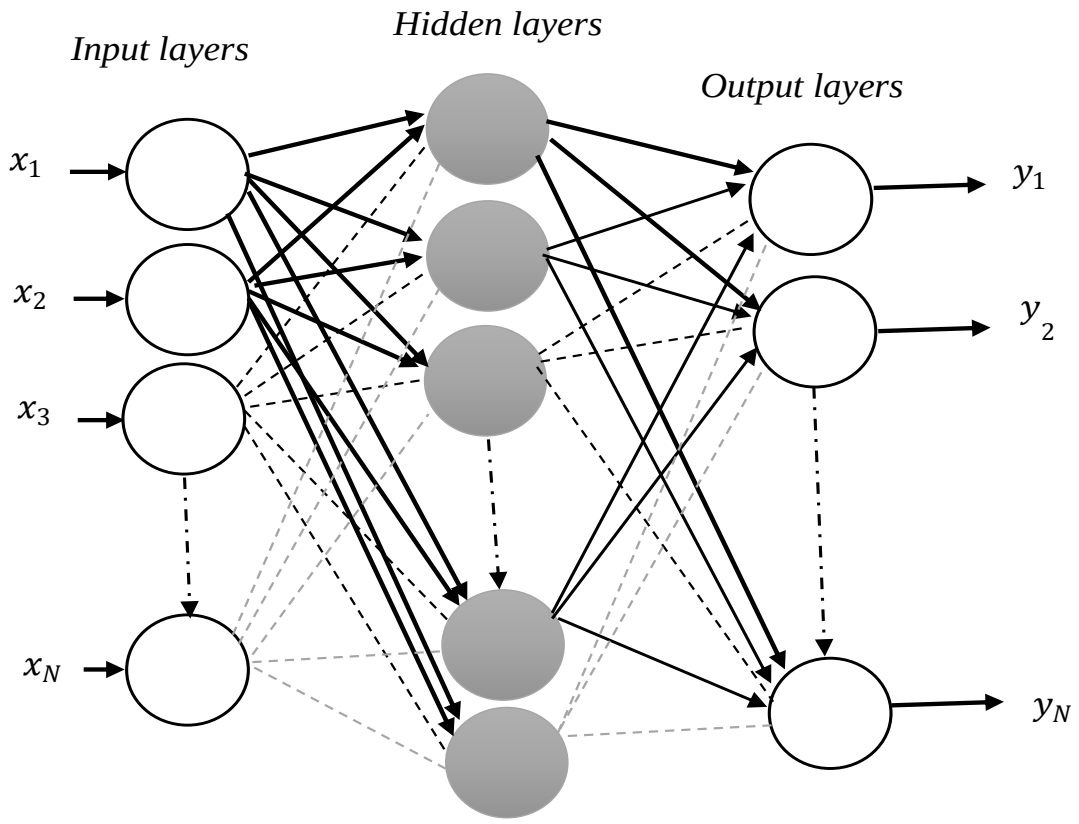

Figure 4. 2 Feed-forward neural network.

Three different layers are the main construction of the ANN, namely input, hidden and output layer, such as the input layer $[x_1, x_2, \dots, x_N]^T$, the hidden layer $[h_1, h_2, \dots, h_N]^T$ and the output layer $[y_1, y_2, \dots, y_N]^T$. The model output, therefore, can be calculated by Eq. (4-1) [91]:

$$y_i = \alpha_0 + \sum_{j=1}^{n} \alpha_j f\left(\sum_{i=1}^{m} \beta_{ij} y_{t-i} + \beta_{0j}\right) + \varepsilon_t \tag{4-1}$$

Where m is the number of nodes at the input layer, while n is the number of nodes at the hidden layer. f is a sigmoid transfer function, which will be the logistic function in this study, $f(x) = \frac{1}{1+\exp(-x)}$. $\{\alpha_j, j = 0,1,\dots,n\}$ is the weights vector that links the hidden layer and output layer and $\{\beta_{ij}, i = 1,2,\dots,m; j = 0,1,\dots,n\}$ are the weights that link the input nodes with the hidden nodes. α_0 and β_{0j} are weights magnitude of arcs leading from the bias terms, which have values equal to 1.

The number of nodes in each hidden layer are optimized by utilizing SSO, PSO and CSO. In this study, the multilayer perceptron (MLP) is selected for the BPNN model, while the Levenberg-Marquardt method is chosen as the training function.

4.3 Support Vector Regression

Support vector machine (SVM) is a supervised learning approach utilized for classification, regression problems or outliers' detection. When two classes cannot be separated, a kernel function is employed to map the input space to another high dimension space [92]. In that new space, the input space can be separated linearly. There are three known kernel functions to conduct the separation: linear, polynomial and radial kernel functions [93]. Hence, SVR inherently employs some of the SVM properties. Unlike SVM, SVR conducts the classification based on the regression process error measures based on the predefined threshold [94].

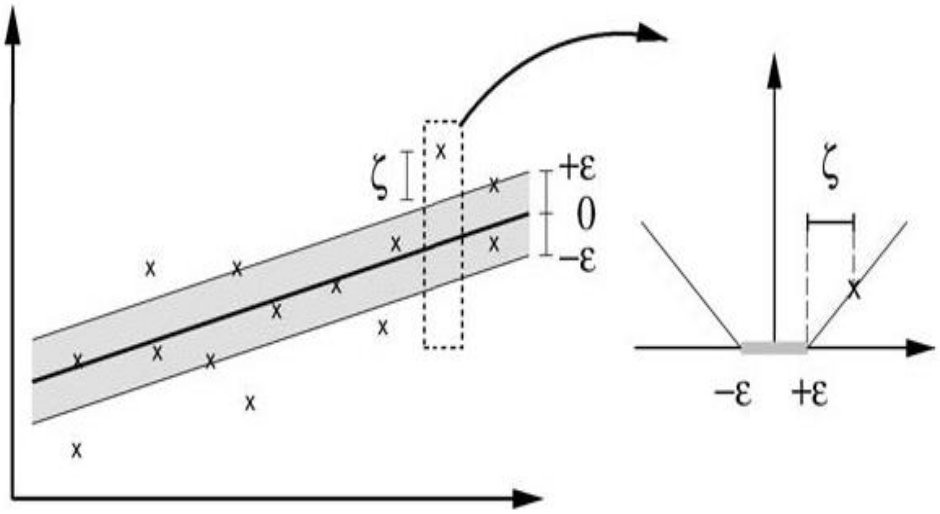

Figure 4. 3 The boundary margin for a linear SVR [94]

The leading optimization can be formulated in Eq. (4-2), and the kernels that are used with the SVR are provided in Eq. (4-3) and (4-4).

The SVR requires solving the following optimization problem:

$$minimize \frac{1}{2}\|w\|^2 + C\sum_{i=1}^{\ell}(\xi_i + \xi_i^*)$$

$$subject\ to \begin{cases} y_i - (w^T\phi(x_i) + b) \leq \varepsilon + \xi_i^* \\ (w^T\phi(x_i) + b) - y_i \leq \varepsilon + \xi_i \\ \xi_i, \xi_i^* \quad \geq 0 \end{cases} \tag{4-2}$$

Where $C > 0$ is a constant that identifies the trade-off between the flatness of f and assesses the tolerated amount of deviation to values larger than ε.

As we have mentioned earlier, our input space represented by the input features, or the training dataset, is transferred into a new space with high dimensions, where the function ϕ is used. This is known as the kernel trick $(x_i, x_j) = \phi(x_i)^T(x_j)$. For kernel functions, the radial basis (RB) and the linear are used. They can be written as [95]:

$$(RB): \qquad K(x_i, x_j) = e^{-\gamma\left(\|x_i - x_j\|^2\right)} \tag{4-3}$$

$$(linear): \qquad K(x_i, x_j) = (x_i^T x_j) \tag{4-4}$$

Where $\gamma\ (Gamma)$ is the kernel parameter and is estimated by the study optimization algorithms.

The selection of the two hyperparameters, C and γ, of the SVR models is essential in improving the model forecasting accuracy. The parameter C controls the level of empirical risk of SVR. On the other hand, the parameter γ controls the width of the radial basis function [72]. Hence, both parameters influence the performance of the SVR model. Researchers typically select these parameters based on their experience, previous knowledge [96] or using methods such as grid search [94]. In this study, the penalty factor, C, and γ, are optimized by using Social Spider Optimization (SSO), Particle Swarm Optimization (PSO) and Cuckoo Search Optimization (CSO) to build the hybrid models. This is described in the next Sections.

4.4 Metaheuristic optimization algorithms for PV power forecast

The meta-heuristic optimization algorithms, including SSO, PSO and CSO, used in this study to optimize the SVR and BPNN parameters, are described in this section. The evaluation function of

which these algorithms are trying to minimize is the normalized Mean Square Error ($nRMSE$), see Eq. (4-7).

4.4.1 Social Spider Optimization Algorithm

Social Spider Optimization (SSO) is explained in Section 3.4. For parameters selection, the SSO is initiated with 50 maximum iterations. For the linear function, the upper and lower bounds for C are between [1,10000], and for the RB function, the boundaries are in the range of [1,10000] and [0.01,3] for C and γ, respectively. For the BPNN models, the upper and lower bounds of neurons at each hidden layer are set to be [1,50].

4.4.2 Particle Swarm Optimization

Particle Swarm Optimization (PSO) is explained in Section 3.5. For parameters selection, the PSO is initiated with 50 maximum iterations and 50 particles are considered as the random population. For the linear function, the upper and lower bounds for C are between [1,10000], and for the RB function, the boundaries are in the range of [1,10000] and [0.01,3] for C and γ, respectively. For the BPNN models, the upper and lower bounds of neurons at each hidden layer are set to be [1,50].

4.4.3 Cuckoo Search Optimization

Cuckoo search optimization (CSO) is explained in Section 3.6. In this study: h= 20, p=0.25, and 50 is the number of iterations. For the linear function, the up and low bound for C are between [1,10000], and for the RB function, the boundaries are in the range of [1,10000] and [0.01,3] for C and γ, respectively. For the BPNN models, the upper and lower bounds of neurons at each hidden layer are set to be [1,50].

4.5 Forecasting models input variables

In this work, the forecasting objective is a day-ahead forecasting of PV power generation from a PV panel located in Riyadh city, Saudi Arabia. Therefore, to obtain the best forecasting model of PV power output, the proposed models are trained and tested using three types of variables considered at the study location. As mentioned in the literature, the PV output is greatly influenced

by time variables, weather variables and historical data of the PV power generation. Table 4.1 lists the input variables used in this study.

Table 4. 1 List of input variables used to forecast PV power output

		Input Variables
Time Variables	v_i^1	Month
	v_i^2	Day
	v_i^3	Hour
Weather Variables	v_i^4	Air Temperature (℃)
	v_i^5	Wind Direction
	v_i^6	Wind Speed (m/s)
	v_i^7	Forecasted direct normal irradiance, DNI $(W\mathrm{h}/m^2)$
	v_i^8	Forecasted global horizontal irradiance, GHI $(W\mathrm{h}/m^2)$
	v_i^9	Pressure (mB)
Lag Variables	v_i^{10}	PV power output at the same hour on the previous day (kW)

The variable (v_i^4), for example, is the air temperature (℃), and i is the temperature value at each hour. On each day, we have 24 values of air temperature. After that, the entire dataset (V) is divided into two subsets, namely: the training dataset, v_{train}, and the test dataset, v_{test}, such that $V = v_{train} \cup v_{test}$. In this study, eighty percent (80%) of the data is utilized as the training dataset, while the remaining (20%) is used as the testing dataset. The Cross-Validation technique is utilized to tune the hyperparameters of the SVR models and the BPNN network configuration.

4.5.1 Feature combinations

In this study, different independent combinations of variables are used as inputs to forecast the PV output (P_{out}). As more input variables do not always indicate good forecasting outcomes, the primary goal of combining different sets of input variables is to identify the suitable variables that give the best forecasting results at this site. Table 4.2 contains the variables for each feature combination. Considering the feature combination (12), for example, the P_{out} $(v_i^1, v_i^2, v_i^3, v_i^8, v_i^{10})$

is a function of Month, Day, Hour, Forecasted global horizontal irradiance, GHI $\left(\frac{\mathrm{Wh}}{m^2}\right)$ and PV power output at the same hour on the previous day (kW).

Table 4. 2 The input variables associated with each feature combination

Feature Combination	Input Variables
1	v_i^3
2	v_i^7
3	v_i^8
4	v_i^{10}
5	v_i^8, v_i^{10}
6	v_i^3, v_i^{10}
7	v_i^4, v_i^{10}
8	v_i^7, v_i^8, v_i^{10}
9	v_i^4, v_i^8, v_i^{10}
10	v_i^3, v_i^8, v_i^{10}
11	$v_i^3, v_i^7, v_i^8, v_i^{10}$
12	$v_i^1, v_i^2, v_i^3, v_i^8, v_i^{10}$
13	$v_i^1, v_i^2, v_i^3, v_i^7 v_i^8, v_i^{10}$
14	$v_i^1, v_i^2, v_i^3, v_i^4, v_i^8, v_i^{10}$
15	$v_i^1, v_i^2, v_i^3, v_i^4, v_i^7, v_i^8, v_i^{10}$
16	$v_i^1, v_i^2, v_i^3, v_i^4, v_i^5, v_i^6, v_i^7, v_i^8, v_i^{10}$
17	$v_i^1, v_i^2, v_i^3, v_i^4, v_i^5, v_i^6, v_i^7, v_i^8, v_i^9, v_i^{10}$

4.5.2 Cross-Validation

To evaluate the performance of the proposed forecasting models, it is not ideal to conduct this evaluation based on one test set. Therefore, to examine the forecasting model performance over different test data, k-fold Cross-Validation should be employed. Cross-validation is a procedure in which the data are split into more k-subsets [97], see Figure 4.4. These k-subsets are further divided into testing and training groups. In the training group, a single subset is used as a validation data set, while the remaining k-subsets are used as training subsets. This technique is repeated k times until the entire k-subsets are used as a validation set. Hence, the overall result is independent of only one training set, which may affect the robustness of the forecasting models [98].

It is worth mention that the k-fold Cross-Validation procedure is conducted in the absence of the testing dataset. The primary goal of Cross-Validation is to examine the generalization of a forecasting model. In this study, 10-fold cross-validation is used. In other words, the training

dataset is divided into 10-subsets. One subset is considered the test set, while the remaining nine subsets are utilized for training the forecasting model. This process is repeated 10 times resulting in 10 training and testing folds, where the $nRMSE$ is recorded for each of them. The average of the 10-folds $nRMSE$ results is then reported.

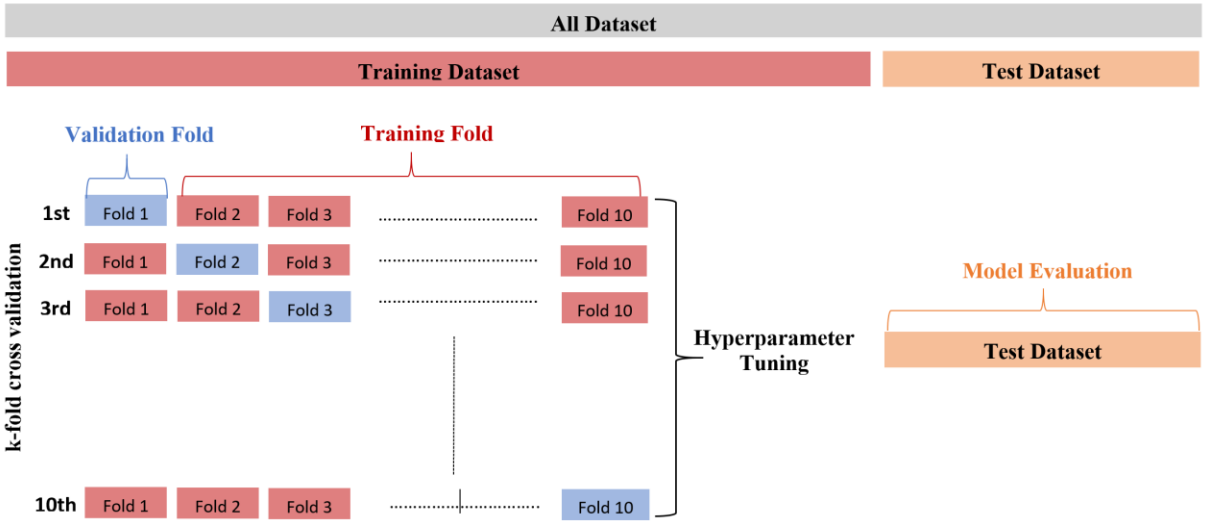

Figure 4. 4 k-fold Cross-Validation process

4.6 Data preparation

The weather and PV power data are required to be prepared. Two main steps are necessary for the data preparation. These steps are data clearing and data normalization. Each of these steps is described below:

4.6.1 Data cleaning

Data cleaning is a very significant step to create a successful forecasting model. Since we are dealing with historical data from different sources, these data could be imprecise impacting the performance of the forecasting models. In this step, all the missing PV power data are removed with all the associated time and weather variables.

4.6.2 Data normalization

Input data normalization plays an essential role in preparing the data before examining the forecasting models. The primary goal of data normalization is to reduce the possibility that features

with high numerical values dominate those with smaller numerical values [99]. In this study, the input data listed in Table 4.2 are normalized between 0 and 1 using Eq. (4-5).

$$x_i^n = \frac{x_i - x_{min}}{x_{max} - x_{min}} \tag{4-5}$$

Where x_i is the actual data value; x_i^n is the normalized value, while x_{max} and x_{min} are the maximum and minimum values corresponding to the actual dataset, respectively.

4.7 Model accuracy criteria

The accuracy and efficiency of the considered forecasting methods are evaluated using the following statistical indicators: Root Mean Square Error ($RMSE$), normalized Mean Square Error ($nRMSE$), Mean Absolute Error (MAE) and normalized Mean Absolute Error ($nMAE$). These metrics show how close the measured values are to the predicted PV power output produced by the proposed models. These metrics are defined in the following equations [100]:

$$RMSE = \sqrt{\frac{1}{n}\sum_{i=1}^{n}(y_i - f_i)^2} \tag{4-6}$$

$$nRMSE = \frac{\sqrt{\frac{1}{n}\sum_{i=1}^{n}(y_i - f_i)^2}}{y_{i,max}} \tag{4-7}$$

$$MAE = \sqrt{\frac{1}{n}\sum_{i=1}^{n}|y_i - f_i|} \tag{4-8}$$

$$nMAE = \frac{\sqrt{\frac{1}{n}\sum_{i=1}^{n}|y_i - f_i|}}{y_{i,max}} \tag{4-9}$$

Where n is the number of testing datasets involved in the analysis; y_i is the actual value to be estimated; $y_{i,max}$ is the maximum value in the testing dataset and f_i is the forecasted value generated by the forecasting models. $RMSE$ measures the deviation between actual values and

speculated values [101], while the MAE is the mean of absolute value of the residuals (forecasting errors).

4.8 PV power forecast simulation results

The proposed methods were applied to forecast the PV power output. In this study, the forecasting objective is to predict the PV power in a day-ahead (24-hours in 1-hour intervals). The forecasting models are described in Section 4.1.

4.8.1 Study site and dataset

The datasets used to develop the PV output forecasting models are obtained from a rooftop PV system placed on a mosque in Riyadh city, Saudi Arabia. Five PV-inverters are installed on this site, making the PV system have a capacity of 120kWp. This location is operated by both King Abdelaziz City for Science and Technology (KACST) and Saudi Electricity Company (SEC). The PV output data gathered from the unit are in 1-hour intervals for the period between June 03rd, 2017, until August 31st, 2018. The maximum power production from the system was found to be on March 25th, 2018, with a total active power production of 105.09285 kW at 11:00 A.M. The hourly data show that there are numerical readings from the PV system at night hours when no irradiance is expected. To deal with such data, all data below 100 W are omitted and set to zero implying that after the sunset and before the sun rises, there is no output power from the PV system. Figure 5.1 shows the solar map of Saudi Arabia.

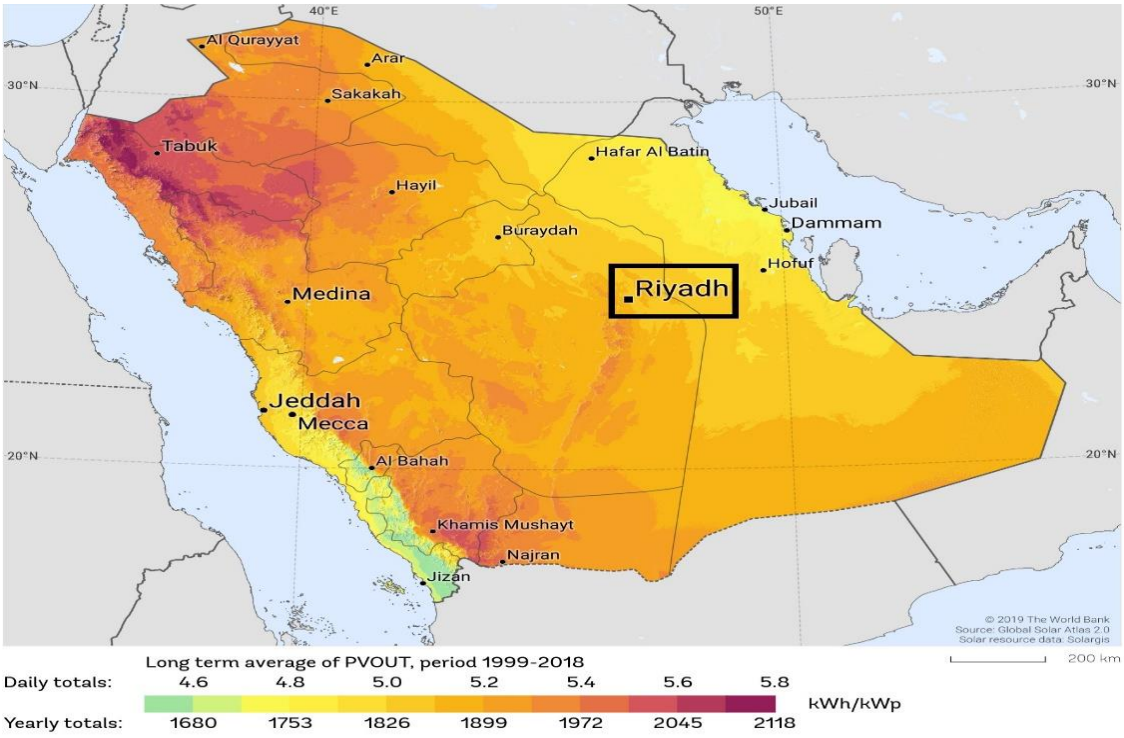

Figure 4. 5 Saudi Arabia solar map [102]

4.8.2 Solcast

Solcast is a company that provide a global solar forecasting and historical solar irradiance data [103]. It provides important data for researchers, and the historical data are available to the public freely. Different atmospheric parameters are available publicly in (https://solcast.com/). Different weather variables can be obtained in several time intervals (5-min, 30-min, 60-min). These variables include global horizontal irradiance (GHI), direct normal irradiance (DNI), diffuse horizontal irradiance (DIF), direct horizontal irradiance, air temperature, solar zenith angle, solar azimuth angle, cloud capacity (a percentage where 0% is completely clear and 100% is completely cloudy), pressure, wind speed and wind direction.

4.8.3 Results and Discussion

A multilayer perceptron (MLP) was selected for the BPNN model with the backpropagation algorithm, while the Levenberg-Marquardt method was selected as the training function. Regarding the number of layers, this study assumes three cases for BPNN:

- Case 1: $BPNN^1$ - one input layer, one hidden layer and one output layer.
- Case 2: $BPNN^2$ - one input layer, two hidden layers and one output layer.
- Case 3: $BPNN^D$ - default BPNN.

The number of neurons (nodes) in the hidden layers in Case 1 ($BPNN^1$) and Case 2 ($BPNN^2$) are obtained based on the optimal number of nodes generated by the three metaheuristic optimization algorithms, namely SSO, PSO and CSO. For Case 3 ($BPNN^D$), which represents the default BPNN, it is assumed that it has one input layer, one hidden layer and one output layer. In $BPNN^D$, the number of neurons is selected equal to the number of input features listed in Table 4.2. For example, with the input feature combination (1), which consists of one input feature, the number of nodes is one. Similarly, five nodes are set for the feature combination (12), which has five input features. The input data in the $BPNN$ were the same as those used in SVR models. Table 4.4 summarizes the $BPNN$ best models' configuration by using different algorithms.

For SVR models, the default parameters are selected based on the default values used in the LIBSVM tool. The default value of the parameter C is set to 1 for the radial basis and linear functions, while parameter γ is equal to (1/number of features). After that, the SVR and $BPNN$ models with the optimal parameters and network configurations were used to predict the PV power output. The performance of the proposed models was evaluated to determine how close the predicted data track the measured data. For this purpose, the output of the testing models was examined based on Root Mean Square Error ($RMSE$), normalized Mean Square Error ($nRMSE$), Mean Absolute Error (MAE) and normalized Mean Absolute Error ($nMAE$). Table 4.3 compares the performance indices of SVR and BPNN models.

- ***Analysis of the forecasting models***

In this section, the forecasting models are compared according to the goodness of fit tests to examine their performance to predict the PV power output from the solar system. Results of the best forecasting models, corresponding optimized parameters of SVR_{RB}, SVR_{Linear}, $BPNN^1$, and $BPNN^2$ models and the statistical errors of the forecasting models are shown in Table 4.3, Table 4.4 and Table 4.5, respectively. Figure 4.6 and Figure 4.7 display graphical representations of the goodness of fit tests of $RMSE$ (in Figure 4.6) and MAE (in Figure 4.7), in the form of heat maps. These figures aim to compare all the 255 models considered at the study site. These are four

forecasting models, SVR_{RB} , SVR_{Linear}, $BPNN^1$ and $BPNN^2$, which obtain their parameters for each of the 17 feature combinations using three optimization approaches, SSO, PSO and CSO, in addition to the three default models SVR_{RB}^{D} , SVR_{Linear}^{D} and $BPNN^D$.

Table 4. 3* Statistical errors of the best-proposed forecasting models using SSO, PSO and CSO

		$\boldsymbol{SVR_{RB}}$	$\boldsymbol{SVR_{Linear}}$	$\boldsymbol{BPNN^1}$	$\boldsymbol{BPNN^2}$
SSO	$RMSE\ (kW)$	4.47513	10.69401	4.84603	5.07423
	$nRMSE$ (%)	4.33744	10.36499	4.69693	4.91811
	$MAE\ (kW)$	2.56999	4.86217	3.17134	3.23656
	$nMAE$ (%)	2.49092	4.71258	3.07377	3.13698
PSO	$RMSE\ (kW)$	4.487	9.1334	4.973575	4.556413
	$nRMSE$ (%)	4.349	8.8524	4.820558	4.422383
	$MAE\ (kW)$	2.5728	4.8617	3.24105	2.873902
	$nMAE$ (%)	2.4936	4.7121	3.141335	2.785483
CSO	$RMSE\ (kW)$	4.4795	10.6932	5.078893	4.5692
	$nRMSE$ (%)	4.3417	10.3642	4.922636	4.4286
	$MAE\ (kW)$	2.5661	4.8637	3.305309	2.9614
	$nMAE$ (%)	2.4871	4.7141	3.203617	2.8703

* The statistical errors are reported for the best feature combination, which is number 14 in Table 4.2.

Table 4. 4* Models' parameters for SVR models and BPNN network configuration (SVR models: $\varepsilon = 0.001$)

	SSO		**PSO**		**CSO**	
	$\boldsymbol{C}$	$\boldsymbol{\gamma}$	$\boldsymbol{C}$	$\boldsymbol{\gamma}$	$\boldsymbol{C}$	$\boldsymbol{\gamma}$
$\boldsymbol{SVR_{RB}}$	9239.9	2.9384	9854	2.8795	9136.8	2.85636
$\boldsymbol{SVR_{Linear}}$	138.55385	-	0.6318801	-	4461.4607	-
	SSO		**PSO**		**CSO**	
	Hidden Layer 1	Hidden Layer 2	Hidden Layer 1	Hidden Layer 2	Hidden Layer 1	Hidden Layer 2
$\boldsymbol{BPNN^1}$	19	-	18	-	17	-
$\boldsymbol{BPNN^2}$	15	7	19	9	19	6

* The SVR parameters and BPNN network configurations are reported for the best feature combination, which is number 14 in Table 4.2.

Table 4. 5 Best proposed forecasting models vs. default models based on SVR and ANN

	$\boldsymbol{CSO-SVR_{RB}}$	$\boldsymbol{SVR_{RB}^{D}}$	$\boldsymbol{PSO-SVR_{linear}}$	$\boldsymbol{SVR_{linear}^{D}}$	$\boldsymbol{SSO-BPNN^1}$	$\boldsymbol{CSO-BPNN^2}$	$\boldsymbol{BPNN^D}$
$\boldsymbol{RMSE}\ (\boldsymbol{kW})$	4.4795	8.9733	9.1334	9.9392	4.8460	4.5692	5.2289
$\boldsymbol{nRMSE}$ (%)	4.3417	8.6972	8.8524	9.6334	4.6969	4.4286	5.0681
$\boldsymbol{MAE}\ (\boldsymbol{kW})$	2.5661	5.2218	4.8617	4.9399	3.1713	2.9614	3.2892
$\boldsymbol{nMAE}$ (%)	2.4871	5.0612	4.7121	4.7879	3.0738	2.8703	3.1879

- ***Hybrid forecasting models vs. default forecasting models***

Table 4.3, Table 4.5, Figure 4.6 and Figure 4.7 show that: (i) Overall, the proposed forecasting models optimized by SSO, PSO and CSO outperform the default forecasting models in predicting the PV power output with low $RMSE$ and MAE values. Regarding models fitting accuracy with the SVR_{RB} models, the proposed models with the optimized hyperparameters show improvements compared to default models, where $RMSE$ improved between 12.001% to 50.079 % and MAE improved between 1.80291% to 59.8847%. Similarly, the prediction models with the $BPNN^1$and $BPNN^2$ using the proposed models with the optimal network configurations have better performance with 1.883%-46.964% and 2.0576%-47.007% improvement in the $RMSE$ and MAE values, respectively, compared to the $BPNN^D$ models.

Using SVR_{RB} models with different optimization algorithms and different feature schemes, Figure 4.6 shows that $RMSE$ values are ≤ 23.12 kW, while $RMSE$ values with the default models are ≤ 28.24 kW. With the feature combination (12), for example, the value of $RMSE$ with the best model ($CSO - SVR_{RB}$) is 4.968 kW and MAE is 2.756 kW. On the other hand, the SVR_{RB}^D gives an $RMSE$ value of 9.206 kW and MAE of 5.269 kW. Similarly, the reduction in the error metrics values has been attained with the proposed $BPNN$ models. For instance, considering the feature combination (9), the value of $nRMSE$ using $BPNN^1$and $BPNN^2$ are 5.767% and 5.804%, respectively, while the $BPNN^D$ generates an error value of 7.25%. Nevertheless, the degree of improvement is somewhat low in the SVR_{Linear} models with the optimized parameters as a comparison to the SVR_{Linear}^D models. This can be attributed to the value of the optimized hyperparameter, C, that has close values to the default ones.

In addition, Figure 4.6, Figure 4.7 and Table 4.5 show that the BPNN with the default models have better performance than the default models of the SVR with the radial base and the linear functions. This is due to the default parameters that are selected for the SVR models. Hence, to obtain the best forecasting performance of the SVR models, the associated parameters should be selected appropriately. The BPNN default models, on the other hand, show good performance as a comparison to the proposed models. For instance, the best model using $SSO - BPNN^1$ and $CSO - BPNN^2$give $RMSE$ values of 4.8460 kW and 4.5692 kW, respectively, while the $BPNN^D$model generates an error value of 5.2289 kW.

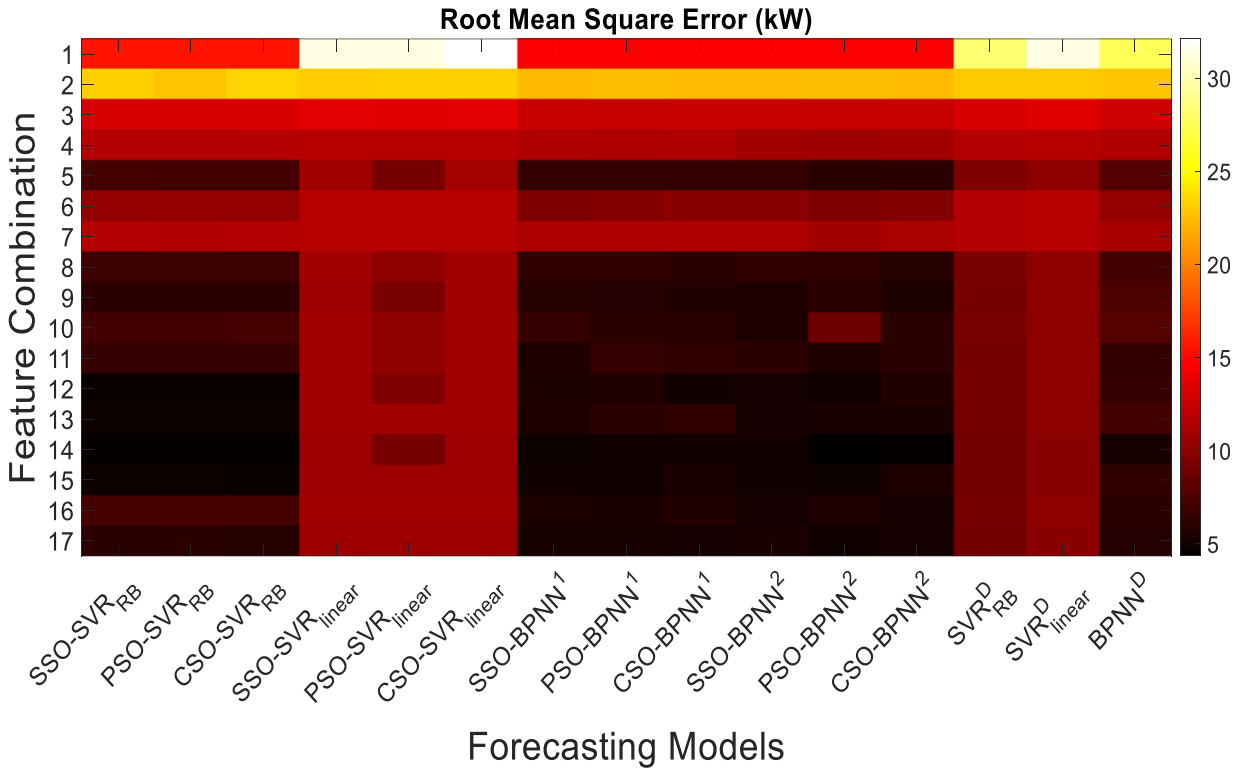

Figure 4. 6 $RMSE$ values of the study models with the considered feature combinations

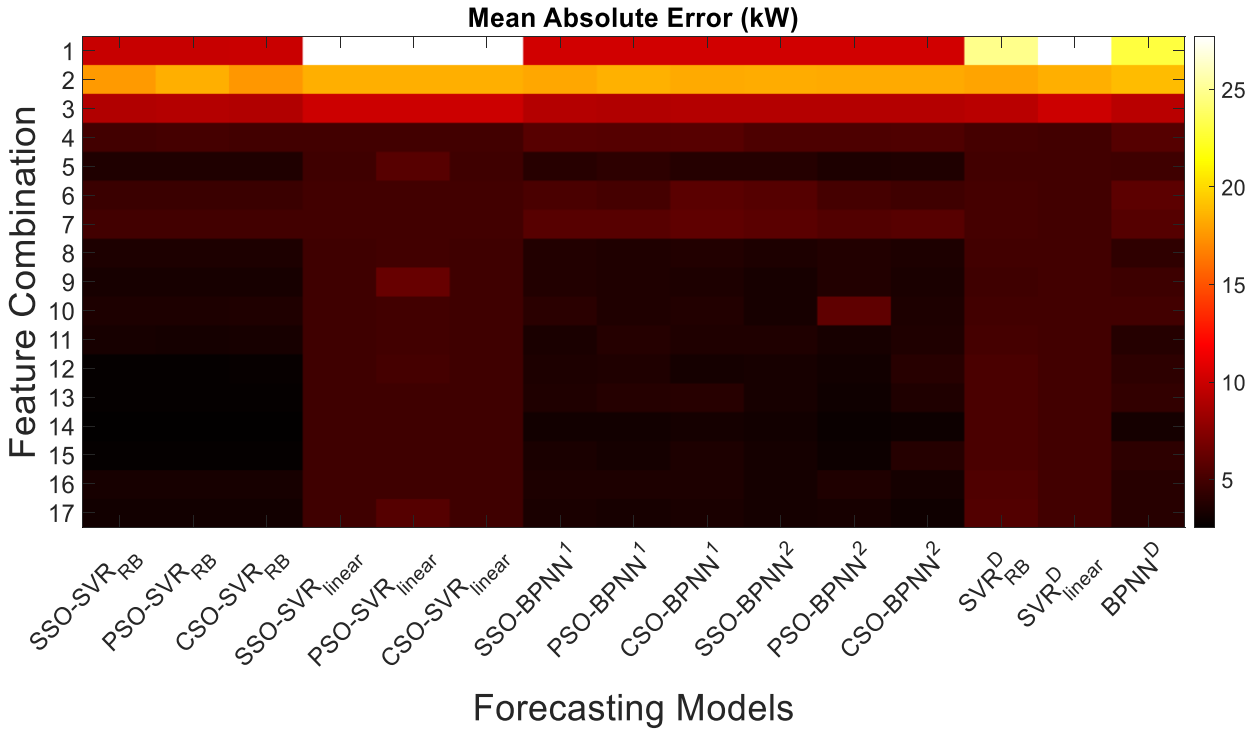

Figure 4. 7 MAE values of the study models with the considered feature combinations

- ***Performance analysis using proposed models***

(ii) From Table 4.3, Figure 4.6 and Figure 4.7, and by comparing different forecasting models using the proposed models, SVR_{RB} models can be considered the best prediction model to best estimate the PV power generation in the study site. SVR_{RB} has better error metrics values than SVR_{Linear}, $BPNN^1$ and $BPNN^2$ with low $RMSE$ and MAE values. For instance, $PSO - SVR_{RB}$ models are better than $PSO - SVR_{Linear}$, $PSO - BPNN^1$ and $PSO - BPNN^2$ for all the considered feature combinations. This result is also found with others optimization methods. $BPNN$ models, on the other hand, have a better performance than the SVR models with the linear function and promising performance compared to the RB models. As a comparison between the proposed $BPNN$ models, overall $BPNN^2$ models have led to better prediction capability than the $BPNN^1$. $PSO - BPNN^2$ with the feature combination (11), for example, gave an $nRMSE$ of 3.251% and $nMAE$ values of 3.251%, while $PSO - BPNN^1$ resulted in error values of 6.297% and 3.819%, respectively. This implies that using more than one hidden layer with optimized node numbers leads to higher forecasting accuracy than a single hidden layer.

Furthermore, as a comparison between the performance of the optimization algorithms, more than one optimization approach has the same accuracy and performance in estimating the parameters of the forecasting models. PSO and SSO methods have a similar or negligible difference in terms of estimating parameter values. Nevertheless, the three optimization algorithms show different performance in obtaining the C parameter of the linear function. Also, the linear models performed the worst due to their limited capacity in dealing with nonlinearity in input data.

- ***Best feature combination***

(iii) From Table 4.3, Figure 4.6 and Figure 4.7, and by comparing different feature combinations, we can see that the best forecasting model is attained with the feature combination (14). This combination includes the month in the year, the day of the month, the hour in the day, air temperature (℃), forecasted global horizontal irradiance, GHI ($W\mathrm{h}/m^2$) and PV power output at the same hour on the previous day (kW). Results show that the best forecasting results for all considered models are obtained using this feature combination. Regarding other feature combinations, using only forecasted global horizontal irradiance, feature combination (3), PV

power output at the same hour on the previous day (kW), feature combination (4), or a mix between them could lead to satisfactory forecasting results. GHI provided good accuracy results due to its significant impact on the PV system production, while the lag power observation is due to the nature of solar radiation in the study site. In Riyadh city, the nature of the weather is less variable, and there are two seasons in the year, summer and winter. Therefore, the power output of the previous day may influence the production of the next day.

4.9 Conclusion

In this study, SVR with the radial basis and the linear kernel functions and BPNN models were examined to predict the PV output power of the rooftop PV unit placed on a mosque located in Riyadh city, Saudi Arabia. The penalty factor (C) and kernel parameter (γ) of the SVR models with the radial and linear functions as well as the number of hidden nodes of the artificial neural network were optimized using three optimization algorithms. These algorithms are Social Spider Optimization (SSO), Particle Swarm Optimization (PSO) and Cuckoo Search Optimization (CSO). Different combinations of the input variables are used in this study, including month, day, hour, global solar radiation, direct normal radiation, temperature, wind speed, wind direction, pressure and PV power generation of the previous day. The efficiency of all selected models was evaluated based on Root Mean Square Error ($RMSE$), normalized Mean Square Error ($nRMSE$), Mean Absolute Error (MAE) and normalized Mean Absolute Error ($nMAE$). Results indicate that the proposed models with the optimized hyperparameter of the SVR with radial basis outperform other models in forecasting PV power output at the study site. The three optimization algorithms almost have the same performance, resulting in high accuracy models that prove their ability to select SVR parameters and BPNN configuration. Furthermore, the proposed BPNN models exhibit a good performance that can be compared with the SVR radial basis models. On the other hand, the SVR based on the linear function showed limited forecasting performance due to its limited capability in capturing the nonlinearity in the input dataset. Finally, the framework that is proposed in this study can be used to forecast the PV power output in other countries.

Chapter 5: Voltage Regulation in the Medium Voltage Distribution Network

In this Chapter, the proposed voltage management strategy is evaluated. The proposed approach is a coordination algorithm consisting of two controlling stages aiming to eliminate the voltage deviation in distribution networks connected with solar PV and wind. The first stage is accomplished by optimal planning of BESS through network-level optimization. The second stage is accomplished by controlling the reactive power of the smart solar PV inverters. The flowchart of the proposed study is depicted in Figure 5.1.

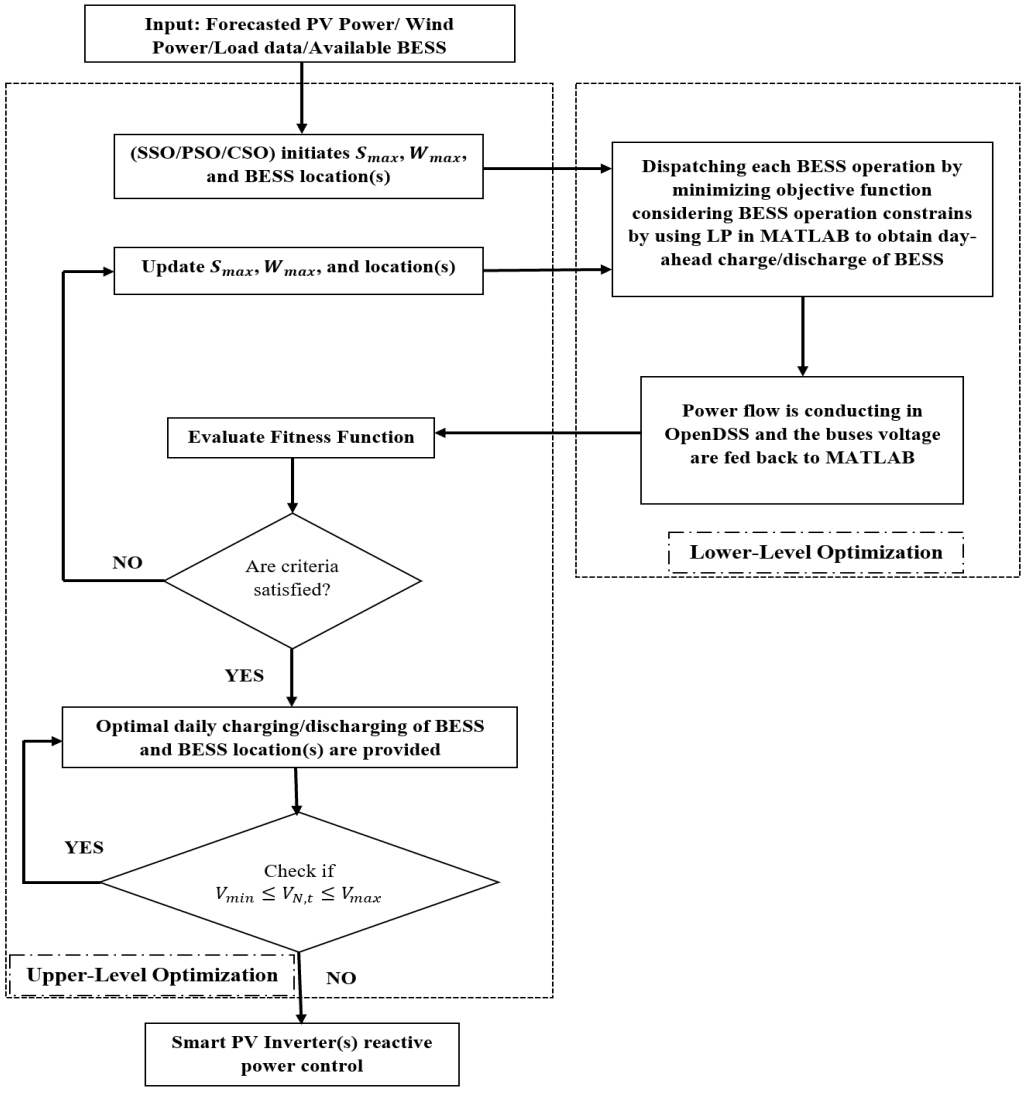

Figure 5. 1 Framework of the voltage management strategy

The algorithm is based on the bi-level optimization method. The full description of the proposed algorithm is described in Chapter 3. In this study, three metaheuristic optimization algorithms are used to represent upper-level optimization, while linear programming (LP) is used in lower-level optimization. The metaheuristic optimization algorithms are Social Spider Optimization (SSO), Particle Swarm Optimization (PSO) and Cuckoo Search Optimization (CSO). The main reason for using these algorithms is to examine their performance and their searching capability in solving the voltage problem in the electrical distribution system. The performance experiment and convergence experiment results (shown in Subsections 5.1.7-5.2.6) indicate that PSO provides better performance than other algorithms.

5.1 High level of PV integration at the feeder's end

The proposed methodology has been applied to the modified IEEE-34 Test Feeder shown in Figure 5.2. The feeder is a radial distribution feeder, and the substation transformer steps down the voltage from 69 kV to 24.9 kV. The transformer at the substation of this test feeder has a rated kVA of 2500, and the tap setting of the secondary part of the transformer is set to 1.03 p.u to make the overvoltage and undervoltage problem more vivid. In this study, there are two locations at which the two PV systems are placed. The two PV systems have sizes of 500 kWp and are located at bus 840 and bus 848. The PV systems sizing is selected to make the impact on voltage level more pronounced. Typically, the acceptable voltage limits in the distribution system should be within $\pm 5\%$ of the nominal voltage. In this study, the maximum and minimum allowed voltage is $V_{max} = 1.05$ and $V_{min} = 0.95$, respectively. In addition, this network is unbalanced; therefore, the study voltage is calculated based on the mean of the three-phase voltages. Furthermore, in this case study, the voltage regulators (VR) are assumed to operate at fixed tap positions in the distribution system, and the simulations are conducted in the absence of VR interference. The power flow simulations are performed utilizing OpenDSS, while the numerical calculations and the daily BESS dispatch are obtained by LP using MATLAB.

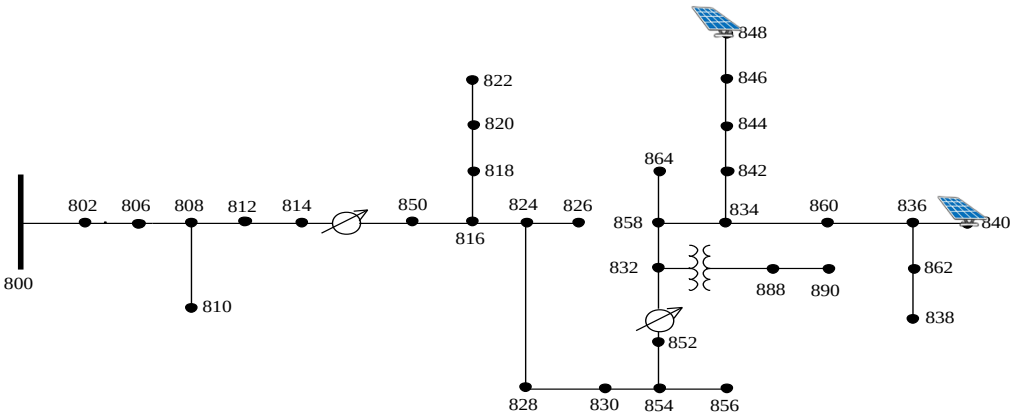

Figure 5. 2 The modified IEEE 34-bus test radial distribution system

5.1.1 Study dataset

The daily load is based on real-time data obtained from a substation transformer that feeds primarily residential and commercial loads in Riyadh city, Saudi Arabia. The spot and distributed loads are calculated based on scaled base values provided by the feeder configuration. The PV output power profile is scaled up from real-time data collected from the 120 kW PV system placed on a rooftop of a mosque in Riyadh. The time resolution of the load and the PV power is 1-hour, and their profile on 07-Nov- 2017 is shown in Figure 5.3. The smart PV inverters are assumed to operate at a unity power factor. The batteries are deployed at the same bus where the PV systems are connected and have the specifications listed in Table 5.1. This study also assumes that the utility has ownership of the PV systems and BESS. Therefore, these equipments are fully controlled by the utility to control the voltage in the distribution system.

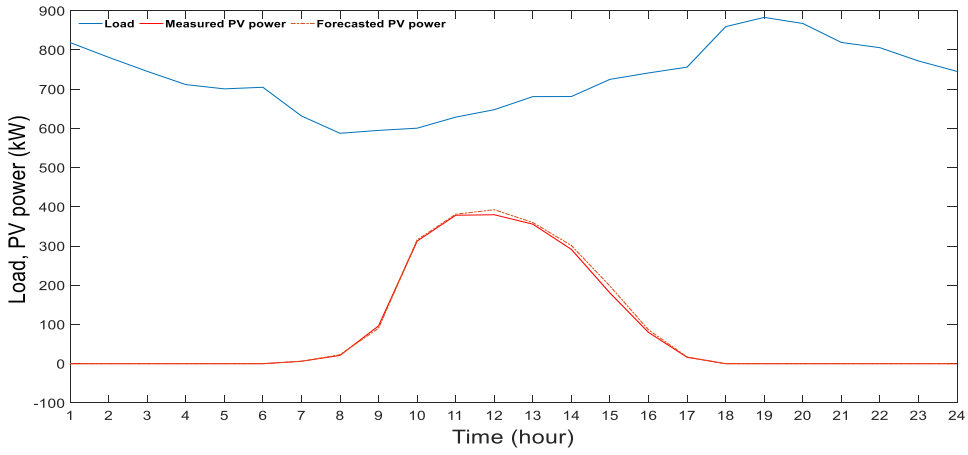

Figure 5. 3 Net daily load and PV power output profiles (07-Nov- 2017)

Table 5. 1 The specification of the battery energy storage system

Specification		Powerpack
AC voltage	AC	380-480 3-phase
Usable Energy	W_{max}	228 kWh
Maximum charging/discharging power	S_{max}	130 kW
Minimum charging/discharging power	S_{min}	0 kW
Maximum State of Charge	SOC_{max}	100%
Minimum State of Charge	SOC_{min}	10%
Round trip efficiency	η	90%

The primary goal of the voltage management strategy is to manage the overvoltage problem in the distribution system. The voltage deviations usually occur when the feeder's load is low and the power generated from the PV systems is high. The distribution feeder in this study is located in Riyadh city, where the net load is low in the winter season compared to the high summer load. Therefore, in this research, the selection of the days on which the overvoltage happens is based on the mean of voltage deviation index, $\overline{VD}$, and it is defined as follows:

$$\overline{VD} = mean(V_i - V_{ref}) \quad \forall \ V_i > V_{ref} \tag{6-1}$$

Where v_i is the voltage magnitude at the PV systems buses, and V_{ref} is the voltage reference which the voltage should be below. $\overline{VD}$ values reflect the degree of voltage deviation on each day. Therefore, to evaluate the effectiveness of the proposed voltage management strategy using BESS and reactive power from the smart PV inverters, the selected days are taken when the voltage is the worst.

5.1.2 Case study simulation results with two PV systems

This section exhibits the impact of the proposed voltage management strategy to control the voltage in the distribution system. In this study, the load demand is assumed to be constant or based on forecasted values with high accuracy; thus, the load forecast error is not considered. On the other hand, the predicted values of the PV system are considered. The forecasted PV power outputs are based on the best forecasting model discussed in Chapter 4. The distribution system is simulated based on the actual and forecasted values of the PV power output to optimize the BESS

operations and PV inverter reactive power, taking into consideration the objective functions of the upper and the lower-level optimizations. These objectives are for adhering to the BESS specifications, the reactive power capability of the smart PV inverters and the voltage objective function. The objective functions are described in Chapter 3.

5.1.3 Real-time simulation

The optimal BESS scheduling obtained from the proposed method, and the exact values of the load and PV generation and the forecasted PV generation for the next 24-hours are utilized to simulate the distribution system for different simulation days. In this study, the smart PV inverters simulation is conducted in real-time based on the measured conditions using the Volt-VAR mode, shown in Figure 3.3. In order to evaluate the effectiveness of the proposed method, five simulation cases were conducted according to different controlling methods and PV generations. These cases are described as follows:

Case 1: $BESS$: In this case, the optimal BESS scheduling is done based on the assumption that the measured PV power generation is used. The charging and discharging rates are considered to show their effect on the distribution system voltage profile. This case represents the *reference case 1*.

Case 2: $BESS - VAR$: In this case, the optimal BESS scheduling is done based on the assumption that the measured PV power generation is used, while the smart PV inverters are simulated in real-time using the Volt-VAR mode. In this case, the charging and discharging rates are considered to show their effect on the distribution system voltage profile. The Volt-VAR mode that has the curve displayed in Figure 3.3 is used. This case represents the *reference case 2*.

Case 3: VAR: In this case, the optimal reactive power from the smart PV inverters is simulated based on the assumption that the measured PV power generation is used. The reactive power values are considered to show their effect on the distribution system voltage profile. The Volt-VAR mode that has the curve displayed in Figure 3.3 is used.

Case 4: $BESS^f$: In this case, the optimal BESS scheduling is done based on the assumption that the forecasted PV power generation is used. That is, the BESS operations are scheduled for the day ahead, 24-hours in 1-hour intervals. In this case, the charging and discharging rates are considered to show their effect on the distribution system voltage profile.

Case 5: $BESS^f - VAR$: In this case, the optimal BESS scheduling is done based on the assumption that the forecasted PV power generation is used, while the smart PV inverters are simulated in real-time using the Volt-VAR mode. That is, the BESS operations are scheduled for the day ahead, 24-hours in 1-hour intervals. In this case, the charging and discharging rates are considered to show their effect on the distribution system voltage profile. The Volt-VAR mode that has the curve displayed in Figure 3.3 is used.

5.1.4 Real-time simulation for VAR and $BESS$

Simulation results of Cases 1, 2, 3, 4, and 5 on 07-Nov-2017 are displayed in Figures 5.4-5.9, respectively. As has been mentioned previously, the simulation horizon of the BESS and the smart PV inverters' reactive power is hourly for the next day. The reactive power absorbed by the smart PV inverters at bus 841 and bus 848 is shown in subplots 1 in Figures 5.6-5.9. The optimized charging and discharging scheduling rates of the BESS placed at Bus 841 and Bus 848 based on actual and forecasted PV generation are shown in subplot 2 in Figures 5.6-5.9, respectively. The BESS's states of charges ($SCOb$) for all different cases are shown in subplot 3 in Figures 5.6-5.9, respectively.

Real-time simulations of the distribution system for the actual and forecasted PV generation have been performed on 07-Nov-17. The voltage profiles at PV buses with different controlling methods for cases 1, 2, 3, 4, and 5 are shown in Figures 5.4-5.5, respectively. In this simulation case study, the excess power from the solar PV reverses the power flow causing the overvoltage problem in the distribution network. From Figures 5.4-5.5, it can be seen that the VAR case and $BESS$ alone were not able to manage the overvoltage problem. This is due to limited capacity of the smart PV inverters and BESS. Reactive power absorption by the smart PV inverters at bus 848 and bus 840 occurs in the midday as a response to the local overvoltage. Also, the BESS starts collectively storing energy from the PV systems in conjunction with the high PV generation to minimize the voltage deviation from the acceptable upper limit. Despite the improvement in the $\overline{VD}$ employing $BESS$ and VAR, as listed in Table 5.2, the voltages deviate most of the time. However, on some days, VAR and $BESS$ alone can maintain the voltage at the desired ranges, as shown in Table 5.2. As a comparison between Case 1, when the measured PV generations are considered, and the Case 4, when the forecasted PV generations are considered, we can notice that BESS operation with the

forecasted values results in a good performance in minimizing the voltage deviation in the distribution system.

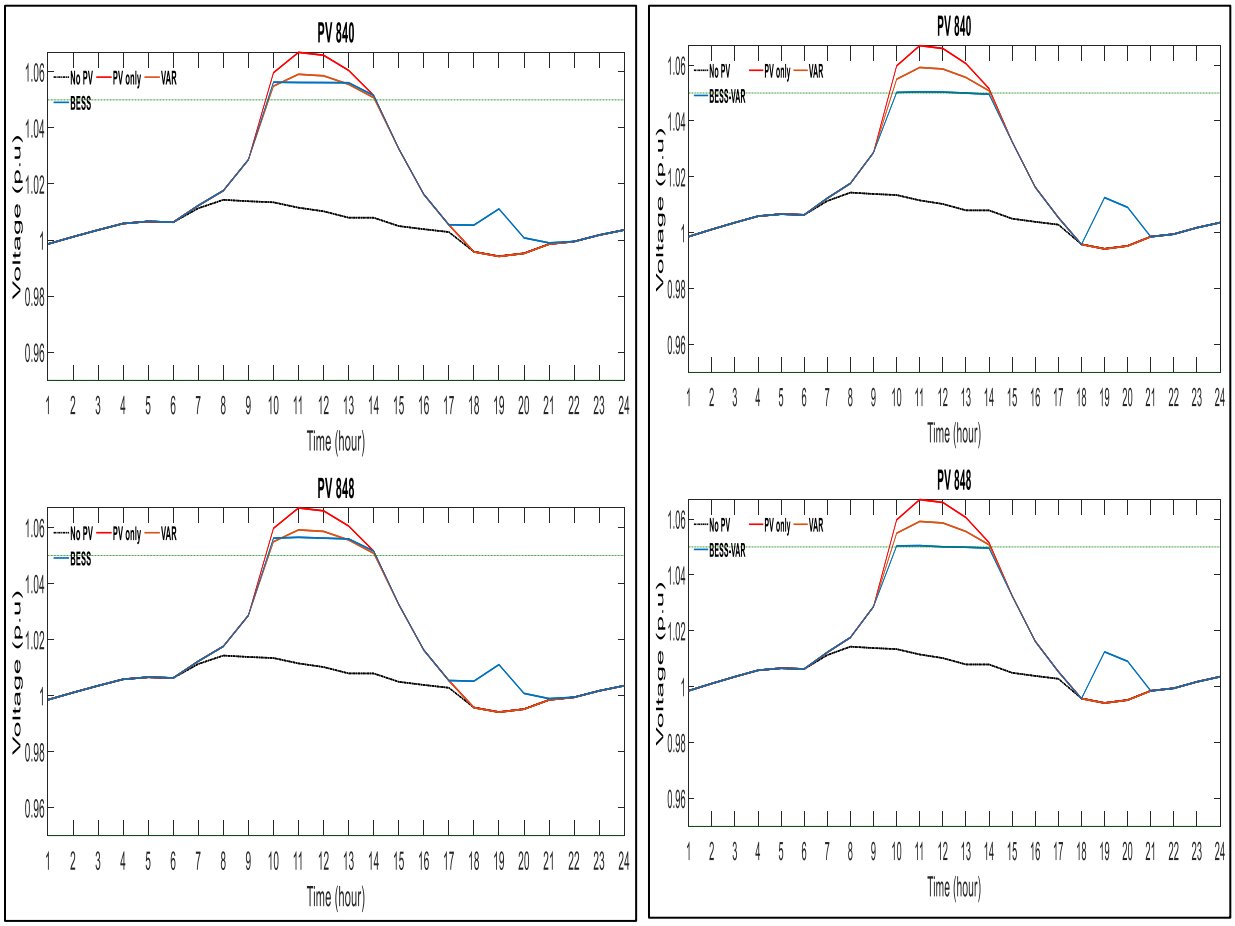

Figure 5. 4 Voltage profile at bus 840 and bus 848 - (Left) $BESS$, (Right) $BESS - VAR$ (PV: Measured)

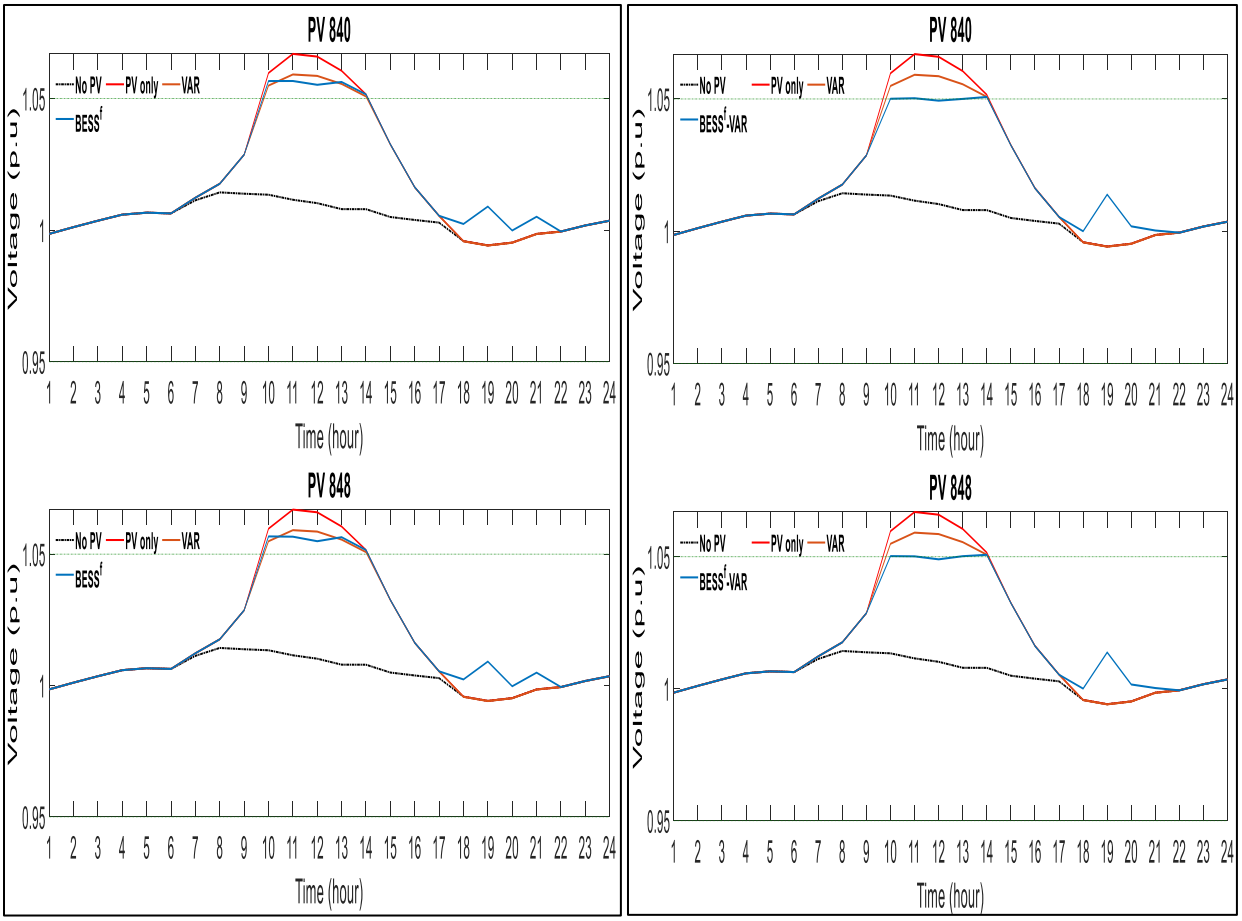

Figure 5. 5 Voltage profile at bus 840 and bus 848- (Left) $BESS^f$, (Right) $BESS^f - VAR$ (PV: Forecasted)

5.1.5 Real-time simulation for $BESS - VAR$

On the other hand, the effectiveness of the proposed model to improve the overvoltage in the distribution system appears when BESS and smart PV inverters are coordinated (Case 2 and Case 5). As shown in Figure 5.4 and Figure 5.5, the overvoltage problem has been significantly minimized and has shown noticeable improvement. The BESS's limited capability of reducing the overvoltage incidents has been supported by the reactive power capability of the smart PV inverters. BESS stored the excess power from the PV system, which causes the voltage problem with respect to the battery operation capacity. The voltage is minimized, but it is still violated. Hence, the reactive power absorption provided by the smart PV inverter assists in further reducing in voltage levels. As a comparison between Case 2 and Case 5, we can see that Case 5 has a close performance to the reference case (Case 2) as the voltage comes within the desired upper and lower limits.

5.1.6 BESS operation with two PV systems

The optimal battery charging and discharging of each battery storage is exhibited in Figures 5.6-5.9. These figures show that all batteries start charging as a response to the excess power from the PV systems (from 10 AM to 13 PM) instead of being injected into the grid and causing reverse power and overvoltage. At peak demand (from 18 PM to 21 PM), the batteries supply the stored energy back to the grid, which accounts for the increase in voltage at this period, as shown in Figures 5.4-5.5. Also, the batteries' energy at the beginning of the day has the same energy at the end of the day, adhering to the BESS operational constraints.

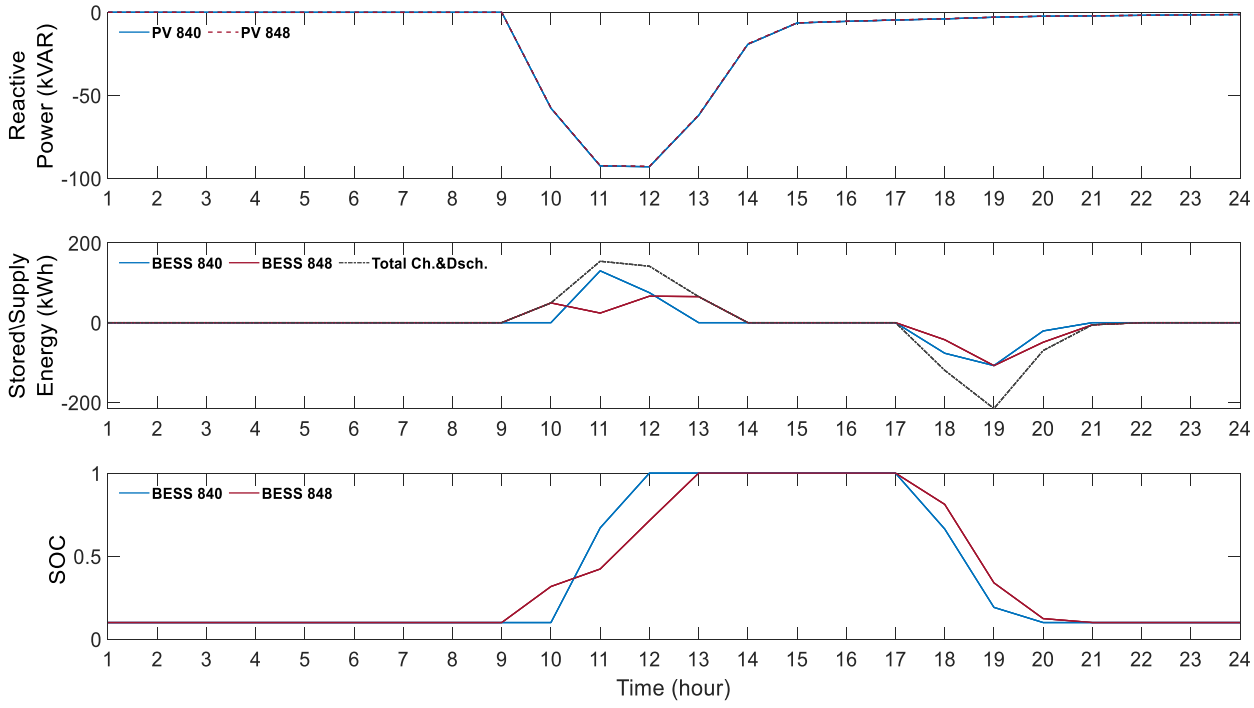

Figure 5. 6 (Top) Reactive power; (Middle) stored and supplied energy; and (Bottom) SOC of the BESS for Case 1 and Case 3 (PV: Measured).

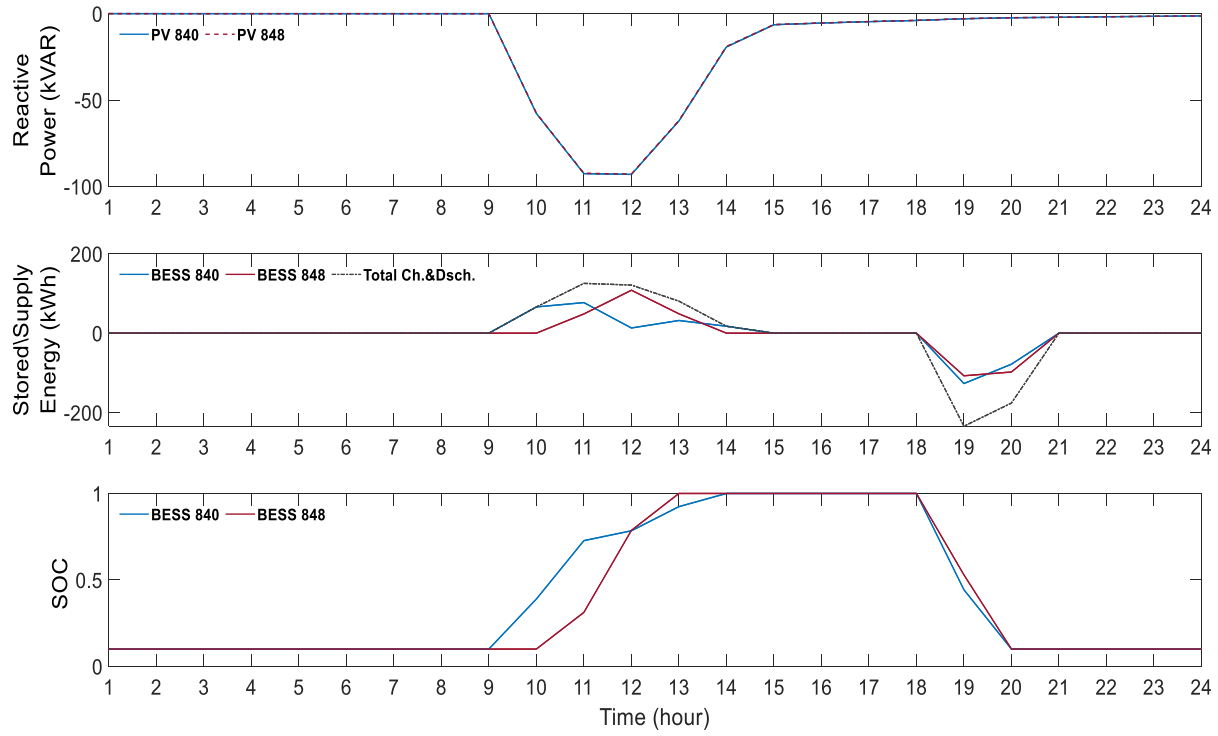

Figure 5. 7 (Top) Reactive power; (Middle) stored and supplied energy; and (Bottom) SOC of the BESS Case 2 (PV: Measured).

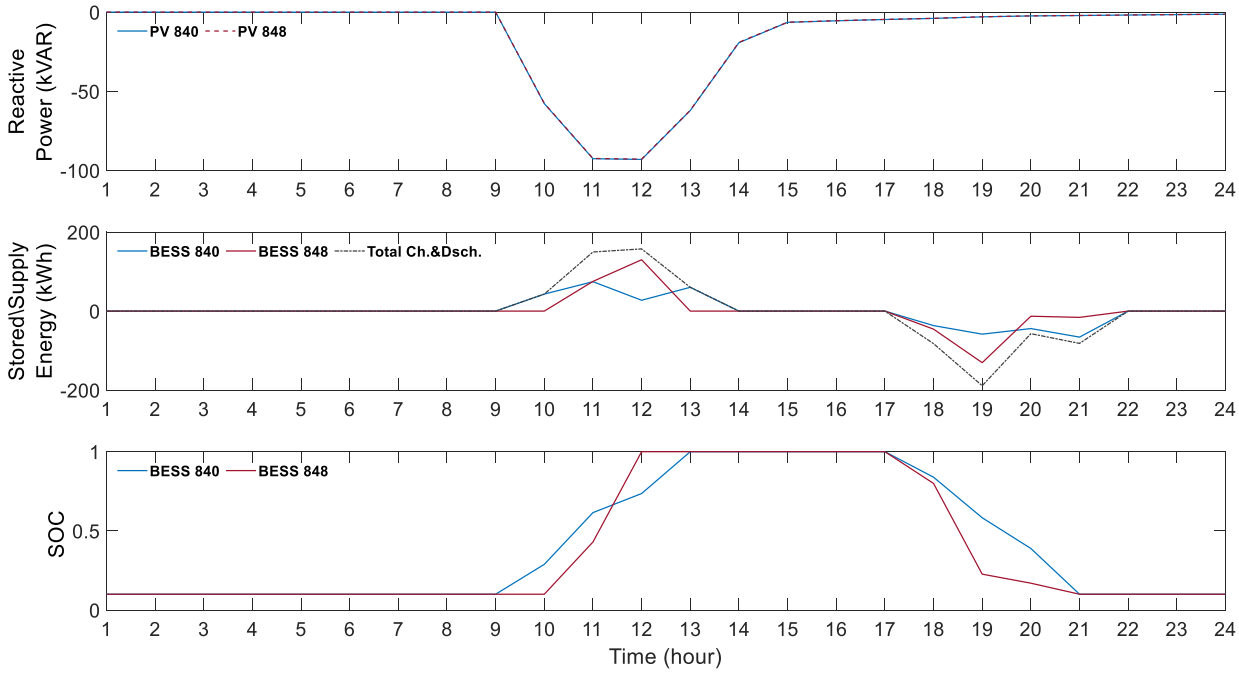

Figure 5. 8 (Top) Reactive power; (Middle) stored and supplied energy; and (Bottom) SOC of the BESS for Case 4 (PV: Forecasted).

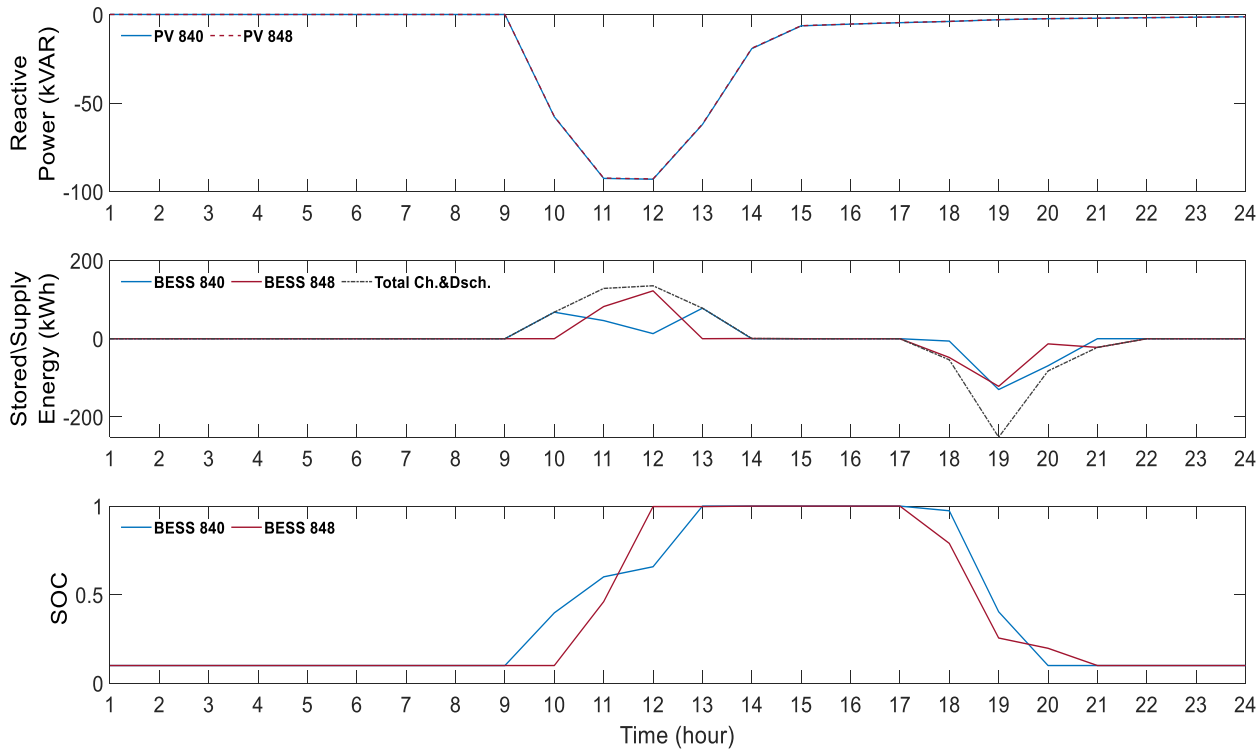

Figure 5. 9 (Top) Reactive power; (Middle) stored and supplied energy; and (Bottom) SOC of the BESS for Case 5 (PV: Forecasted)

5.1.7 Average voltage deviation ($\overline{VD}$)

Average voltage deviation ($\overline{VD}$) results, see Eq. (6-1), for the selected days that satisfy the predefined criteria are listed in Table 5.2 by using different cases and different metaheuristic optimization algorithms, namely SSO, PSO and CSO. Table 5.2 contains the $\overline{VD}$ results based on the real-time simulation using measured and forecasted values of the PV power.

Table 5. 2 Average voltage deviation ($\overline{VD}$) generated by SSO, PSO and CSO on different simulation days

	Day	*Only PV*	*VAR*	*BESS*	*BESS − VAR*	*BESS^f*	*BESS^f − VAR*
SSO	7-Nov-17	0.228133	0.120966	0.111953	0.004885	0.112317	0.007892
	6-Dec-17	0.268555	0.142868	0.151411	0.025425	0.152159	0.026239
	18-Jan-18	0.047982	0.025582	0	0	0.005078	0
	31-Jan-18	0.076453	0.038093	0	0	0.015794	0
	8-Feb-18	0.033301	0.017649	0	0	0	0
	2-Mar-18	0.335016	0.181497	0.218965	0.064097	0.219461	0.073657
	19-Mar-18	0.106487	0.058178	0	0	0.002237	0

	Day	*Only PV*	*VAR*	*BESS*	*BESS − VAR*	$BESS^f$	$BESS^f - VAR$
PSO	7-Nov-17	0.228133	0.120966	0.110159	0.004016	0.110156	0.004714
	6-Dec-17	0.268555	0.142868	0.150942	0.02423	0.150938	0.024215
	18-Jan-18	0.047982	0.025582	0	0	0.004652	0
	31-Jan-18	0.076453	0.038093	0	0	0.011689	0
	8-Feb-18	0.033301	0.017649	0	0	0	0
	2-Mar-18	0.335016	0.181497	0.218169	0.063666	0.218028	0.06732
	19-Mar-18	0.106487	0.058178	0	0	0.001322	0
	Day	***Only PV***	***VAR***	***BESS***	***BESS − VAR***	$BESS^f$	$BESS^f - VAR$
CSO	7-Nov-17	0.228133	0.120966	0.110162	0.003844	0.110161	0.00544
	6-Dec-17	0.268555	0.142868	0.150945	0.024228	0.150938	0.024229
	18-Jan-18	0.047982	0.025582	0	0	0.00495	0
	31-Jan-18	0.076453	0.038093	0	0	0.011206	0
	8-Feb-18	0.033301	0.017649	0	0	0	0
	2-Mar-18	0.335016	0.181497	0.218212	0.063674	0.218036	0.067577
	19-Mar-18	0.106487	0.058178	0	0	0.001487	0

As a comparison between the metaheuristic optimization algorithms in reducing the $\overline{VD}$, all three algorithms have led to a reduction either by $BESS$ or $BESS - VAR$ based on the measured or forecasted PV power generation (the two cases in which the study algorithm is used). PSO and CSO methods have a similar or negligible difference in terms of the $\overline{VD}$ values. Yet, PSO has the best velocity in attaining these values, as shown in Subsection 5.1.8. For example, considering (06-Dec-17) with $BESS - VAR$ based on the forecasted PV values, the $\overline{VD}$ using SSO was found to be 0.026239, while using PSO and CSO led to values of 0.024215 and 0.024229, respectively. Similar results were found on all simulation days. In this respect, PSO presents the most accurate and fastest approach to minimize the $\overline{VD}$ and solve the voltage deviation problem in the distribution system in question. The CSO and SSO could be considered as the following best algorithms, respectively.

Overall, and as it can be seen from Table 5.2, VAR and $BESS$ have provided a reduction in the $\overline{VD}$ when considering the measured and forecasted PV power values. This is due to the capability of the reactive power of the smart PV inverters and BESS in minimizing the voltage deviation. However, $BESS$ alone has better $\overline{VD}$ values compared to the VAR case. On some simulation days, the optimal operation of $BESS$ resulted in managing the overvoltage at the PV buses. For example, on (31-Jan-2018) and by using PSO, $BESS^f$ reduced the $\overline{VD}$ to 0.011689 compared to 0.038093

by using VAR. If we compare the $\overline{VD}$ based on the measured and forecasted values of PV power using $BESS$, Table 5.2 shows that on some days $BESS^f$ with the forecasted values could not control the overvoltage, which it is supposed to accomplish based on the measured PV generation ($BESS$). This is due to the PV forecasting error that influenced the batteries' operations. On the other hand, $BESS - VAR$, which is the proposed technique in this study, minimizes the $\overline{VD}$ significantly through the optimal scheduling of the BESS and the reactive power provided by the smart PV inverter, as shown in Figure 5.10. This figure shows the level of reduction in the $\overline{VD}$ by all considered cases based on the measured and forecasted PV power using PSO. The results of $BESS^f - VAR$ using forecasted values are close to $BESS - VAR$ based on measured PV values. This can be attributed to the size of the batteries and the increase in the smart PV inverters' capacities. Therefore, increasing the size of the battery storage or the capacity of the PV inverter can assist in minimizing the PV forecasting error.

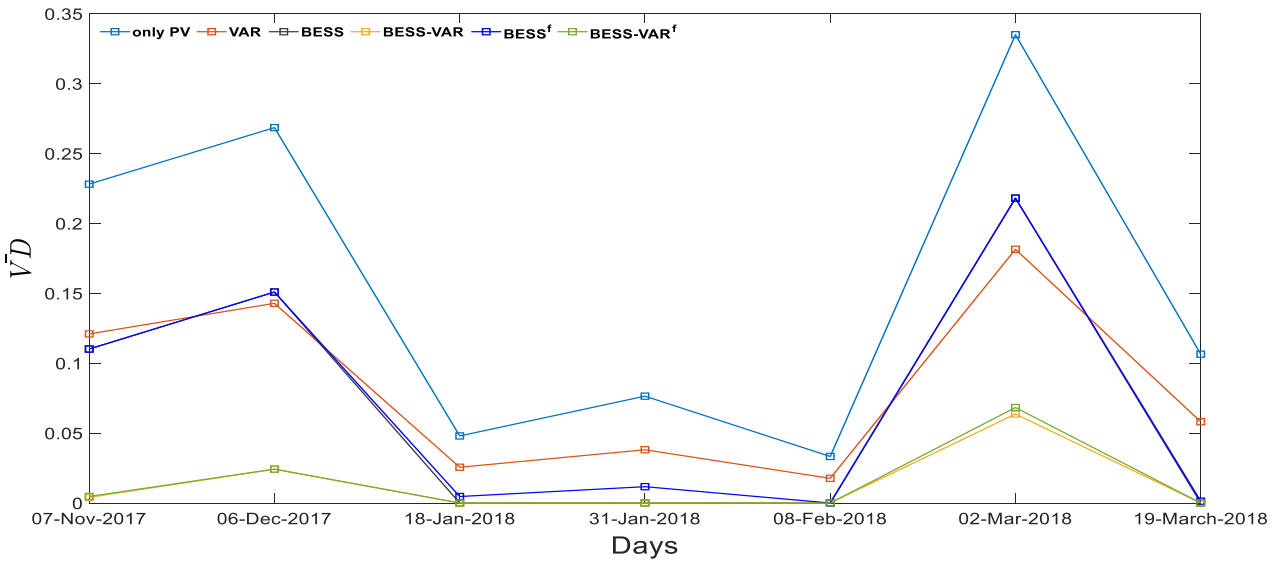

Figure 5. 10 Levels of reduction in $\overline{VD}$ by all considered cases using PSO

5.1.8 Performance comparison between metaheuristic optimization algorithms

To compare the performance of the three metaheuristic optimization algorithms, namely Social Spider Optimization (SSO), Particle Swarm Optimization (PSO) and Cuckoo Search Optimization (CSO), these algorithms are used to minimize the objective function, Eq. (3-2) in Chapter 3, that minimizes the voltage deviation. The results of every algorithm consider the output of 5 runs with

a stopping criterion of 250 iterations. The choice of the final fitness values considers the median values of those 5 executions. Accordingly, the performance experiment has been conducted, and the comparison considers the following five performance measure indexes: Best Fitness Value (BFV), Worst Fitness Value (WFV), Average of Best Fitness Values (ABFV), Median of Best Fitness Values (MBFV) and Standard Deviation of Best Fitness Values (SDBV). The simulations are run on a setup with Intel Core i7-8550 CPU @ 1.80GHz.

Table 5. 3 Results of five indexes for minimizing the objective function of the upper-level optimization for Case 5

		BFV	**WFV**	**ABFV**	**MBFV**	**SDFV**
07-Nov-2017	**SSO**	1.65E-05	5.13E-05	2.23E-05	2.03E-05	6.03E-06
	PSO	1.56E-05	**5.26E-05**	1.61E-05	1.56E-05	3.48E-06
	CSO	**1.48E-05**	**2.26E-05**	**1.54E-05**	**1.49E-05**	**1.16E-06**
06-Dec-2017	**SSO**	2.68E-05	6.32E-05	3.41E-05	3.36E-05	7.19E-06
	PSO	**2.48E-05**	**6.71E-05**	**2.53E-05**	**2.48E-05**	**3.07E-06**
	CSO	2.48E-05	7.01E-05	2.93E-05	2.48E-05	1.01E-05
18-Jan-2018	**SSO**	1.36E-08	1.40E-06	1.84E-07	7.88E-08	3.19E-07
	PSO	**4.45E-14**	**1.39E-06**	**5.04E-08**	**8.08E-14**	**1.69E-07**
	CSO	4.58E-14	1.53E-06	7.93E-08	2.27E-10	2.10E-07
31-Jan-2018	**SSO**	3.76E-08	1.45E-05	1.13E-06	7.42E-07	1.55E-06
	PSO	**9.47E-19**	**1.07E-05**	**1.97E-07**	**3.46E-13**	**1.06E-06**
	CSO	2.26E-10	1.30E-05	1.12E-06	2.91E-08	3.09E-06
08-Feb-2018	**SSO**	1.10E-08	4.93E-06	2.42E-07	9.71E-08	6.75E-07
	PSO	**1.55E-16**	**3.45E-06**	**3.91E-08**	**8.77E-15**	**2.77E-07**
	CSO	1.45E-11	3.74E-06	4.26E-08	1.46E-11	2.77E-07
02-Mar-2018	**SSO**	5.56E-05	8.27E-05	6.29E-05	6.38E-05	6.30E-06
	PSO	**5.34E-05**	7.96E-05	**5.39E-05**	**5.35E-05**	**1.76E-06**
	CSO	**5.34E-05**	**7.08E-05**	5.47E-05	**5.35E-05**	3.32E-06
19-Mar-2018	**SSO**	8.00E-07	2.89E-05	2.67E-06	2.22E-06	2.95E-06
	PSO	**1.74E-07**	3.04E-05	**7.22E-07**	**1.74E-07**	**2.45E-06**
	CSO	6.64E-07	**1.43E-05**	2.58E-06	1.72E-06	2.73E-06

Table 5.3 shows the results of the five indexes by minimizing the objective function, Eq. (3-2), using SSO, PSO and CSO. The results are for the Case 5 on the selected simulation days. Overall, results show that PSO performance is better than SSO and CSO with the best BFV and lowest WFV, ABFV, MBFV and SDBV. This is because of the stochastic factor of the PSO algorithm that permits the balance between exploitation and exploration [85]. Similar results were found on all simulation days with different simulation cases.

The evaluation based on the final fitness values cannot always provide an insight into the capability of an optimization algorithm. Hence, the convergence experiment has been conducted to analyze how fast an algorithm reaches optimal values. Figures 5.11-5.12 display the convergence rate plots of SSO, PSO and CSO with the simulations of Case 4 and Case 5 on different selected days. From these figures, it can be noticed that PSO converges faster than SSO and CSO and can reach optimal values in ≤ 50 iterations.

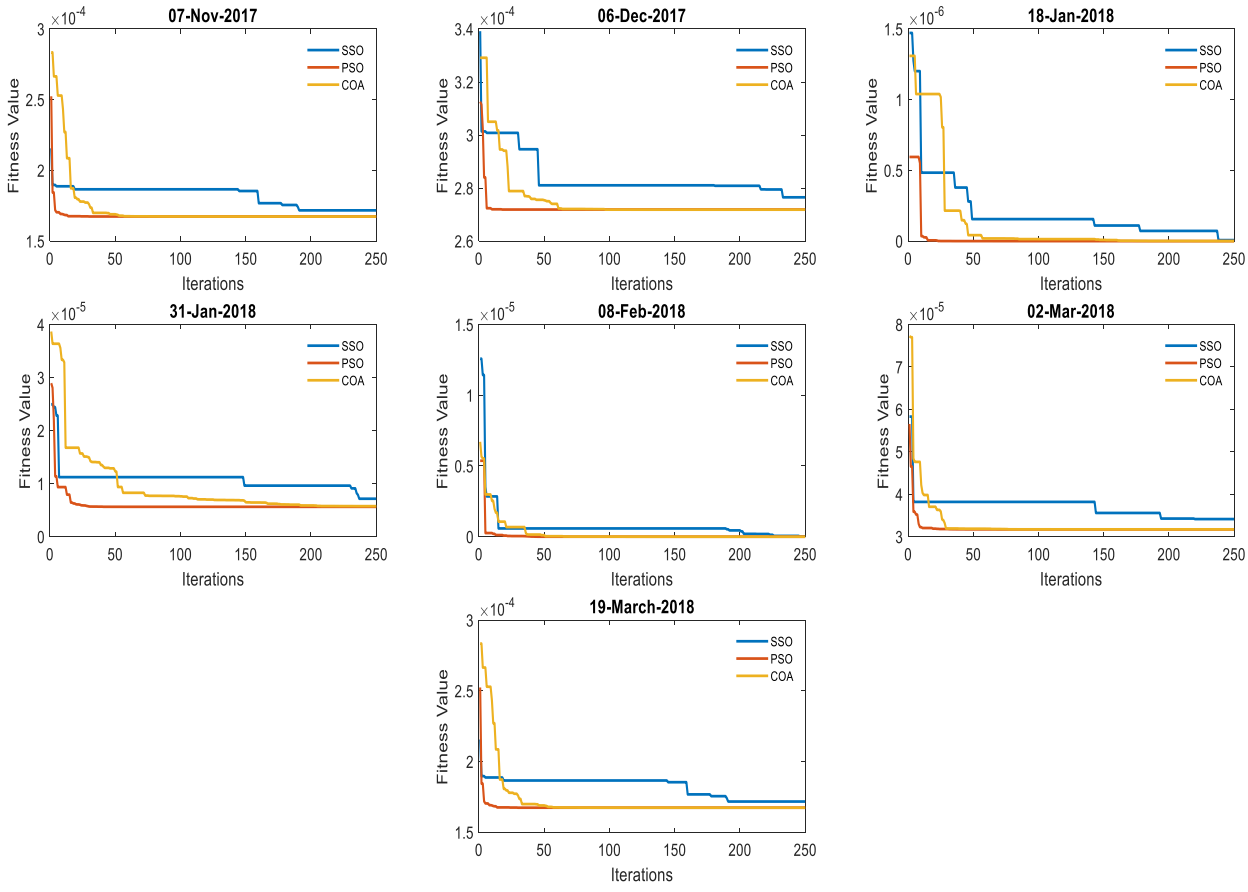

Figure 5. 11 The convergence plots of SSO, PSO and CSO for minimizing the objective function of the upper-level optimization for Case 4

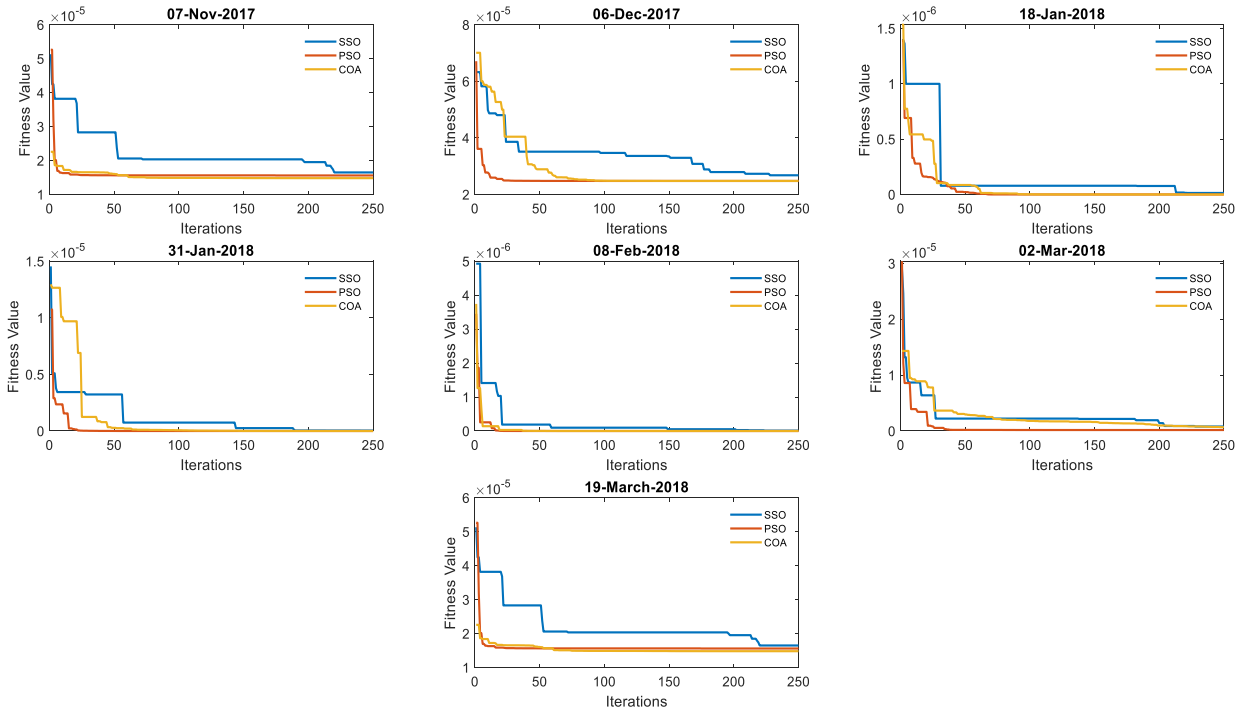

Figure 5. 12 The convergence plots of SSO, PSO and CSO for minimizing the objective function of the upper-level optimization for Case 5

5.2 High level of PV and wind integrations at the feeder's end

In this case study, a wind turbine has been placed at the location of a PV system, see Figure 5.13. The primary reason for this study is to show the effect of the hybridization of energy generated from the PV system and wind turbine on the distribution system's voltage profile compared to installing PV systems alone. In addition, this case study is to examine the potential impact of such hybridization on BESS operations. Besides the 500 kWp PV system located at Bus 848, a 500 kWp wind turbine is placed at bus 840 to represent a high wind penetration. The PV system and wind turbine sizing are selected to make the impact on voltage level more pronounced. Typically, acceptable voltage limits in the distribution systems should be within $\pm 5\%$ of the nominal voltage. In this study, the maximum and minimum allowed voltage is $V_{max} = 1.05$ and $V_{min} = 0.95$, respectively. In addition, this network is unbalanced; therefore, the study voltage is calculated based on the mean of the three-phase voltages. Similar to the case study in Section 5.1, the voltage regulators (VR) are assumed to operate at fixed tap positions in the distribution system, and the simulations are conducted in the absence of VR interference. The power flow simulations are

performed utilizing OpenDSS, while the numerical calculations and the daily BESS dispatch are obtained by LP using MATLAB.

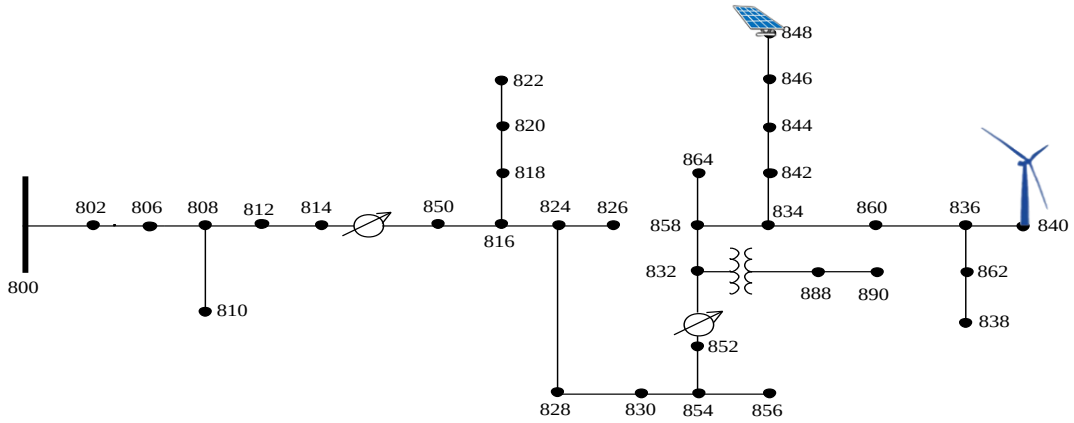

Figure 5. 13 The modified IEEE 34-bus test radial distribution system

- **Study dataset**

Similar to the previous study, the daily load is based on real-time data obtained from a substation transformer that feeds primarily residential and commercial loads in Riyadh city. The PV output power profile is scaled up from real-time data collected from the 120kWp PV system placed on a rooftop of a mosque in Riyadh.

5.2.1 Wind data

The wind speed data utilized to conduct this study are obtained from King Abdulla City for Atomic and Renewable Energy, K.A.CARE. In this study, hourly wind speed data are collected at 40m above ground level are used. The wind data are obtained from the same station that has the geographic feature in Table 5.4. The wind map of Saudi Arabia is depicted in Figure 5.14. In order to convert wind speed to wind power, a wind turbine (Vestas V39) with a rated power of 500 kW is used. The turbine specification is listed in Table 5.5, and the associated power curve is shown in Figure 5.15 [104].

Table 5. 4 Selected site geographic features

Latitude ($\boldsymbol{North}$)	24.90689
Longitude ($\boldsymbol{East}$)	46.39721
Elevation ($\boldsymbol{meter}$)	764.0

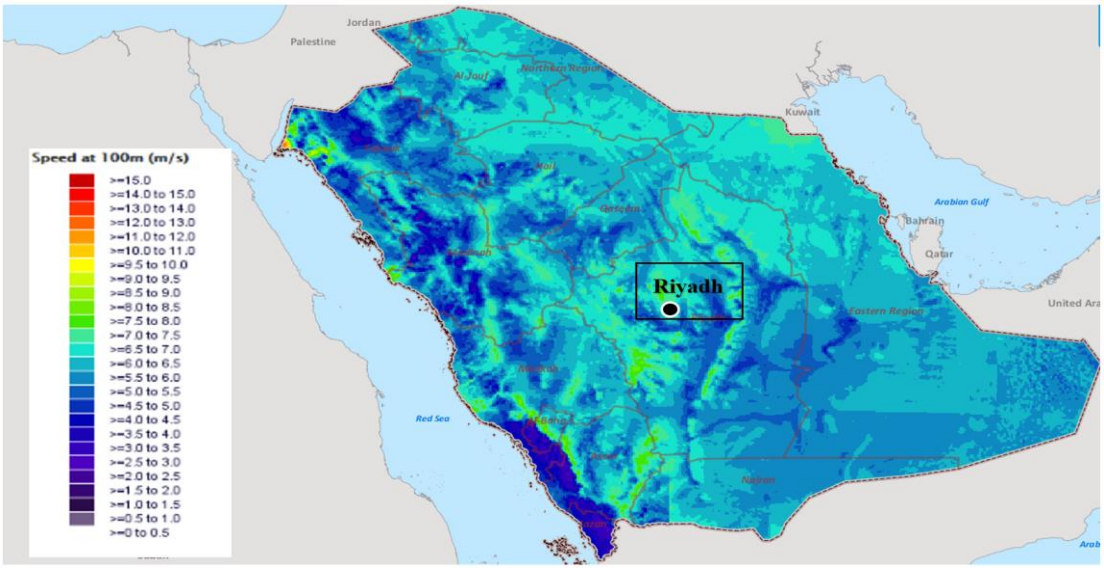

Figure 5. 14 Saudi Arabia wind map [105]

Table 5. 5 The specification of Wind turbine, Vestas V39

Voltage $(\boldsymbol{V})$	690
Hub Height $(\boldsymbol{meter})$	40
Rated Power $(\boldsymbol{kW})$	500
Rotor Diameter $(\boldsymbol{meter})$	39
Cut-in Speed $(\boldsymbol{m/s})$	4.5
Rated Speed $(\boldsymbol{m/s})$	15.5
Cut-off Speed $(\boldsymbol{m/s})$	25

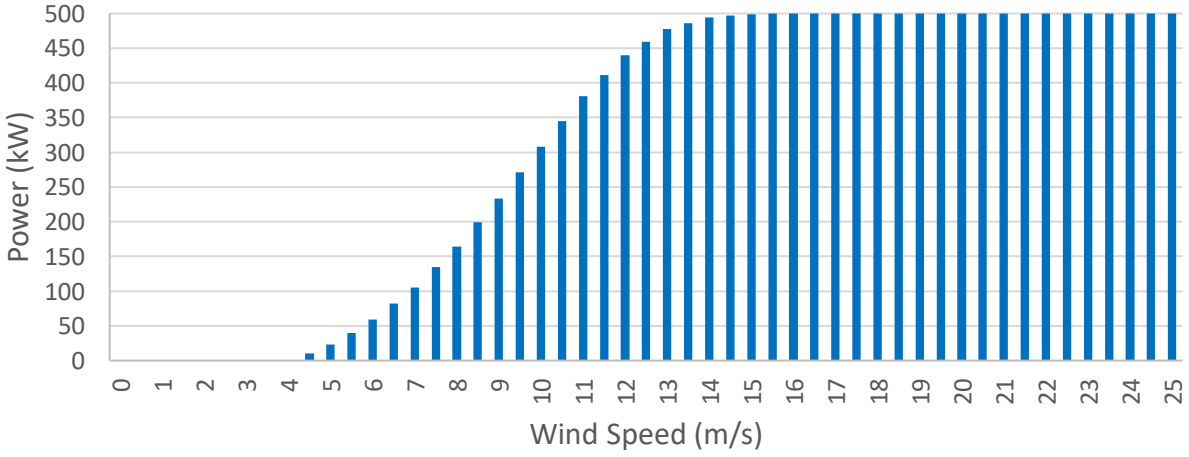

Figure 5. 15 Power curve of the wind turbine, Vestas V39 [104]

The time resolution of the load, PV power and wind power is in1-hour intervals, and their profiles on 07-Mar-2018 are shown in Figure 5.16. The inverters are set at unity power factors. The batteries are deployed at the same bus where the PV system and wind turbine are connected and have the specifications listed in Table 5.5. This study also assumes that the utility has ownership of the PV system, wind turbine and BESS. Therefore, these components are fully controlled by the utility to control the voltage in the distribution systems. In this study, the load and wind power are assumed to be constant or based on forecasted values with high accuracy; thus, the load and wind forecast errors are not considered in this study. On the other hand, the predicted values of the PV system are based on the best forecasting model discussed in Chapter 4.

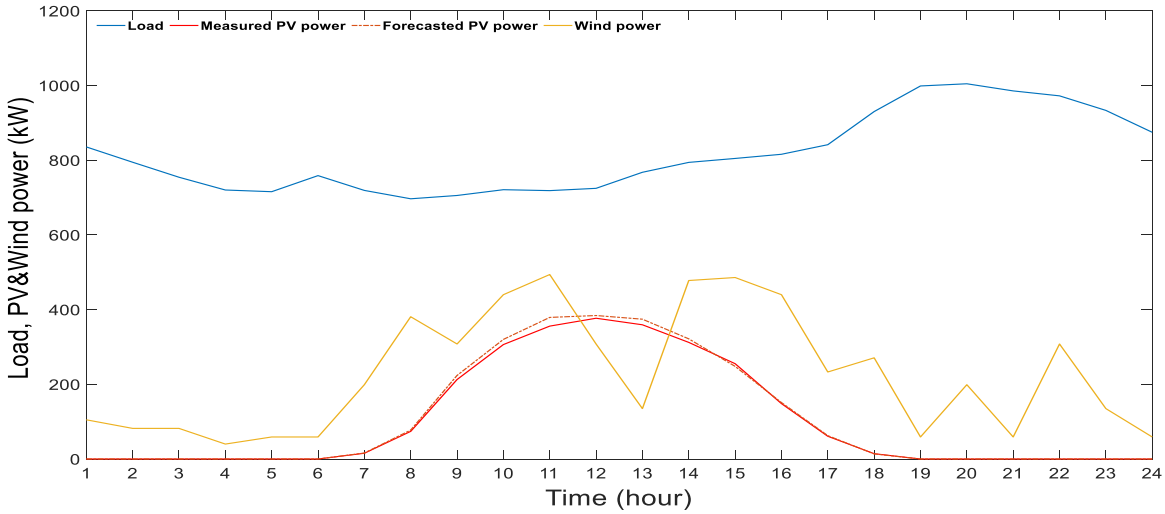

Figure 5. 16 Net daily load and PV power output profiles (07-Mar-2018)

As mentioned in the case study in Section 5.1, the voltage deviations usually occur when the feeder load is low and the power generated from the PV system and wind is high. The distribution feeder in this study is in Riyadh city, in Saudi Arabia, where the net load is low in the winter season compared to the high summer load. Also, the performance of the proposed voltage management approach is evaluated according to the index in Eq. (6-1). Furthermore, Case 1, Case 2, Case 3, Case 4, and Case 5, defined in Subsection 5.1.2, are also considered in this case study.

5.2.2 Real-time simulation for VAR and $BESS$

The excess power from the solar PV and wind turbine reverses the power flow causing overvoltage in the distribution network. Figures 5.17-5.18 show the voltage profiles at bus 840 and bus 848 on 07-Mar-2018 for Case 1, Case 2, Case 3, Case 4, and Case 5. These figures indicate that the

voltages deviate and exceed the predefined upper limit ($V_{max} = 1.05$) during the peak generation hours from the PV and wind. From Figures 5.17-5.18, we can see that the VAR case and the $BESS$ case could not prevent the overvoltage problem. This is due to the limited capacity of the smart PV inverter and BESS. Reactive power absorption by the smart PV inverter at bus 848 occurs in the midday as a response to the local voltage, as appears in subplots 1 in Figures 5.19-5.22, respectively. Also, the BESS starts storing energy associated with high PV and wind to minimize the voltage deviation, as appears in subplots 2 in Figures 5.19-5.22, respectively. Despite the improvement in the $\overline{VD}$ by these cases, as listed in Table 5.6, the voltages violate the upper limit. However, on some days, VAR and $BESS$ alone can maintain the voltage at the desired ranges, as shown in Table 5.6. As a comparison between $BESS$, when the measured PV generations are considered, and $BESS^f$, when the forecasted PV generations are considered, we can notice that $BESS$ alone in both cases has a good performance in minimizing the voltage deviation in the distribution system.

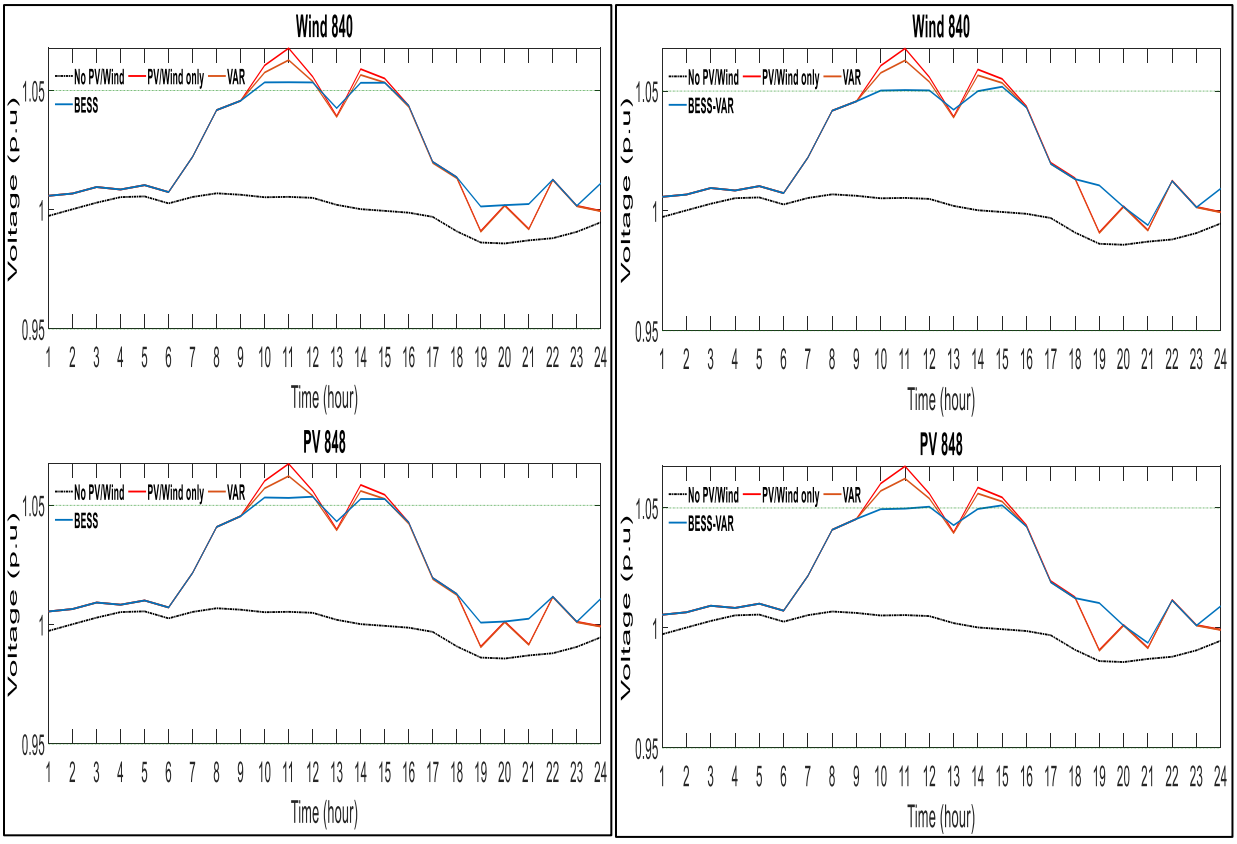

Figure 5. 17 Voltage profile at bus 840 and bus 848 - (Left) $BESS$, (Right) $BESS - VAR$ (PV: Measured)

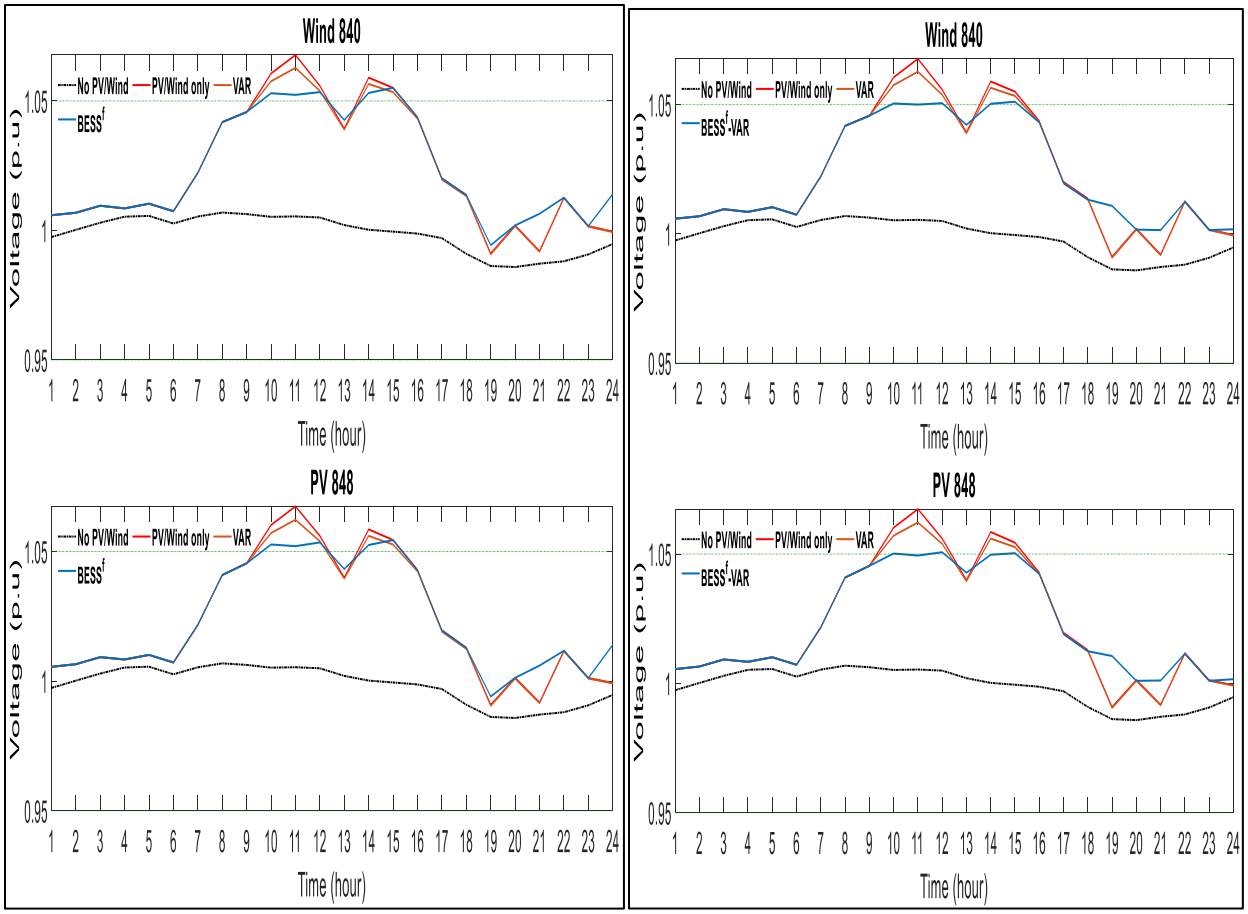

Figure 5. 18 Voltage profile at bus 840 and bus 848- (Left) $BESS^f$, (Right) $BESS^f - VAR$ (PV: Forecasted)

In addition, it can be noticed that the voltage profile of the PV system (Bus 848) has been shaped by the voltage at the wind turbine bus (Bus 840), see Figures 5.17-5.18. This is due to the high power coming from the wind turbine on this particular day compares to the power generated from the PV system. Hence, the charging and discharging rates are collectively operated between the two BESS placed in the network to clear the overvoltage, as shown in the subplots.

5.2.3 Real-time simulation for $BESS - VAR$

On the other hand, the effectiveness of the proposed model to improve the overvoltage in the distribution system appears when BESS and PV inverters are coordinated. As shown in Figures 5.17-5.18, the overvoltage profiles have been significantly minimized and have shown noticeable improvement. As a comparison between Case 2 and Case 5, we can see that Case 5 has a close

performance as the reference case (Case 2) as the voltage comes within the desired upper and lower limits.

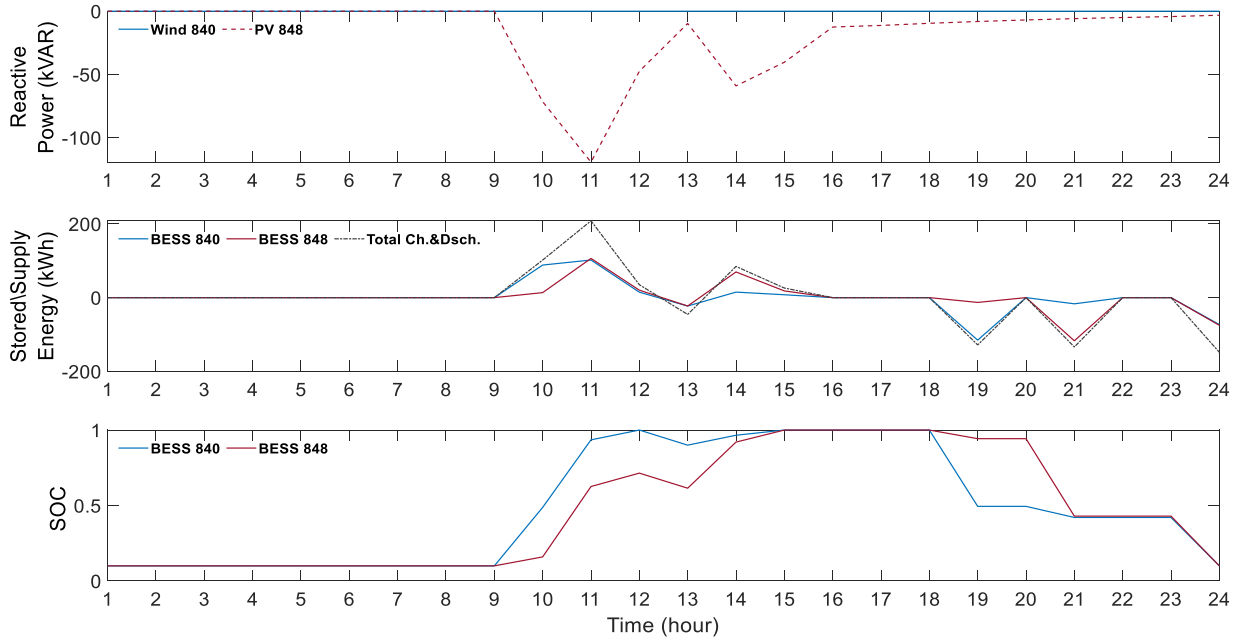

Figure 5. 19 (Top) Reactive power; (Middle) stored and supplied energy; and (Bottom) SOC of the BESS for Case 1 and Case 3 (PV: Measured)

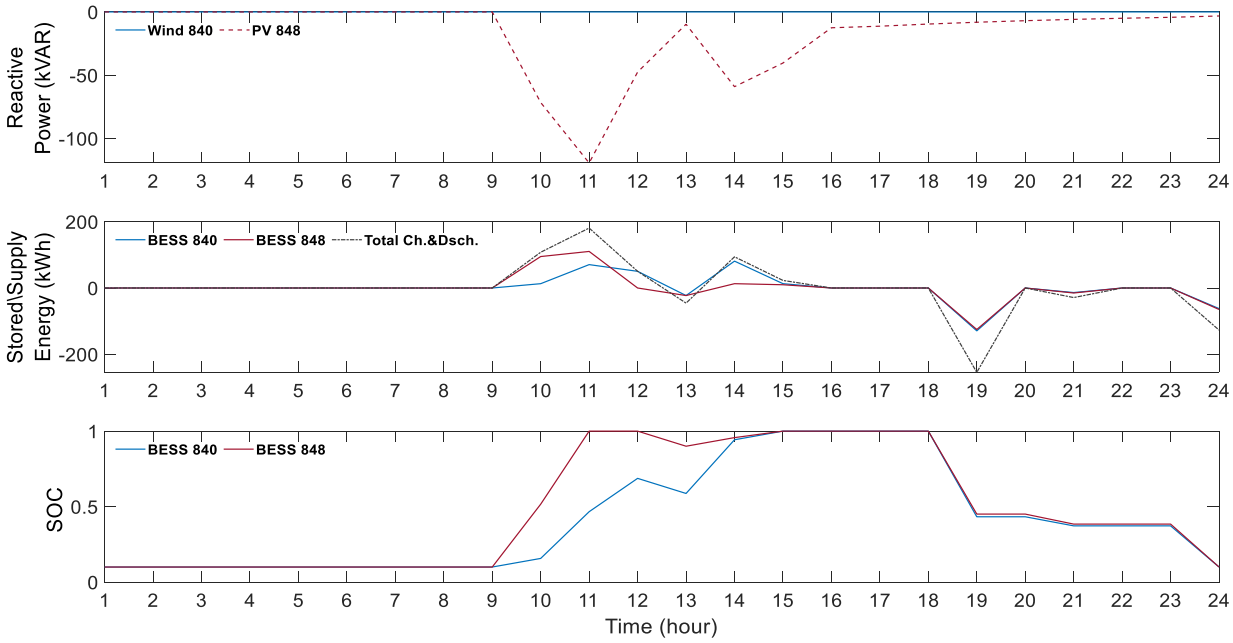

Figure 5. 20 (Top) Reactive power; (Middle) stored and supplied energy; and (Bottom) SOC of the BESS for Case 2 (PV: Measured)

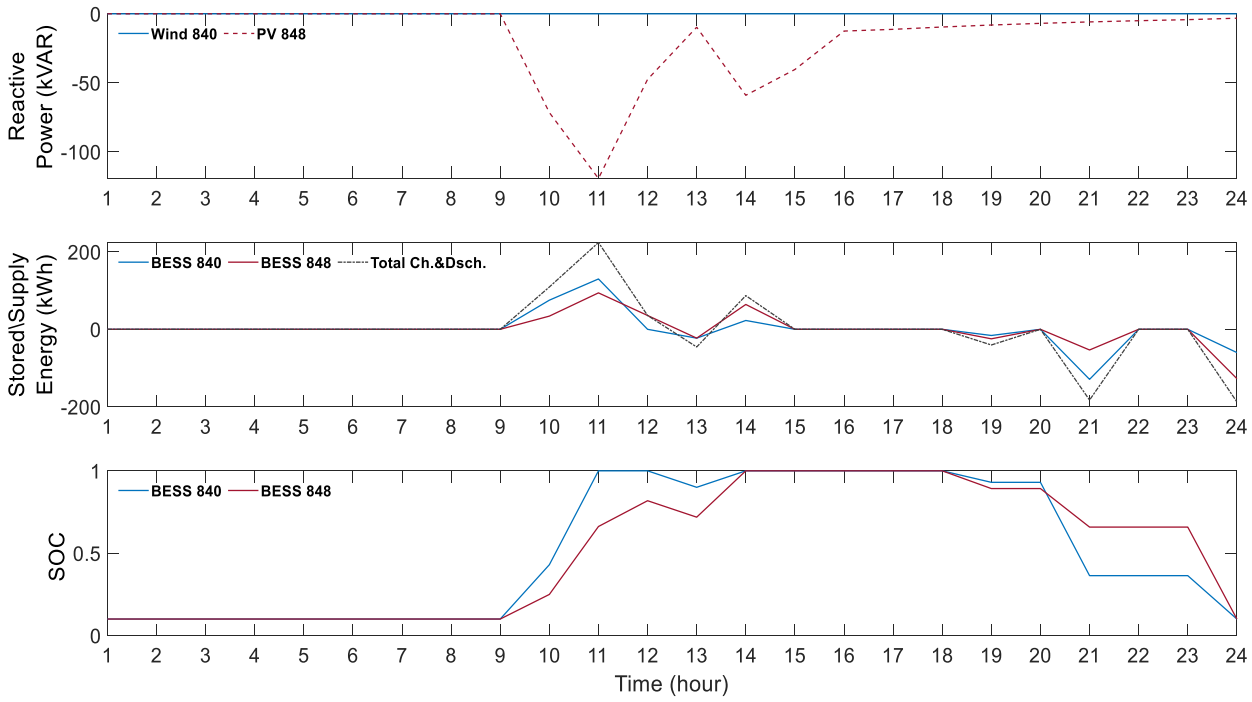

Figure 5. 21 (Top) Reactive power; (Middle) stored and supplied energy; and (Bottom) SOC of the BESS for Case 4 (PV: Forecasted)

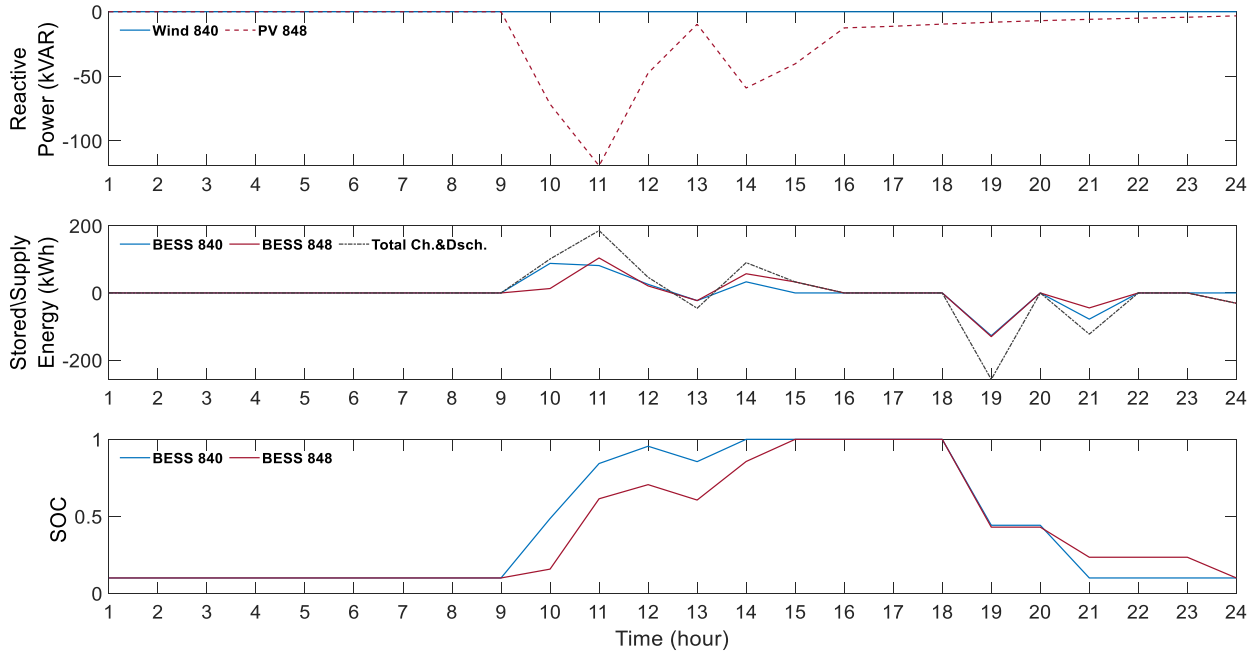

Figure 5. 22 (Top) Reactive power; (Middle) stored and supplied energy; and (Bottom) SOC of the BESS for Case 5 (PV: Forecasted)

5.2.4 BESS operation with the PV system and wind turbine

The optimal battery charging and discharging of each battery storage is exhibited in subplots 2 in Figures 5.19-5.22. These figures show that all batteries start charging the excess power from the PV system and wind turbine (from 10 AM to 15 PM) instead of being injected to the grid and causing reverse power and overvoltage at peak PV and wind incidents. At peak demand (from 19 PM to 21 PM), the batteries supply the stored energy back to the load and the grid, which accounts for the increase in the voltage at this period. Also, the batteries' energy at the beginning of the day has the same energy at the end of the day, adhering to the BESS operational constraints.

5.2.5 Average voltage deviation ($\overline{VD}$)

Similar to the previous case study's outcomes, the results in this case study are consistent in terms of the performance of the metaheuristic optimization algorithms and the level of reduction in the $\overline{VD}$ provided by the $BESS-VAR$ cases, as shown in Table 5.6. In terms of optimization algorithms, the performance experiment and convergence experiment results show that PSO also offers better performance than other algorithms, namely SSO and CSO.

As a comparison between the metaheuristic optimization algorithms in reducing the $\overline{VD}$, all three algorithms have led to a reduction either by $BESS$ or $BESS-VAR$ based on the measured or forecasted PV power generation (the two cases in which the proposed algorithm is used). PSO and CSO methods have a similar or negligible difference in terms of the $\overline{VD}$ values. Yet, PSO has the best velocity in attaining these values, as shown in Subsection 5.2.6. For example, considering (19-Mar-2018) with $BESS^{f}-VAR$ based on the forecasted PV values, the $\overline{VD}$ using SSO was found to be 0.018541, while using PSO and CSO led to 0.011258 and 0.011263, respectively. Similar reduction was found on all simulation days. In this respect, PSO presents the most accurate and fastest approach to minimize the $\overline{VD}$ and solve the voltage deviation problem in the distribution system in question. The CSO and SSO could be considered as the following best algorithms, respectively.

Table 5. 6 Average voltage deviation ($\overline{VD}$) generated by SSO, PSO and CSO on different simulation days

	Day	Only PV	VAR	$BESS$	$BESS-VAR$	$BESS^f$	$BESS^f-VAR$
SSO	7-Nov-17	0.024645	0.017962	0	0	0	0
	6-Dec-17	0.113878	0.07825	0	0	0.002082	0
	18-Jan-18	0.053442	0.037122	0	0	0	0
	8-Feb-18	0.116546	0.082386	0.005687	0	0.014133	0
	19-Mar-18	0.201085	0.142409	0.073196	0.017945	0.071085	0.018541
	Day	*Only PV*	*VAR*	$BESS$	$BESS-VAR$	$BESS^f$	$BESS^f-VAR$
PSO	7-Nov-17	0.024645	0.017962	0	0	0	0
	6-Dec-17	0.113878	0.07825	0	0	0.001164	0
	18-Jan-18	0.053442	0.037122	0	0	0	0
	8-Feb-18	0.116546	0.082386	0	0	0.014133	0
	19-Mar-18	0.201085	0.142409	0.070459	0.011152	0.070385	0.011258
	Day	Only PV	VAR	$BESS$	$BESS-VAR$	$BESS^f$	$BESS^f-VAR$
CSO	7-Nov-17	0.024645	0.017962	0	0	0	0
	6-Dec-17	0.113878	0.07825	0	0	0.001183	0
	18-Jan-18	0.053442	0.037122	0	0	0	0
	8-Feb-18	0.116546	0.082386	0	0	0.007925	0
	19-Mar-18	0.201085	0.142409	0.070546	0.011182	0.070388	0.011263

Overall, and as it can be seen from Table 5.6, VAR and $BESS$ have provided a reduction in the $\overline{VD}$ when considering the measured and observed PV power values. This is attributed to the capability of the reactive power of the smart PV inverter and BESS. However, on most days, $BESS$ alone has better $\overline{VD}$ values compared to VAR alone. On some selected days, the optimal operation of $BESS$ resulted in the prevention of the voltage deviation. For example, on 08-Feb-2018 and by using PSO, $BESS^f$ reduced the $\overline{VD}$ to 0.014133 compared to 0.082386 using VAR. If we compared the $\overline{VD}$ based on the measured and forecasted values of PV power using $BESS$, it shows that on some days $BESS^f$ with the forecasted values could not control the overvoltage, which it is supposed to accomplish based on the measured PV generation. This is due to the PV forecasting error that influenced the batteries' operations. On the other hand, $BESS-VAR$, which is the proposed technique in this study, minimizes the $\overline{VD}$ significantly through the optimal scheduling of the BESS and reactive power provided by the smart PV inverter, as shown in Figure 5.23. The results of $BESS^f-VAR$ using forecasted values are close to $BESS-VAR$ based on measured PV values,

as depicted in Figure 5.23. This can be attributed to the size of the batteries and the increase in the smart PV inverter's capacity. Therefore, increasing the size of the battery storage or the capacity of the smart PV inverter can assist in minimizing the forecasting error.

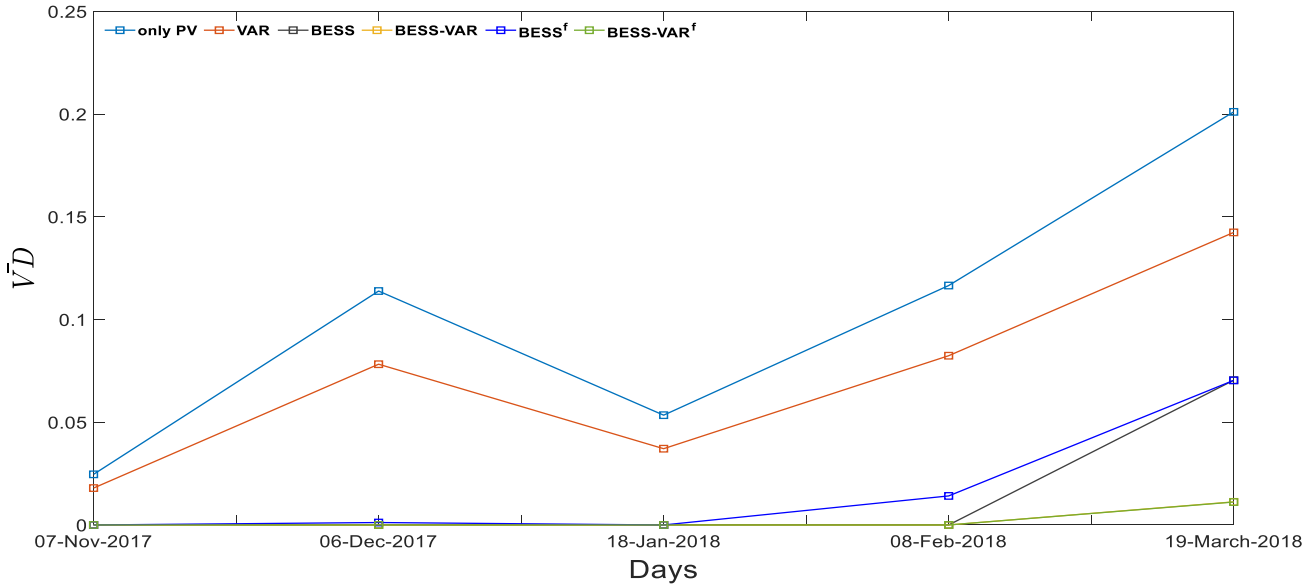

Figure 5. 23 Levels of reduction in $\overline{VD}$ by all considered cases using PSO

5.2.6 Performance comparison between metaheuristic optimization algorithms

To compare the performance of the three metaheuristic optimization algorithms namely, Social Spider Optimization (SSO), Particle Swarm Optimization (PSO) and Cuckoo Search Optimization (CSO), these algorithms are used to minimize the objective function, Eq. (3-2) in Chapter 3, that minimizes the voltage deviation. The results of every algorithm contemplate the output of 5 runs with a stopping criterion of 250 iterations. The choice of the ultimate fitness values considers the median values of those 5 executions. Accordingly, the performance experiment has been conducted, and the comparison considers the following five performance measure indexes: Best Fitness Value (BFV), Worst Fitness Value (WFV), Average of Best Fitness Values (ABFV), Median of Best Fitness Values (MBFV) and Standard Deviation of Best Fitness Values (SDBV). The simulations are run on a setup with Intel Core i7-8550 CPU @ 1.80GHz.

Table 5. 7 Results of five indexes for minimizing the objective function of the upper-level optimization for Case 5

		BFV	WFV	ABFV	MBFV	SDFV
07-Nov-2017	**SSO**	7.52E-09	1.75E-06	9.81E-08	1.34E-07	1.61E-07
	PSO	1.03E-10	**2.09E-06**	1.61E-07	6.44E-09	**3.81E-07**
	CSO	**3.05E-25**	2.33E-06	**4.61E-08**	**9.48E-19**	2.45E-07
06-Dec-2017	**SSO**	1.13E-07	2.01E-05	2.74E-06	2.04E-06	2.69E-06
	PSO	**1.10E-15**	**1.76E-05**	**3.22E-07**	**2.35E-10**	**1.74E-06**
	CSO	1.99E-10	1.60E-05	6.87E-07	1.00E-09	3.10E-06
18-Jan-2018	**SSO**	9.06E-08	1.62E-06	2.83E-07	1.76E-07	3.42E-07
	PSO	7.73E-08	**6.26E-07**	**1.13E-07**	7.96E-08	**8.68E-08**
	CSO	**3.98E-08**	8.79E-07	1.25E-07	**7.30E-08**	1.64E-07
08-Feb-2018	**SSO**	4.26E-06	2.34E-05	8.13E-06	6.41E-06	3.54E-06
	PSO	**3.13E-06**	2.82E-05	**3.63E-06**	**3.13E-06**	**2.42E-06**
	CSO	**3.12E-06**	**2.74E-05**	**4.63E-06**	3.14E-06	**4.42E-06**
19-Mar-2018	**SSO**	3.51E-05	6.03E-05	4.15E-05	4.05E-05	5.39E-06
	PSO	**2.83E-05**	5.67E-05	**2.92E-05**	**2.83E-05**	**3.24E-06**
	CSO	3.30E-05	**4.46E-05**	3.49E-05	3.33E-05	**3.24E-06**

Table 5.7 shows the results of the five indexes by minimizing the objective function, Eq. (3-2), using SSO, PSO and CSO. The results are for the Case 5 on the selected simulation days. Overall, results show that PSO performance is better than SSO and CSO with the best BFV and lowest WFV, ABFV, MBFV and SDBV. This is because of the stochastic factor of the PSO algorithm that permits the balance between exploitation and exploration [85]. Similar results were found on all simulation days with different simulation cases.

The evaluation based on the final fitness values cannot always provide an insight into the capability of an optimization algorithm. Hence, the convergence experiment has been conducted to analyze how fast an algorithm reaches the optimal values. Figure 5.24 and Figure 5.25 display the convergence rate plots of SSO, PSO and CSO with the simulations of Case 4 and Case 5 on different selected days. From these figures, it can be noticed that PSO converges faster than SSO

and CSO and can reach optimal values in ≤ 100 iterations.

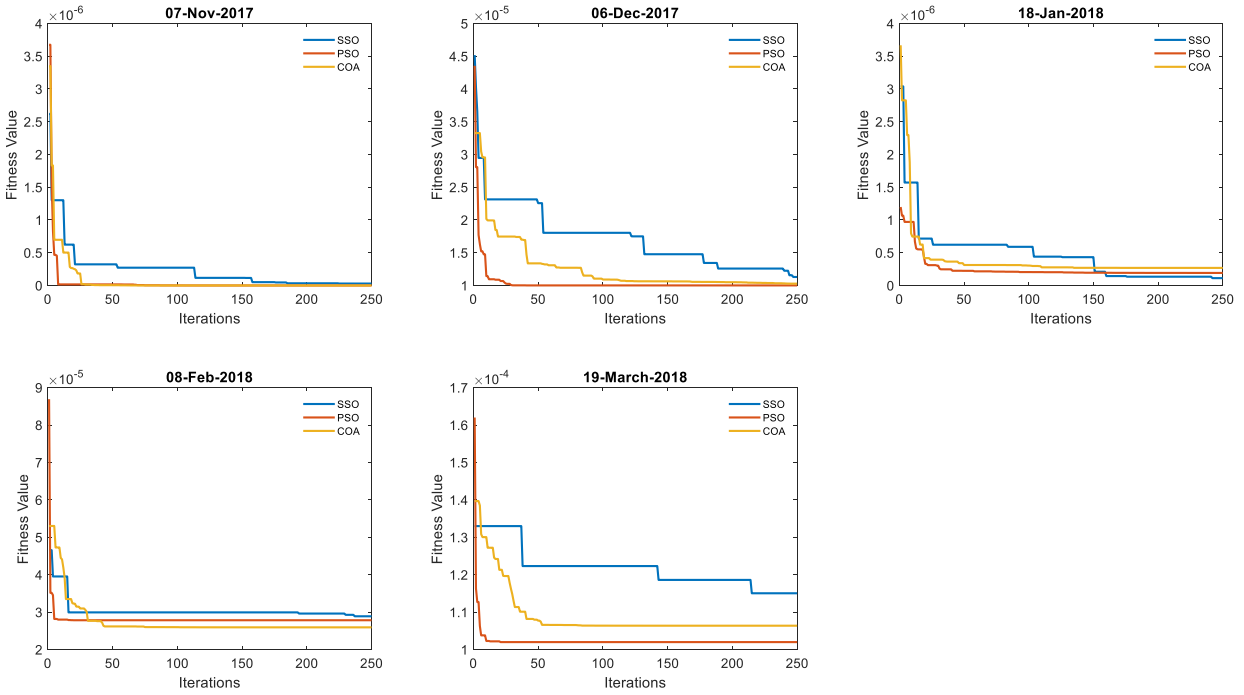

Figure 5. 24 The convergence plots of SSO, PSO and CSO for minimizing the objective function of the upper-level optimization for Case 4

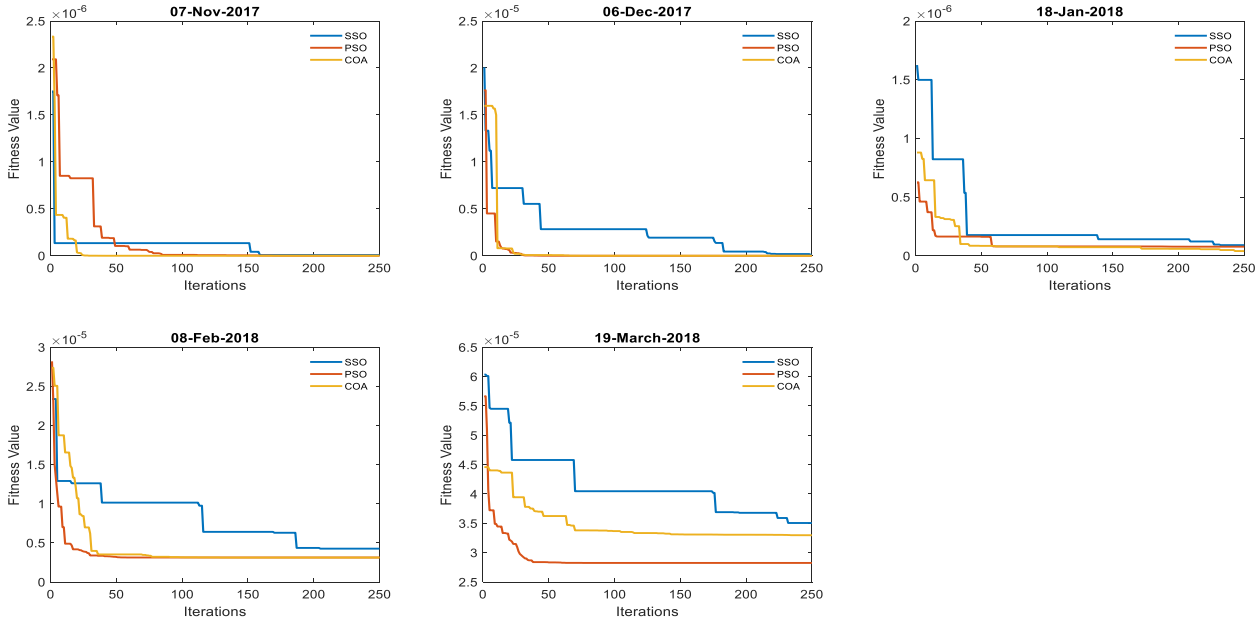

Figure 5. 25 The convergence plots of SSO, PSO and CSO for minimizing the objective function of the upper-level optimization for Case 5

Chapter 6: Voltage Regulation in the Low Voltage Distribution Network

In this Chapter, the proposed voltage management strategy is evaluated in the low voltage distribution system. Unlike the study in Chapter 5, the proposed approach in this study is using only the battery energy storage systems for voltage control. The primary objective of this study is to plan multi-BESS through network-level optimization optimally. The optimal scheduling of each installed BESS and optimal location of these batteries are accomplished in this study. The flowchart of the proposed algorithm is depicted in Figure 6.1.

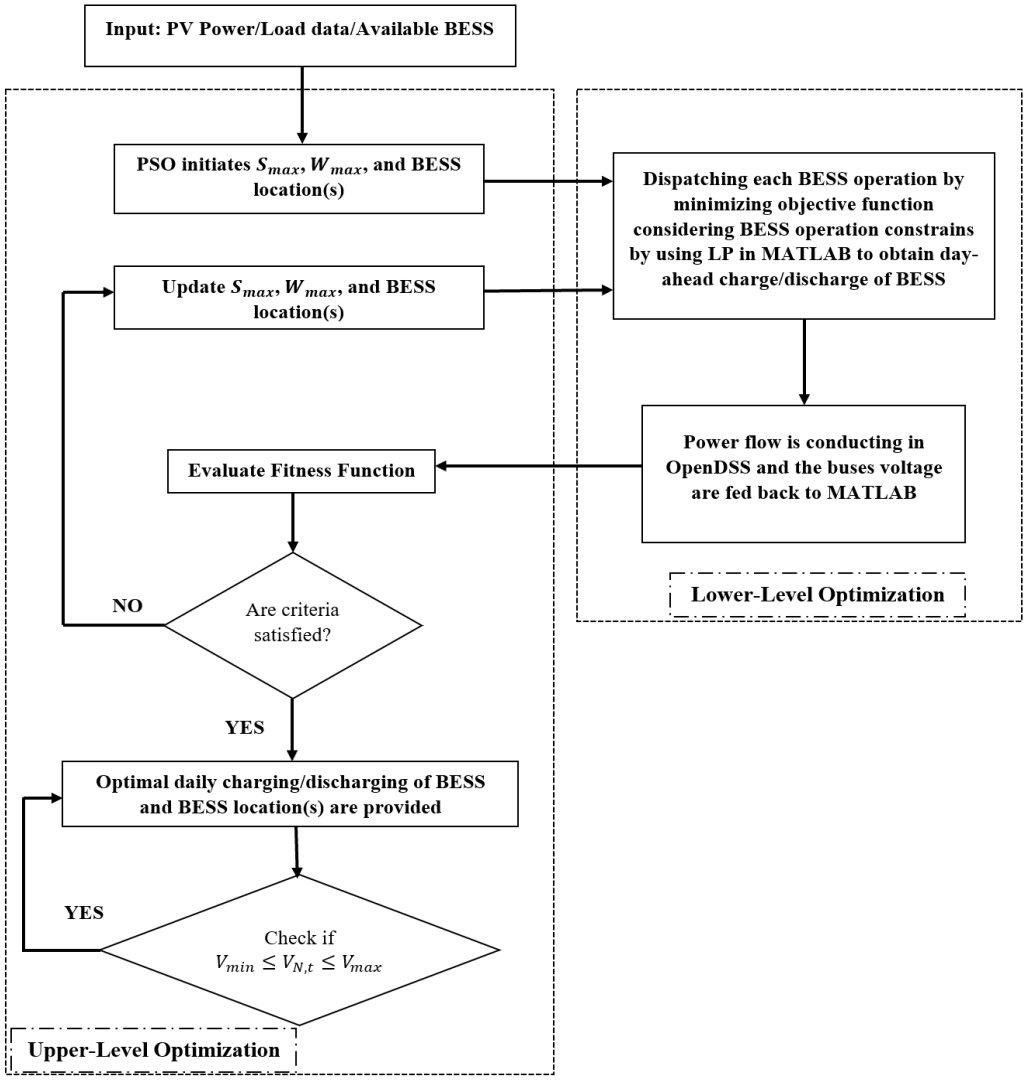

Figure 6. 1 Framework of the voltage management strategy

6.1 Simulation results and analysis

The algorithm is based on the bi-level optimization method. The full description of the proposed algorithm is described in Chapter 3. In this study, Particle Swarm Optimization (PSO) is used as the upper-level optimization, while linear programming (LP) is used in the lower-level optimization. PSO is selected in this study due to its good performance in the studies conducted in Chapter 5.

6.1.1 Test system

The proposed methodology has been applied to the IEEE Low Voltage Test Feeder shown in Figure 6.2. The feeder is a radial distribution feeder, and the substation transformer steps down the voltage from 11 kV to 416 V. The transformer at the substation of this test feeder has a rated kVA of 800, and the tap setting of the secondary part of the transformer is set to 1.02 p.u. to make the overvoltage and undervoltage problem more vivid. It is assumed in this study that each bus in the distribution network is a load bus and is equipped with a rooftop solar PV rated of 10kWp. The power flow simulations are conducted utilizing OpenDSS, while the numerical calculations and the daily BESS dispatch are obtained by LP using MATLAB.

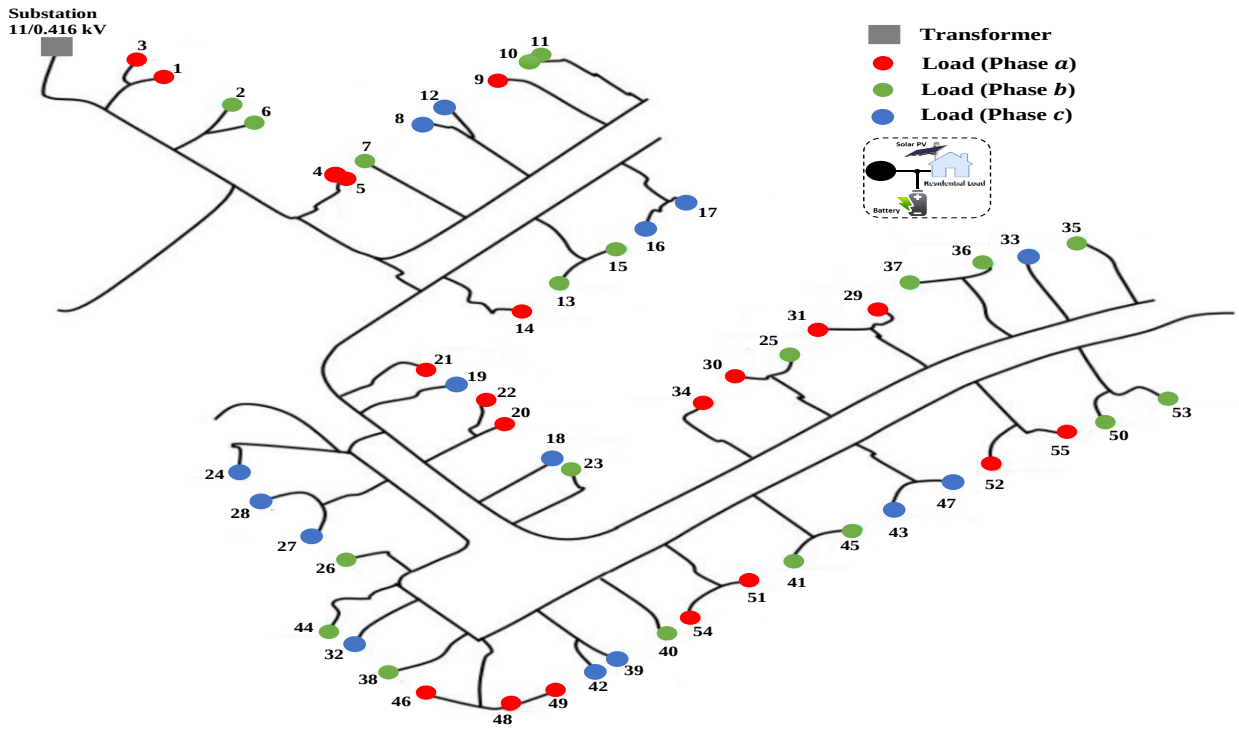

Figure 6. 2 The modified IEEE low voltage test feeder

6.1.2 Study dataset

The load profile is based on real data obtained from a home located in Riyadh, Saudi Arabia. The data are recorded by SEC. In this study, three load profiles have been considered to make the overvoltage and undervoltage phenomena in the LV distribution system more pronounced and account for load profile diversity. Therefore, load profile 1, shown in Figure 6.3, is time-shifted back by seven hours to form the load profile 2 and two hours later to form the load profile 3. The PV output power is scaled down from real-time data collected from the 120kWp PV system placed on a rooftop of a mosque in Riyadh city. The time resolution of the load and the PV power is 1-hour, and their profiles on 31-Jan-2018 are shown in Figure 6.2. The PV inverters are assumed to operate at a unity power factor. This study assumes that the utility has ownership of the PV systems and BESS. Therefore, these equipments are fully controlled by the utility to prevent the voltage in the distribution systems.

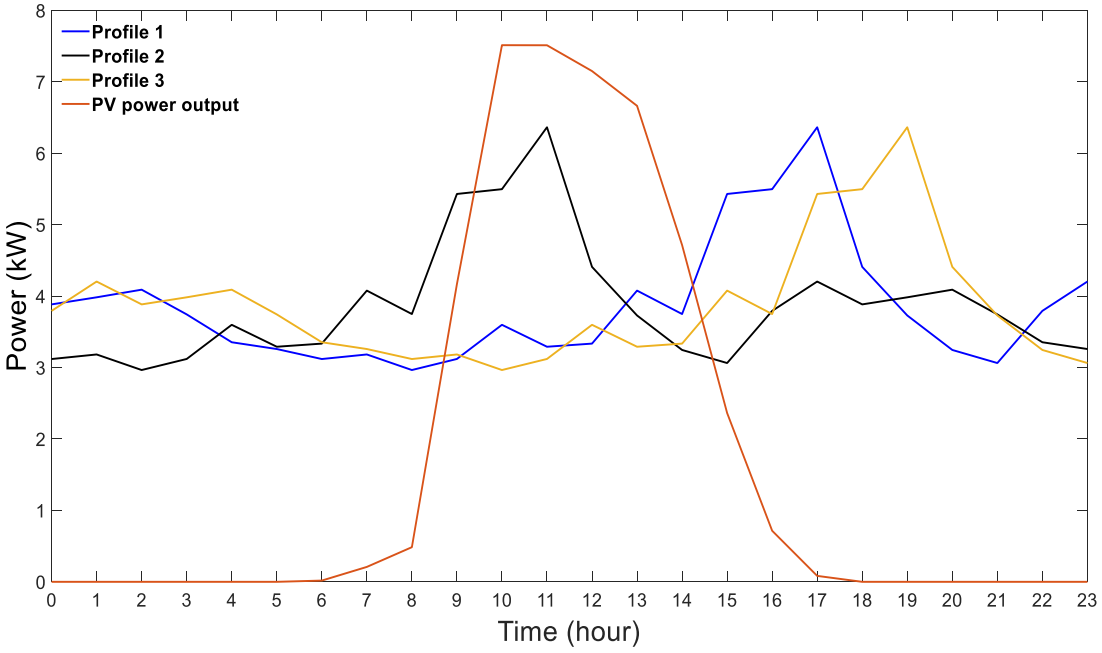

Figure 6. 3 Daily load and PV power output profiles (31-Jan-2018).

6.2 Case studies and simulation results

The excess power from the solar PV reverses the power flow causing overvoltage in the distribution network. In contrast, the high load level results in the undervoltage problem along the feeder. Typically, the acceptable voltage limits in the distribution systems should be within $\pm 5\%$

of the nominal voltage. In this study, the maximum and minimum allowed voltages are $V_{max} = 1.05$ and $V_{min} = 0.95$, respectively. In addition, this network is unbalanced; therefore, the voltage is calculated based on the mean of the three-phase voltages. Figure 6.4 shows the voltage values at the critical bus, load 53, with and without PV systems at the peak PV production. Prior to installing the PV units in the network, buses at the end of the feeder encounter the worst voltage drop. However, this situation is altered with the newly installed rooftop PV units. The voltages start to rise as we go away from the feeder, causing a violation of the upper limit of the grid voltage. Therefore, the proposed voltage management strategy determines optimal BESS characteristics, including capacity, location, number and the optimal BESS charging/discharging operation to regulate the voltage. The analysis of BESS and their impact on the distribution system voltage profile is also shown in this case study.

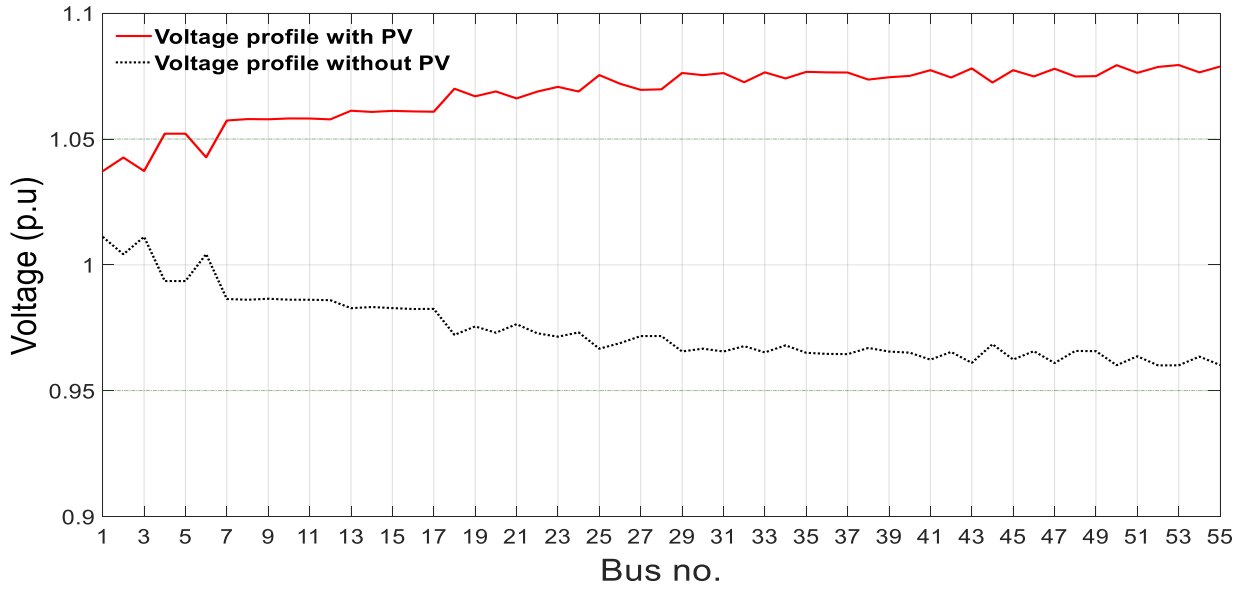

Figure 6. 4 Overvoltage problem with PV systems at the peak PV production at 11 a.m.

- **LV distribution network**

In this case, the effect of adding numbers of BESS on the distribution system voltage is investigated. Different numbers of BESS are selected, and their sizes and locations are determined through the developed management approach. For example, if we have two (three, four, …etc.) available BESS, the hybrid management algorithm identifies two critical buses to place BESS that contribute more to improve the distribution system voltage profile.

6.2.1 Voltage with and without PV systems

Figures 6.5-6.6 present the net transformer loading and the buses voltage profile with and without PV systems. Figure 6.5 shows the total power supplied by the substation transformer (utility). The positive power denotes the export power to the network from the PV units, while the negative power is the imported power from the utility. Power starts to be supplied locally from the PV units in the daytime associated with the power generated from the PV systems. The positive power (at midday) implies that the power starts to be injected back to the main grid from of the PV units, causing overvoltage problems in the network.

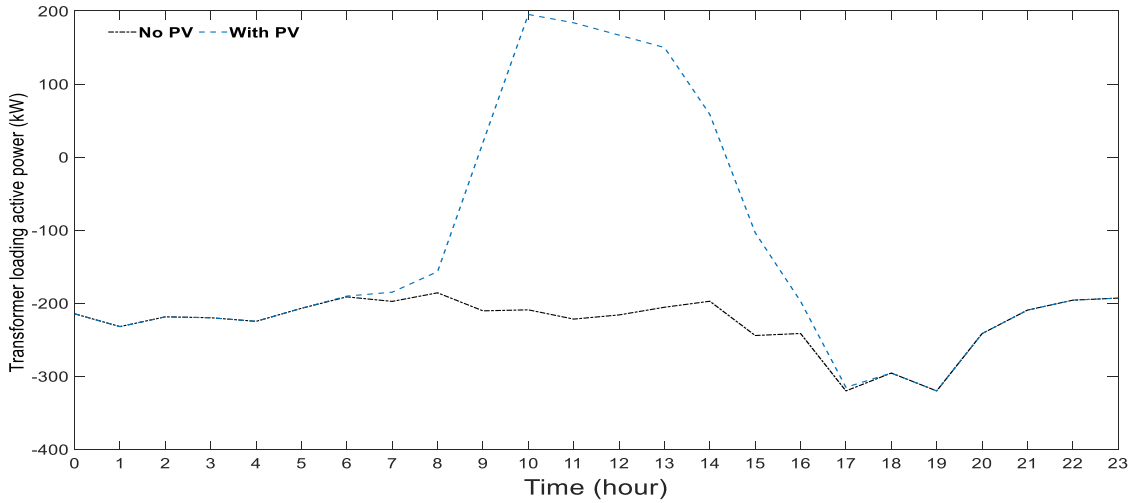

Figure 6. 5 Transformer loading with and without PV units

The voltage profiles with and without the PV systems at buses 1, 15, 44, 35, and 53 are shown in Figure 6.6. In the case without PV systems, Figure 6.6 and Figure 6.7 exhibit that the voltage levels at each load bus are within the voltage operation thresholds during daytime hours. However, the lower threshold is violated during the peak load time. Between 17 PM and 20 PM, the voltage starts dropping as we go further away from the main transformer due to the heavy load. This situation is expected in the conventional distribution systems where the demand levels are the utilities' primary concerns. However, with PV systems operation, the voltage rise is observed at midday due to the excess power from the PV systems. At the same time, the undervoltage problem happens at night coincided with peak load and low renewable energy from the PV systems. Figure 6.6 and Figure 6.7 indicate that the buses at the end of the feeder encounter the worst voltage rise.

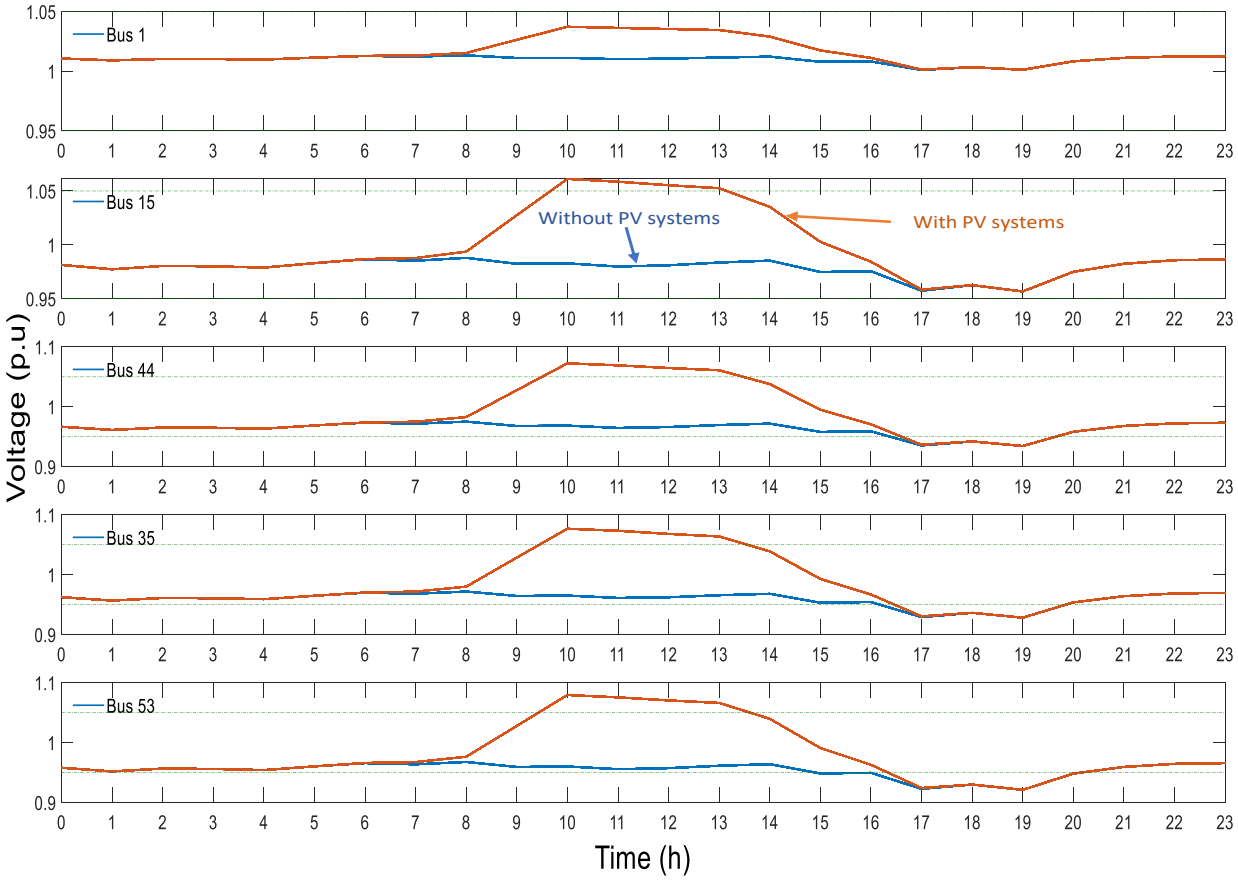

Figure 6. 6 Network daily voltage profile with and without PV system at different load buses

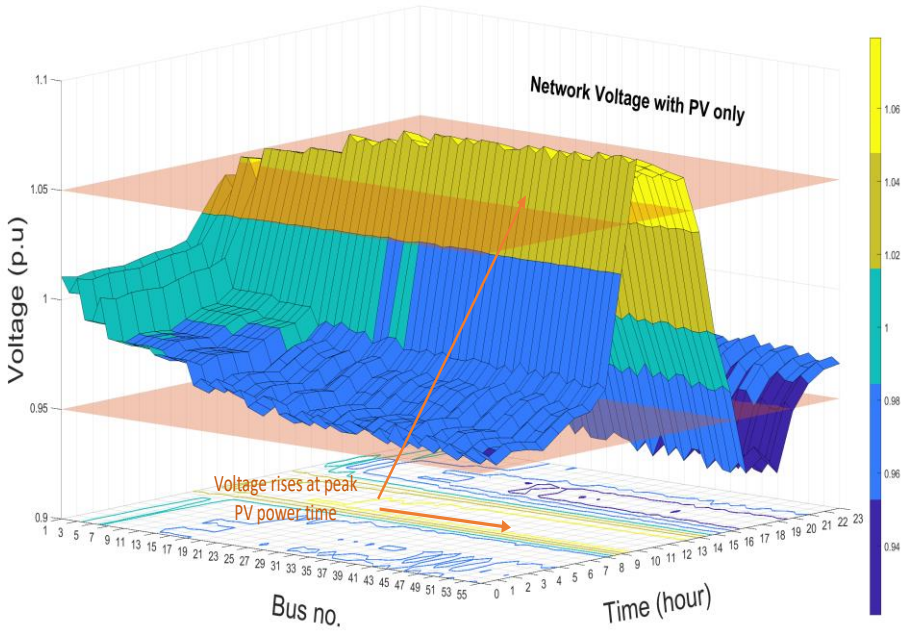

Figure 6. 7 Network daily voltage profile with PV system only

6.2.2 System losses

The daily distribution system losses with and without PV systems are shown in Figure 6.8. System losses refer to the transformer and line losses. In this network, the line losses represent 98% of the system losses, while the transformer losses account for 2%. As it can be observed from Figure 6.8, the PV systems installation in the distribution system assists in reducing the daily system losses by 15.3%, from 339.8 kW to 287.7 kW. This is due to the reduction in the power flowing in the distribution lines since the power supply is located at the end-user terminals. However, at the peak PV generation (10 AM–13 PM), the system losses start to increase due to the injected power into the main grid from the conventional load buses, which also coincided with voltage rise. At 10 AM and as it is shown in Figure 6.8, the power is reversed from the load buses toward the main grid causing the system losses of 11.144 kW compared to 11.408 kW without PV units. This power brings about losses that may cancel out the advantages of deploying the PV units in distribution systems without proper controls. At the peak load hours, when there is insufficient amount of PV power, high current flows in the distribution lines from the main feeder to feed the load. Thus, the system losses will be at the highest levels. Figure 6.8 exhibits coincident peak system losses with peak load at 19 PM with an amount of 28.412 kW.

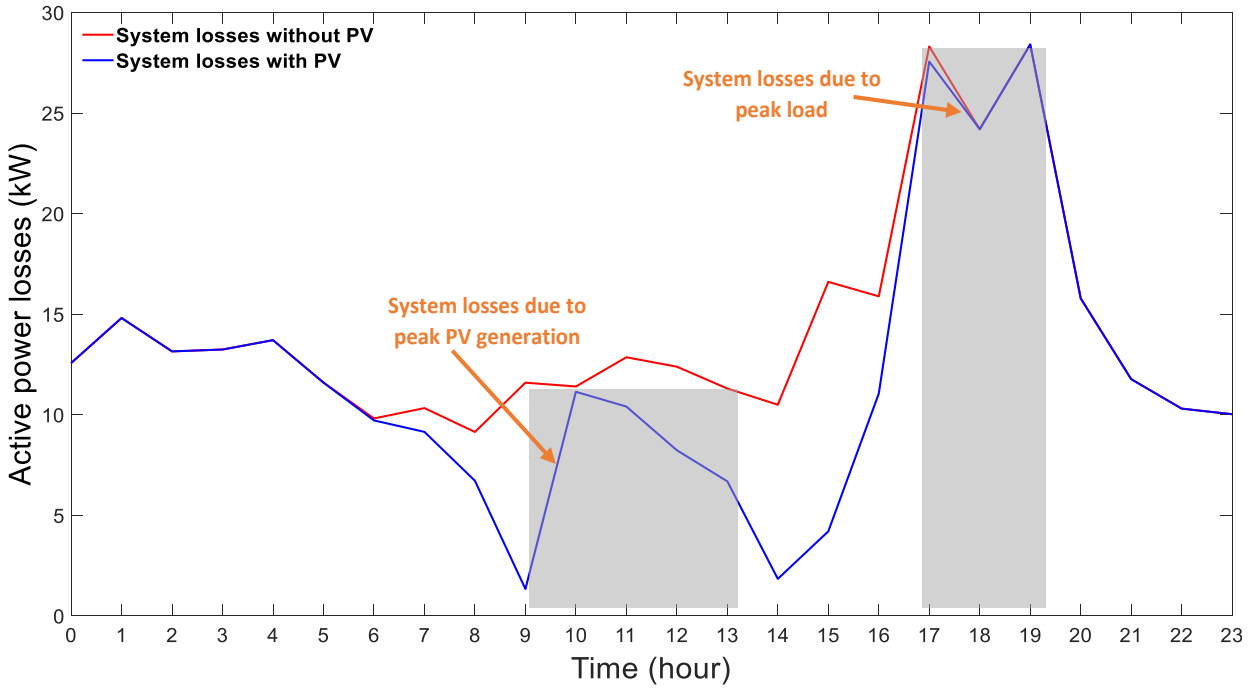

Figure 6. 8 Daily variation of total active system losses with and without PV systems

6.3 Effect of adding BESS

Table 6.1 summarizes the simulation results of the optimal location, size and the numbers of BESS. After applying the proposed voltage management strategy, the network's voltage is enhanced with increasing the installed BESS. Bus 53 is the optimal location to install the BESS if we have only one available battery. Adding more BESS, it can be noticed that the BESS tends to be placed at the end of the feeder. This is because the voltage is more violated as we go away from the main feeder, as appears in Figure 6.6 and Figure 6.7. Furthermore, the maximum and minimum voltage magnitudes are improved to their corresponding voltage limits as the availability of BESS increases. The voltage profile has become within the predefined operation limits at each bus when 21 BESS are installed at 21 different buses with a total energy of 281.6 kWh. Moreover, optimal operation and placing of 17 BESS is enough to overcome the undervoltage problem in the network.

Table 6. 1 The ranks, capacities and locations of the BESS in the network

Rank	S_{max} (kw)	W_{max} (kWh)	Location (Bus)
1	5	13.5	53
2	5	13.5	50
3	5	13.5	55
4	5	13.5	45
5	5	13.5	54
6	5	13.5	29
7	5	13.5	51
8	5	13.5	31
9	5	13.5	41
10	5	13.5	25
11	5	13.5	43
12	5	13.5	35
13	5	13.5	33
14	5	13.5	30
15	5	13.5	36
16	5	13.5	39
17	5	13.5	49
18	5	13.5	40
19	5	13.5	48
20	5	13.5	46
21	5	11.6	52

6.3.1 BESS operation

The optimal battery charging and discharging of each battery storage is exhibited in Figure 6.9. At the peak PV incidents, Figure 6.9 shows that batteries start charging the excess power from PV systems (from 10 AM to 14 PM) instead of being injected to the grid and causing reverse power and overvoltage. At peak demand (from 17 PM to 21 PM), the batteries supply stored energy back to the local load to increase the system voltage. The charging and discharging rates of batteries located at the end of the feeder happen frequently at the peak PV and peak load periods. The main reason is that these buses have the worst voltage profile and contribute greatly to minimizing the over and under voltage in the network. Considering 5 BESS cases, for instance, the capacity of each of them is 13.5 kWh at rated power of 5 kW. Their charging and discharging rates are higher at the hours when the voltage is deviated (rise/drop). After that, the charging and discharging rates differ among the remaining batteries. This is because the overvoltage has been reduced locally at different hours, and there is no need to charge the batteries at the peak PV moments. Also, it can be seen from Figure 6.9 that the energy of the batteries at the beginning of the day is the as their energy at the end of the day, adhering to the batteries' operational constraints.

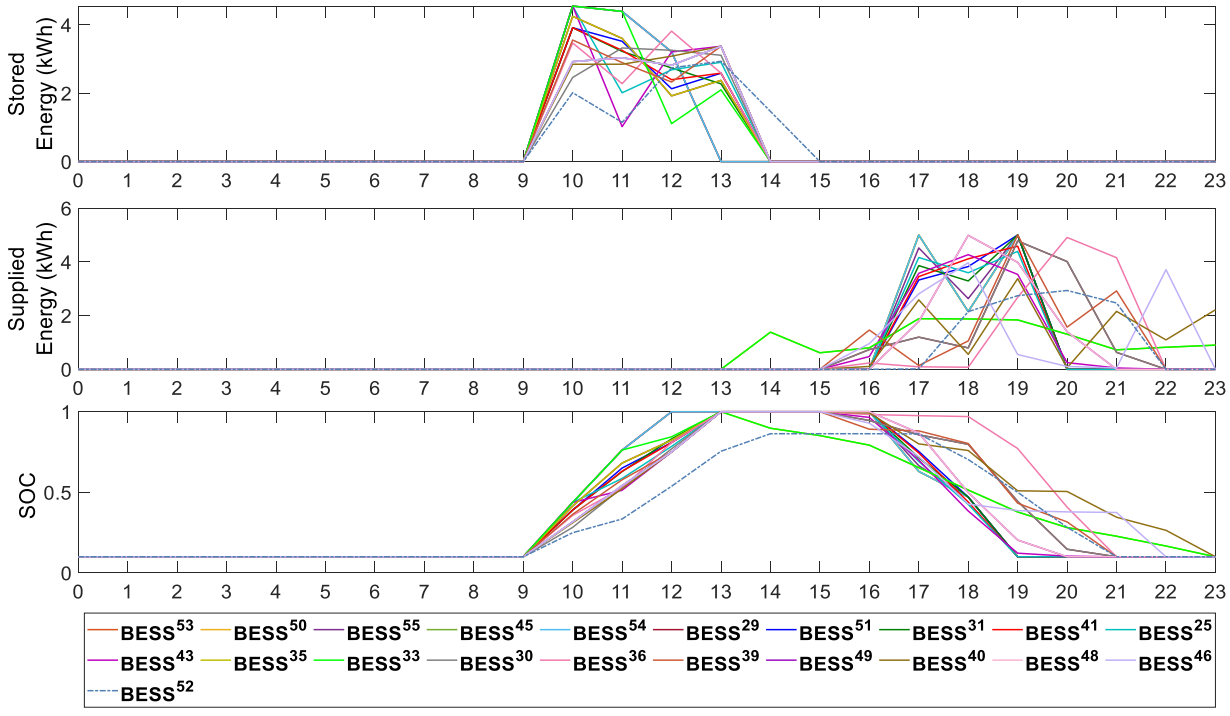

Figure 6. 9 Stored energy, supplied energy, and SOC for each BESS when coordinated for over/under voltage enhancement.

6.3.2 Transformer loading and system losses

Figure 6.10 shows the net transformer loading with the optimal addition of the BESS in the network. From this figure, both export and import peak power are minimized considerably by increasing the number of batteries installed in the network. With 21 BESS, BESS's optimal location and operation reduced the export peak and import peak by 40.14% (from 195.211 kW to 116.845 kW) and 29.76% (from 320.088 kW to 224.838 kW), respectively. Moreover, BESS's optimal operations improved the system losses, as illustrated in Figure 6.11. As the BESS number increases, the line losses decrease caused by minimizing the reverse power during high PV output and supporting the load during high load. By adding 21 BESS, the peaks of the line losses, due to the reverse power and due to the peak load, are reduced by 65.43% and 53.11%, respectively. Finally, peak shaving is also accomplished by the accumulated optimal discharge of BESS along the feeder. All installed batteries worked collectively to prevent reverse power, improve network voltage profile and peak shaving. Finally, the operation behaviors of BESS are highly impacted by the distribution system voltage magnitudes.

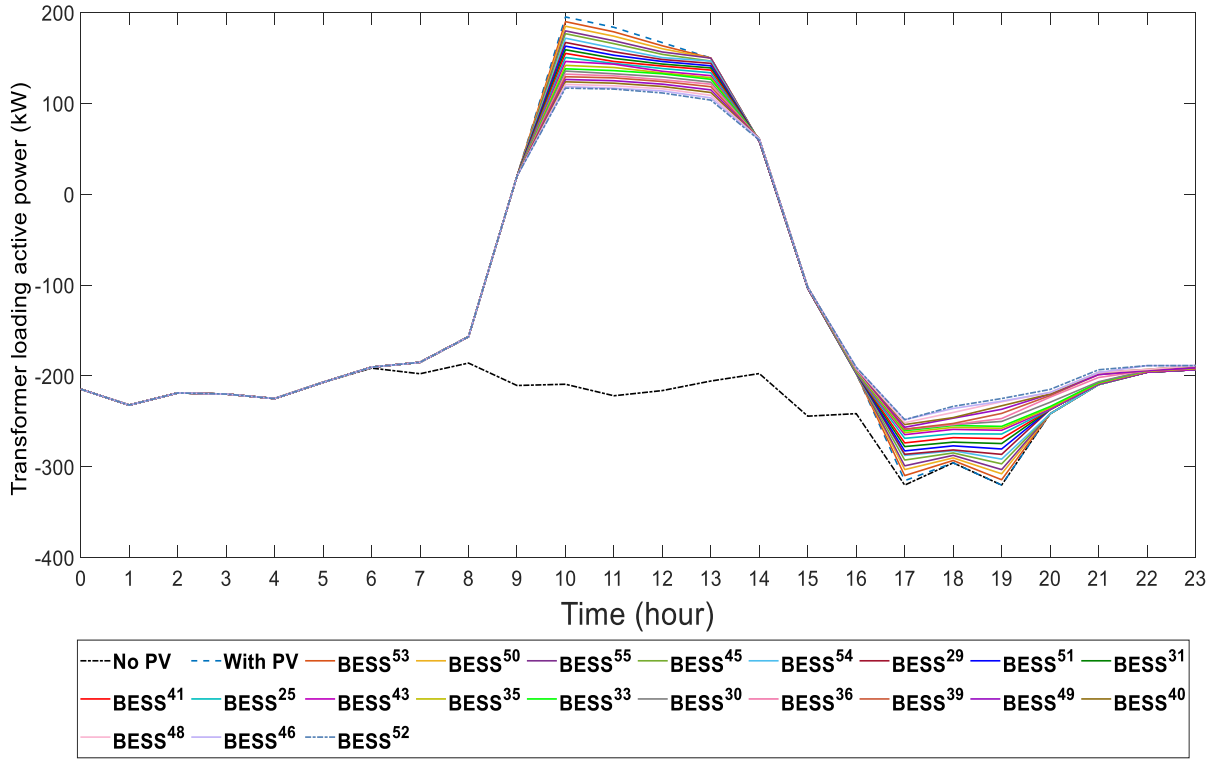

Figure 6. 10 Transformer loading with different number of BESS

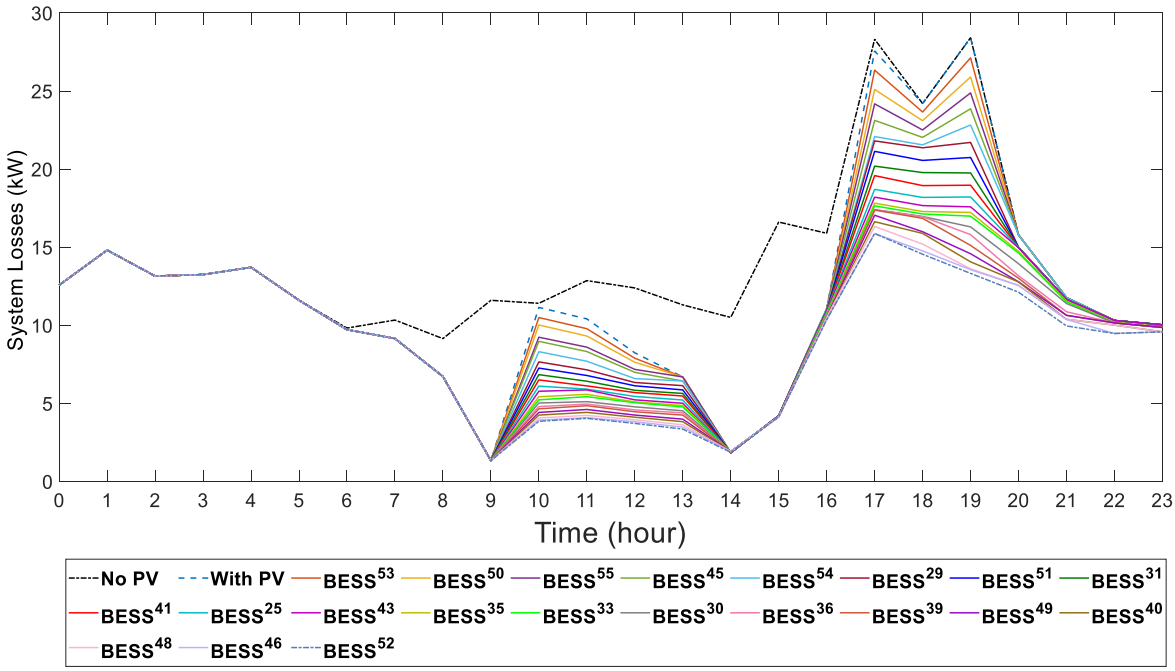

Figure 6. 11 System losses with different number of BESS

6.3.3 Optimal sizing and allocation

A total of 21 BESS were able to improve the over and under voltage along the feeder, while 17 BESS were able to overcome the undervoltage problem, see Figure 6.15 and Figure 6.16. In the study network, there are 55 load/PV buses across the three phases. As shown in Figure 6.2, there are 20 loads/PVs connected to phase a, 20 loads/PVs connected to phase b and 15 loads/PVs connected to phase c. The simulation results in Table 6.1 indicate that the size and the location of batteries are highly influenced by the voltage magnitudes. Thus, the locations of BESS are mostly at the end of the feeder. In addition, among the optimal 21 BESS locations, 10, 8, and 3 batteries are connected to phase a, b and c, respectively. Phases a and b encounter the worst voltage profile; thus, the optimal locations of the batteries are mostly co-located with the PV systems connected with these phases. Despite that bus 47 is at the end of the feeder, no battery is installed there. This is because the load profile at bus 47 is profile 2, which minimizes the contribution from this bus in supporting the network voltage. At this bus, the peak PV generation coincides with local peak load. Similar situation is found with bus 37 that is connected to phase b. Therefore, the optimal siting and sizing of the available BESS are highly impacted by network topology, load and the amount of PV power that flows into the grid.

6.3.4 Network voltage with BESS

Results of the voltage profiles with and without BESS at buses 1, 15, 44, 35, and 53 are shown in Figure 6.12. As we can see from this figure, the voltage profile accepts the upper and lower network voltage when the BESS are optimally installed and operated in the network. In addition, the levels of improvements in the network voltage when 5, 10, 17, and 21 BESS are installed are shown in Figures 6.13-6.16, respectively. Finally, the optimal management of the capacity and allocation of BESS in the distribution system results in enhancement in overall grid voltage, reduction in system losses and peak shaving.

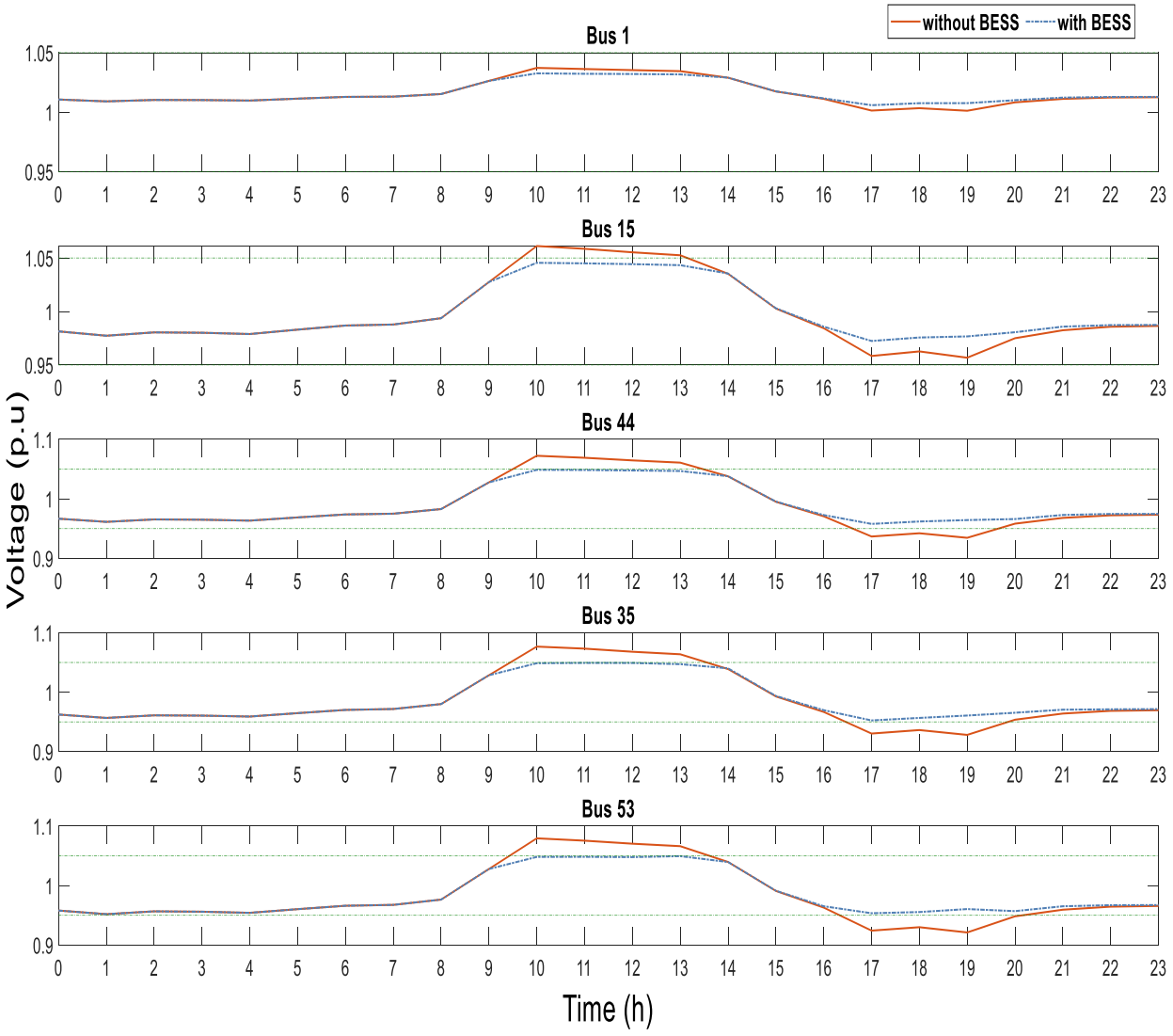

Figure 6. 12 Network daily voltage profile with and without BESS at different load buses

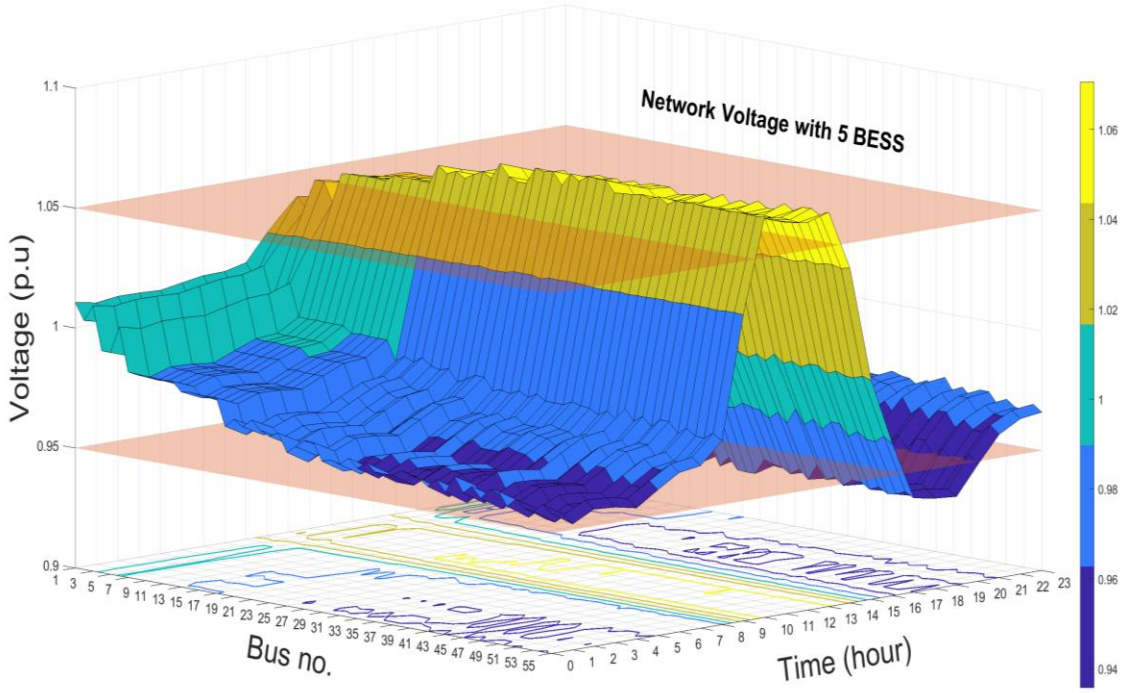

Figure 6. 13 Network voltage profile with installing 5 BESS

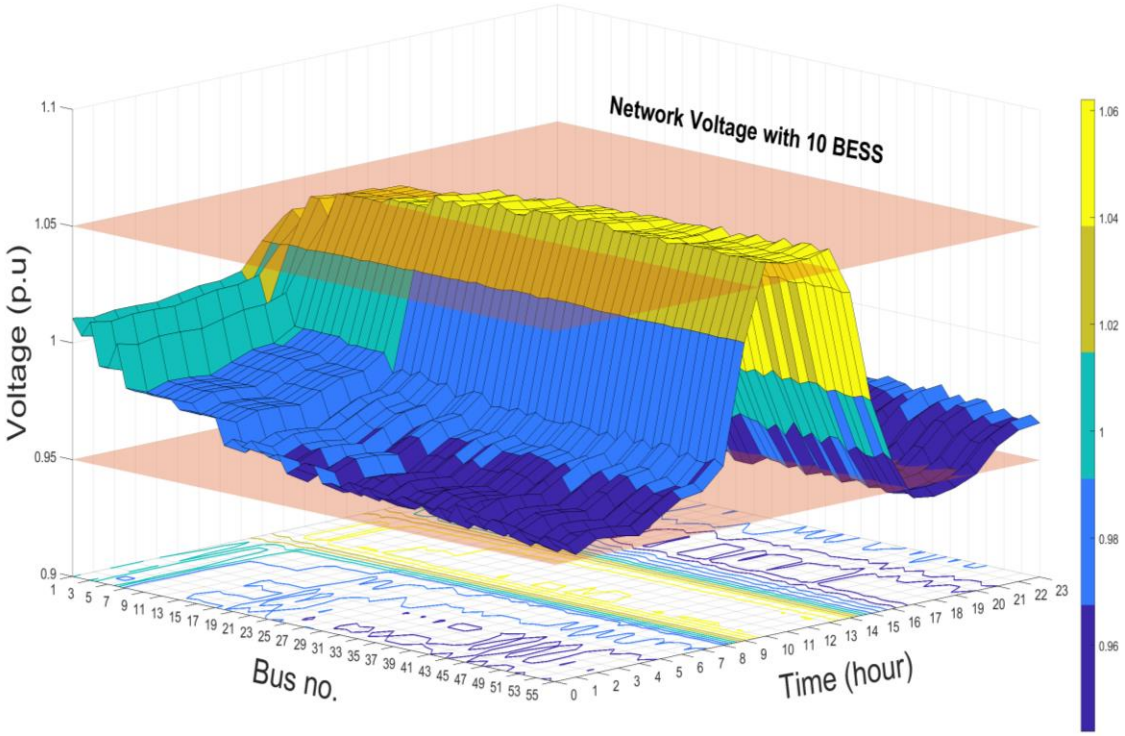

Figure 6. 14 Network voltage profile with installing 10 BESS

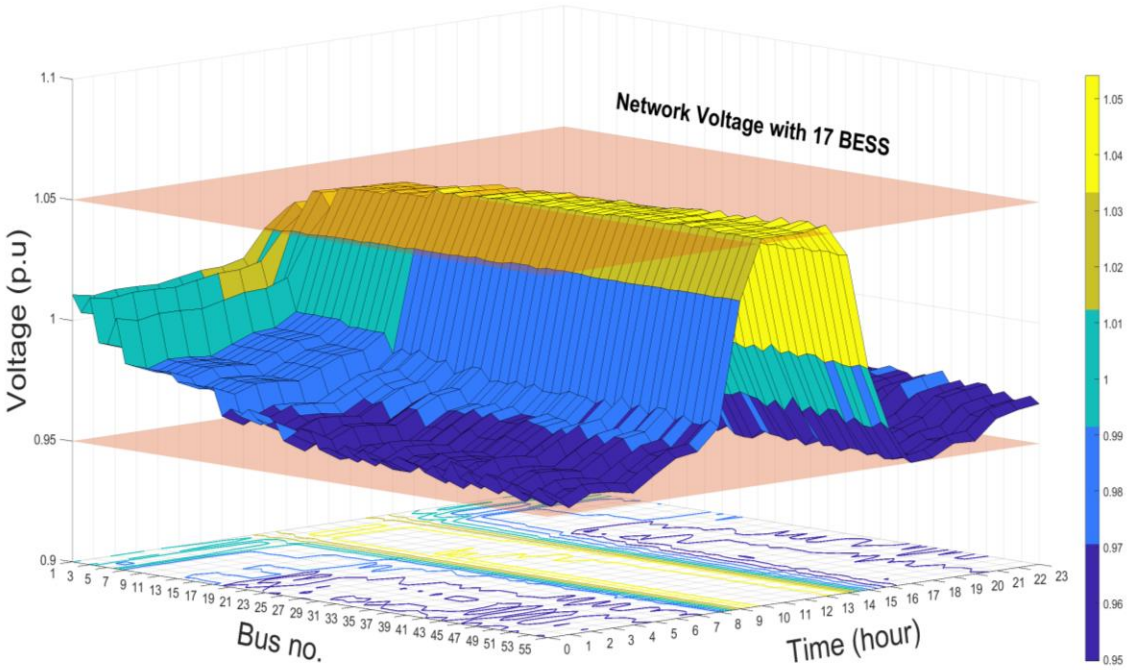

Figure 6. 15 Network voltage profile with installing 17 BESS

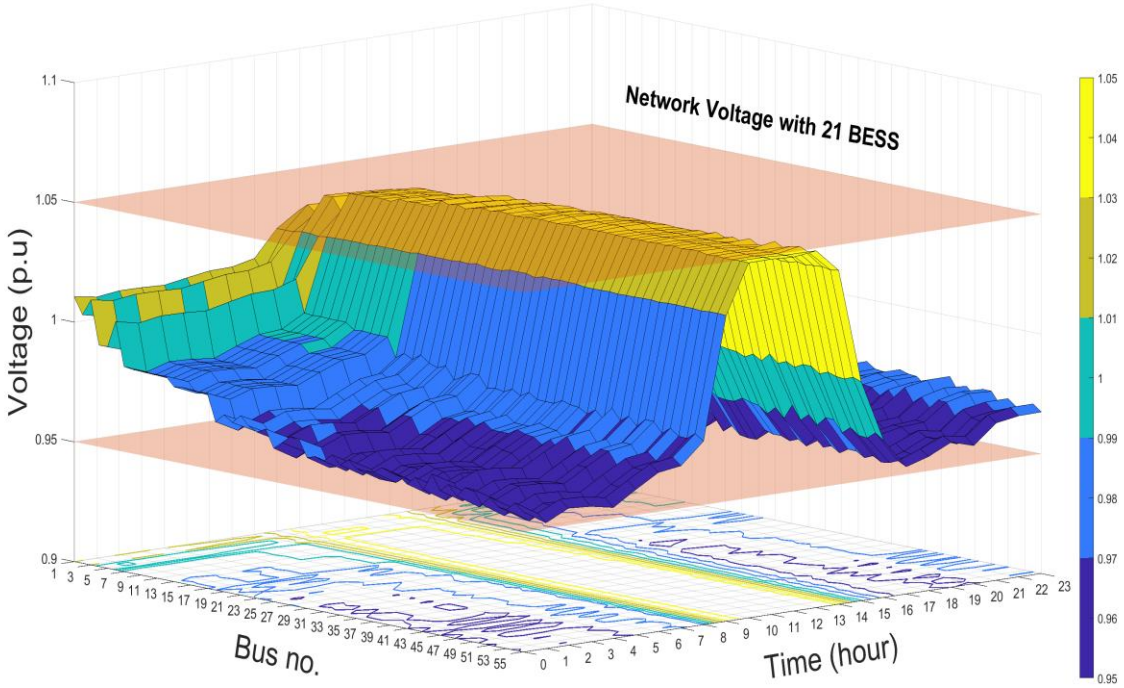

Figure 6. 16 Network voltage profile with installing 21 BESS

Chapter 7: Summary, conclusions and future work

7.1 Summery

The integration of renewable distributed generation (DG), such as PV systems and wind, into the distribution networks brings about several operational issues that are required to be addressed by the distribution systems operators (DSO). The voltage quality problem is considered the most severe obstacle to the DSOs. Surplus energy from the DG units causes the voltage to deviate from the operating grid voltage. DSOs typically maintain the voltage profile by utilizing on-load tap changers, voltage regulator taps and capacitor banks. However, due to the frequent variability of the output energy from DG, these devices cannot function as necessary. Therefore, this dissertation proposes a voltage management strategy to regulate the voltage in distribution systems with high PV and wind energy penetrations. The proposed method coordinates the battery energy storage systems (BESS) with the smart PV inverters to minimize the impacts of DG penetration on the system voltage profile.

Furthermore, the successful deployment of BESS primarily relies on the planning strategies, where the size, location, number and optimal operation of BESS should be considered for managing the voltage problems and enhancing the distribution system reliability. The proposed voltage management method is applied to the modified IEEE 34-bus test feeder and the modified IEEE low voltage test feeder. The proposed management strategy is applied to these two cases to show the impacts of the BESS and smart PV inverters on the network voltage profile.

This dissertation is supported by day-ahead forecasting of PV power outputs based on machine learning algorithms. These models are hybrid forecasting models using support vector regression and backpropagation neural networks with three metaheuristic optimization algorithms, namely Social Spider Optimization (SSO), Particle Swarm Optimization (PSO) and Cuckoo Search Optimization. Utilizing the day-ahead forecasting of PV permits the DSOs to precisely estimate the amount of PV energy available the next day and support the battery operation process. The performance of the forecasting models is evaluated to see how the forecasted values deviate from the measured values. The evaluation is based on Root Mean Square Error ($RMSE$), normalized

Mean Square Error ($nRMSE$), Mean Absolute Error (MAE) and normalized Mean Absolute Error ($nMAE$).

The voltage management method is conducted in the IEEE-34 bus test feeder considering a grid connected with large-size PV system and wind turbine. The high PV and wind integrations and its impact on the distribution systems volage is studied. Also, the validation of the proposed voltage management approach on regulating the voltage and determining the optimal operation of BESS is analyzed. The efficacy of the PV inverters in controlling the voltage and their coordination with BESS is also examined.

The voltage deviation in the LV distribution system due to the newly installed rooftop PV systems is mitigated by utilizing the BESS. The proposed voltage mitigation strategy helps the distribution system planners decide on the location where the available BESS should be installed, the capacity of each BESS and the optimal charging and discharging characteristics of the BESS to overcome the overvoltage and undervoltage problems.

7.2 Conclusions

The data utilized in this research work reflect the behavior of the loads and wind and solar PV generations in Riyadh City, Saudi Arabia. This geographic area is selected as a case study, where the effectiveness of the proposed voltage management strategy is evaluated. The solar PV generation data are obtained from a PV system located in Riyadh to reflect the amount of energy coming from the sun. Also, the wind data are obtained at the same location to depict the wind regime. In addition, in the medium voltage distribution system (Chapter 5), the load data are collected from a substation transformer that feeds primarily residential and commercial loads in Riyadh. On the other hand, the load data in Case 2 (Chapter 6) represent the load of residential homes located in Riyadh. Therefore, the simulation results shown in this dissertation are the outcomes with this dataset, at Riyadh, when the proposed voltage management strategy is applied. The results may change if different sets of data or different geographic areas in other countries are considered. However, the voltage control algorithm presented in this dissertation can be generalized and will stand to control the voltage to the desired range.

Hence, according to the simulation results of this dissertation, the main conclusions that can be drawn show the effectiveness of the proposed methods. These are presented as follows:

- ***Day-ahead hybrid PV power output forecast using machine learning algorithms***

The proposed hybrid PV power forecasting models outperform the default models using SVR with the RB and linear functions and BPNN algorithms. Overall, results indicate that the proposed models with the optimized hyperparameter of the SVR with radial basis outperform other models in forecasting PV power output at the study site. Regarding models fitting accuracy with the SVR_{RB} models, the proposed models show improvements compared to the default models, where $RMSE$ improved between 12.001% to 50.079% and MAE improved between 1.80291% to 50.8847%. Similarly, the prediction models with the $BPNN^1$and $BPNN^2$ using the proposed models, with optimal network configurations, have better performance with 1.883%-46.964% and 2.0576%-47.007% improvement in the $RMSE$ and MAE values, respectively, compared to the default $BPNN$ models. The three optimization algorithms almost have the same performance, proving their ability to select SVR parameters and BPNN network configurations. Furthermore, the BPNN model exhibits a good performance that can compare with the SVR radial basis models.

- ***Proposed voltage strategy in the medium voltage distribution network***

The simulation results presented in Chapter 5 show that the overvoltage problem is the main concern in the distribution network with high PV and wind integrations. Utilizing BESS or smart PV inverters to control the overvoltage may not be sufficient due to their limited capacity. However, the real-time simulation results proved the efficiency of the proposed algorithm in controlling the voltage through coordination between the operation of the BESS and the smart PV inverters. Regarding the metaheuristic optimization algorithms, the performance and convergence experiments exhibit that PSO is better than SSO and CSO. PSO can obtain the optimal BESS scheduling at a fast pace.

- ***Proposed voltage strategy in the low voltage distribution network***

The simulation results presented in Chapter 6 show that the overvoltage and undervoltage problems appear in the distribution network with high PV integration represented by the rooftop PV units. Optimal sizing, placement and operating through utilizing the proposed voltage mitigation method helped overcome the voltage problems. In terms of the locations of the BESS

units, the end of the feeder homes are the ideal sites to install batteries as they encounter the worst voltage scenarios. In addition, results showed that the optimal siting and sizing of the available BESS are highly impacted by network topology, load and the amount of PV power that flows into the grid.

7.2 Future work

This research work proposed a voltage control strategy that coordinates BESS and smart PV inverters. The following are the potential topics to be further explored using the work presented in this dissertation:

1. Considering BESS in distribution networks, several benefits can be obtained to improve the system operation while ensuring cost-effective installation. BESS modeling can be formulated as a multi-objective optimization problem. These objectives can be economic, technical and environmental. First, the capital, maintenance and degradation costs associated with the battery installation can also be considered in the objective function. Second, energy price arbitrage can also be obtained when the battery is charged at high energy prices and discharged when the energy price is low. For technical objectives, minimizing the line losses, for instance, can also be added to the objective function. Finally, for environmental objectives, BESS can contribute to minimizing the harmful greenhouse emissions produced from the conventional power plant when operating at low and high emission periods.

2. The operation of the smart PV inverter with the Volt-VAR mode primarily depends on the pre-identified Volt-VAR curve. This curve has different parameters that are set to keep the voltage within an upper and lower threshold. As the distribution networks' voltage profile levels differ, the Volt-VAR curve parameters could be optimized to get the most benefits of the inverter reactive power capability.

3. To improve the BESS operation while keeping the voltage within upper and lower limits, the BESS scheduling can be updated by a one-hour PV power forecast. Hence, besides the day-ahead forecast of the PV system generated at midnight before the day of operation, the charging and discharging of batteries can be updated based on the one-hour forecast

generated at each hour. This way, the BESS operation will be optimal as the forecasting error associated with the day-ahead forecast will be minimized.

4. Demand response programs can assist in shifting some load and alter the load profile. Most demand response programs incorporate other forecasting models in their applications, such as wind and load forecasts. Hence, incorporating PV, wind and load forecast models with the BESS and smart PV inverter operation would lead to a robust algorithm to overcome voltage problems in the distribution systems. In this study, the overvoltage incidents are observed when the load is low and the power coming from PV and wind is high. On the other hand, the undervoltage usually occurs at the time of heavy load and low renewable generation. Therefore, if the demand response program can shift some load (based on signals received from the load, wind and PV forecast models) from the time of high load and low renewable power (undervoltage) to the time of low load and high renewable power (overvoltage), the voltage violation could be minimized.

5. In this research study, the model is built, and the proposed voltage management algorithm is examined based on data obtained at Riyadh City in Saudi Arabia. This region is selected as a case study to evaluate the efficacy voltage control algorithm. Other researchers can use this algorithm and test it on different data set at different geographic regions and then compare their findings with the results displayed in this work.

References

[1] REN21. 2020. Renewables 2020 Global Status Report. (Paris: REN21 Secretariat): 2020.

[2] IEA (2020). Global Energy Review 2020. Glob Energy Rev 2020 n.d. https://www.iea.org/reports/global-energy-review-2020.

[3] Novoa L, Flores R, Brouwer J. Optimal renewable generation and battery storage sizing and siting considering local transformer limits. Appl Energy 2019;256:113926. doi:10.1016/j.apenergy.2019.113926.

[4] Razavi SE, Rahimi E, Javadi MS, Nezhad AE, Lotfi M, Shafie-khah M, et al. Impact of distributed generation on protection and voltage regulation of distribution systems: A review. Renew Sustain Energy Rev 2019:157–67. doi:10.1016/j.rser.2019.01.050.

[5] Barrero-González F, Pires VF, Sousa JL, Martins JF, Milanés-Montero MI, González-Romera E, et al. Photovoltaic Power Converter Management in Unbalanced Low Voltage Networks with Ancillary Services Support. Energies 2019;12:1–16. doi:10.3390/en12060972.

[6] Mahmud N, Zahedi A. Review of control strategies for voltage regulation of the smart distribution network with high penetration of renewable distributed generation. Renew Sustain Energy Rev 2016;64:582–95. doi:10.1016/j.rser.2016.06.030.

[7] El-Khattam W, Sidhu TS. Resolving the impact of distributed renewable generation on directional overcurrent relay coordination: A case study. IET Renew Power Gener 2009;3:415–25. doi:10.1049/iet-rpg.2008.0015.

[8] Tonkoski R, Lopes LAC, El-Fouly THM. Coordinated active power curtailment of grid connected PV inverters for overvoltage prevention. IEEE Trans Sustain Energy 2011;2:139–47. doi:10.1109/TSTE.2010.2098483.

[9] Alboaouh KA, Mohagheghi S. Impact of Rooftop Photovoltaics on the Distribution System. J Renew Energy 2020;2020:1–23. doi:10.1155/2020/4831434.

[10] Unigwe O, Okekunle D, Kiprakis A. Smart coordination schemes for multiple battery energy storage systems for support in distribution networks with high penetration of photovoltaics. IET Smart Grid 2019;2:347–54. doi:10.1049/iet-stg.2019.0094.

[11] Torquato R, Salles D, Pereira CO, Meira PCM, Freitas W. A Comprehensive Assessment of PV Hosting Capacity on Low-Voltage Distribution Systems. IEEE Trans Power Deliv 2018;33:1002–12. doi:10.1109/TPWRD.2018.2798707.

[12] U.S. Department of Energy (DOE). Combined Heat and Power Technology 2016:1–4.

[13] Wang L, Yan R, Kumar Saha T. Voltage regulation challenges with unbalanced PV integration in low voltage distribution systems and the corresponding solution. Appl Energy 2019;256:113927. doi:10.1016/j.apenergy.2019.113927.

[14] Company SE. The Saudi Arabian Distribution Code. 2008.

[15] Chaudhary P, Rizwan M. Voltage regulation mitigation techniques in distribution system with high PV penetration: A review. Renew Sustain Energy Rev 2018;82:3279–87. doi:10.1016/j.rser.2017.10.017.

[16] Karimi M, Mokhlis H, Naidu K, Uddin S, Bakar AHA. Photovoltaic penetration issues and impacts in distribution network-A review. Renew Sustain Energy Rev 2016;53:594–605. doi:10.1016/j.rser.2015.08.042.

[17] Ziadi Z, Oshiro M, Senjyu T, Yona A, Urasaki N, Funabashi T, et al. Optimal voltage control using inverters interfaced with PV systems considering forecast error in a distribution system. IEEE Trans Sustain Energy 2014;5:682–90. doi:10.1109/TSTE.2013.2292598.

[18] Yan R, Marais B, Saha TK. Impacts of residential photovoltaic power fluctuation on on-load tap changer operation and a solution using DSTATCOM. Electr Power Syst Res 2014;111:185–93. doi:10.1016/j.epsr.2014.02.020.

[19] Mak D, Choi DH. Hierarchical look-ahead conservation voltage reduction framework considering distributed energy resources and demand reduction. Energies 2018;11:1–20. doi:10.3390/en11123250.

[20] Morin J, Colas F, Dieulot JY, Grenard S, Guillaud X. Embedding OLTC nonlinearities in predictive Volt Var Control for active distribution networks. Electr Power Syst Res 2017;143:225–34. doi:10.1016/j.epsr.2016.10.015.

[21] Daratha N, Das B, Sharma J. Coordination between OLTC and SVC for voltage regulation in unbalanced distribution system distributed generation. IEEE Trans Power Syst 2014;29:289–99. doi:10.1109/TPWRS.2013.2280022.

[22] Howlader AM, Sadoyama S, Roose LR, Chen Y. Active power control to mitigate voltage and frequency deviations for the smart grid using smart PV inverters. Appl Energy 2020;258:114000. doi:10.1016/j.apenergy.2019.114000.

[23] Riquelme-Dominguez JM, Martinez S. A photovoltaic power curtailment method for operation on both sides of the power-voltage curve. Energies 2020;13:1–17. doi:10.3390/en13153906.

[24] Ghasemi MA, Parniani M. Prevention of distribution network overvoltage by adaptive droop-based active and reactive power control of PV systems. Electr Power Syst Res 2016;133:313–27. doi:10.1016/j.epsr.2015.12.030.

[25] Ma W, Wang W, Chen Z, Wu X, Hu R, Tang F, et al. Voltage regulation methods for active distribution networks considering the reactive power optimization of substations. Appl Energy 2021;284:116347. doi:10.1016/j.apenergy.2020.116347.

[26] Tina GM, Garozzo D, Siano P. Scheduling of PV inverter reactive power set-point and battery charge/discharge profile for voltage regulation in low voltage networks. Int J Electr Power Energy Syst 2019;107:131–9. doi:10.1016/j.ijepes.2018.11.009.

[27] Pompodakis EE, Drougakis IA, Lelis IS, Alexiadis MC. Photovoltaic systems in low-voltage networks and overvoltage correction with reactive power control. IET Renew Power Gener 2016;10:410–7. doi:10.1049/iet-rpg.2014.0282.

[28] Wang Y, Tan KT, Peng XY, So PL. Coordinated Control of Distributed Energy-Storage Systems for Voltage Regulation in Distribution Networks. IEEE Trans Power Deliv 2016;31:1132–41. doi:10.1109/TPWRD.2015.2462723.

[29] Kabir MN, Mishra Y, Ledwich G, Xu Z, Bansal RC. Improving voltage profile of residential distribution systems using rooftop PVs and Battery Energy Storage systems. Appl Energy 2014;134:290–300. doi:10.1016/j.apenergy.2014.08.042.

[30] Kerdphol T, Fuji K, Mitani Y, Watanabe M, Qudaih Y. Optimization of a battery energy storage system using particle swarm optimization for stand-alone microgrids. Int J Electr Power Energy Syst 2016;81:32–9. doi:10.1016/j.ijepes.2016.02.006.

[31] IEEE Standard for Interconnecting Distributed Resources with Electric Power Systems. IEEE Std 2003:1–28. doi:10.1109/IEEESTD.2003.94285.

[32] Institute of Electrical and Electronics Engineers. IEEE Standard for Interconnecting Distributed Resources with Electric Power Systems - Amendment 1. IEEE Std 1547-2003 2014;2014:1–16. doi:10.1109/IEEESTD.2014.6818982.

[33] Demirok E, González PC, Frederiksen KHB, Sera D, Rodriguez P, Teodorescu R. Local reactive power control methods for overvoltage prevention of distributed solar inverters in low-voltage grids. IEEE J Photovoltaics 2011;1:174–82. doi:10.1109/JPHOTOV.2011.2174821.

[34] Samadi A, Eriksson R, Söder L, Rawn BG, Boemer JC. Coordinated Active Power-Dependent Voltage Regulation in Distribution Grids With PV Systems. IEEE Trans POWER Deliv 2014;29:1454–64. doi:10.1109/TPWRD.2014.2298614.

[35] Samadi A, Shayesteh E, Eriksson R, Rawn B, Soder L. Multi-objective coordinated droop-based voltage regulation in distribution grids with PV systems. Renew Energy 2014;71:315–23. doi:10.1016/j.renene.2014.05.046.

[36] Howlader AM, Sadoyama S, Roose LR, Sepasi S. Distributed voltage regulation using Volt-Var controls of a smart PV inverter in a smart grid: An experimental study. Renew Energy 2018;127:145–57. doi:10.1016/j.renene.2018.04.058.

[37] Weckx S, Driesen J. Optimal Local Reactive Power Control by PV Inverters. IEEE Trans Sustain Energy 2016;7:1624–33. doi:10.1109/TSTE.2016.2572162.

[38] Hashemi S, Østergaard J. Methods and strategies for overvoltage prevention in low voltage distribution systems with PV. IET Renew Power Gener 2017;11:205–14. doi:10.1049/iet-rpg.2016.0277.

[39] Kryonidis GC, Kontis EO, Chrysochos AI, Demoulias CS, Papagiannis GK. A Coordinated Droop Control Strategy for Overvoltage Mitigation in Active Distribution Networks. IEEE Trans Smart Grid 2018;9:5260–70. doi:10.1109/TSG.2017.2685686.

[40] Ghosh S, Rahman S, Pipattanasomporn M. Distribution Voltage Regulation Through Active Power Curtailment With PV Inverters and Solar Generation Forecasts. IEEE Trans Sustain Energy 2017;8:13–22. doi:10.1109/TSTE.2016.2577559.

[41] Su X, Masoum MAS, Wolfs PJ. Optimal PV inverter reactive power control and real

power curtailment to improve performance of unbalanced four-wire LV distribution networks. IEEE Trans Sustain Energy 2014;5:967–77. doi:10.1109/TSTE.2014.2313862.

[42] Das CK, Bass O, Kothapalli G, Mahmoud TS, Habibi D. Overview of energy storage systems in distribution networks: Placement, sizing, operation, and power quality. Renew Sustain Energy Rev 2018;91:1205–30. doi:10.1016/j.rser.2018.03.068.

[43] IRENA (2019). Future of solar photovoltaic:Deployment, investment, technology, grid integration and socio-economic aspects (A Global Energy Transformation: paper). Int Renew Energy Agency, Abu Dhabi 2019:1–88.

[44] Jayasekara N, Masoum MAS, Wolfs PJ. Optimal operation of distributed energy storage systems to improve distribution network load and generation hosting capability. IEEE Trans Sustain Energy 2016;7:250–61. doi:10.1109/TSTE.2015.2487360.

[45] Mehrjerdi H. Simultaneous load leveling and voltage profile improvement in distribution networks by optimal battery storage planning. Energy 2019;181:916–26. doi:10.1016/j.energy.2019.06.021.

[46] Lakshmi S, Ganguly S. Multi-objective planning for the allocation of PV-BESS integrated open UPQC for peak load shaving of radial distribution networks. J Energy Storage 2019;22:208–18. doi:10.1016/j.est.2019.01.011.

[47] Barzkar A, Hosseini SMH. A novel peak load shaving algorithm via real-time battery scheduling for residential distributed energy storage systems. Int J Energy Res 2018;42:2400–16. doi:DOI: 10.1002/er.4010.

[48] Alam MJE, Muttaqi KM, Sutanto D. Distributed energy storage for mitigation of voltage-rise impact caused by rooftop solar PV. IEEE Power Energy Soc Gen Meet San Diego, CA 2012:1–8. doi:10.1109/PESGM.2012.6345726.

[49] Jayasekara N, Wolfs P, Masoum MAS. An optimal management strategy for distributed storages in distribution networks with high penetrations of PV. Electr Power Syst Res 2014;116:147–57. doi:10.1016/j.epsr.2014.05.010.

[50] Babacan O, Torre W, Kleissl J. Optimal allocation of battery energy storage systems in distribution networks considering high PV penetration. IEEE Power Energy Soc Gen Meet Boston, MA 2016:1–5. doi:10.1109/PESGM.2016.7741191.

[51] Sardi J, Mithulananthan N, Gallagher M, Hung DQ. Multiple community energy storage planning in distribution networks using a cost-benefit analysis. Appl Energy 2017;190:453–63. doi:10.1016/j.apenergy.2016.12.144.

[52] Chedid R, Sawwas A. Optimal placement and sizing of photovoltaics and battery storage in distribution networks. Energy Storage 2019;1:1–12. doi:10.1002/est2.46.

[53] Kabir MN, Mishra Y, Ledwich G, Member S, Dong ZY, Wong KP. Coordinated Control of Grid-Connected Photovoltaic Reactive Power and Battery Energy Storage Systems to Improve the Voltage Profile of a Residential Distribution Feeder. IEEE Trans Ind Informatics 2014;10:967–77. doi:10.1109/TII.2014.2299336.

[54] Ranaweera I, Midtgård OM, Korpås M. Distributed control scheme for residential battery

energy storage units coupled with PV systems. Renew Energy 2017;113:1099–110. doi:10.1016/j.renene.2017.06.084.

[55] Wang L, Bai F, Yan R, Saha TK. Real-Time Coordinated Voltage Control of PV Inverters and Energy Storage for Weak Networks with High PV Penetration. IEEE Trans Power Syst 2018;33:3383–95. doi:10.1109/TPWRS.2018.2789897.

[56] (MITEI) MEI. Managing Large-Scale Penetration of Intermittent Renewables. 2011.

[57] Haque MM, Wolfs P. A review of high PV penetrations in LV distribution networks: Present status, impacts and mitigation measures 2016. doi:10.1016/j.rser.2016.04.025.

[58] Antonanzas J, Osorio N, Escobar R, Urraca R, Martinez-De-Pison FJ, Antonanzas-Torres F. Review of photovoltaic power forecasting 2016. doi:10.1016/j.solener.2016.06.069.

[59] Akhter MN, Mekhilef S, Mokhlis H, Shah NM. Review on forecasting of photovoltaic power generation based on machine learning and metaheuristic techniques. IET Renew Power Gener 2019;13:1009–23. doi:10.1049/iet-rpg.2018.5649.

[60] Ahmed R, Sreeram V, Mishra Y, Arif . D. A review and evaluation of the state-of-the-art in PV solar power forecasting: Techniques and optimization. Renew Sustain Energy Rev 2020;124:109792. doi:10.1016/j.rser.2020.109792.

[61] Sampath Kumar D, Gandhi O, Rodríguez-Gallegos CD, Srinivasan D. Review of power system impacts at high PV penetration Part II: Potential solutions and the way forward. Sol Energy 2020. doi:10.1016/j.solener.2020.08.047.

[62] Sobri S, Koohi-Kamali S, Rahim NA. Solar photovoltaic generation forecasting methods: A review. Energy Convers Manag 2017;156:459–97. doi:10.1016/j.enconman.2017.11.019.

[63] Antonanzas J, Osorio N, Escobar R, Urraca R, Martinez-De-Pison FJ, Antonanzas-Torres F. Review of photovoltaic power forecasting. Sol Energy 2016;136:78–111. doi:10.1016/j.solener.2016.06.069.

[64] de Freitas Viscondi G, Alves-Souza SN. Sustainable Energy Technologies and Assessments A Systematic Literature Review on big data for solar photovoltaic electricity generation forecasting. Sustain Energy Technol Assessments 2018;31:54–63. doi:10.1016/j.seta.2018.11.008.

[65] Sharadga H, Hajimirza S, Balog RS. Time series forecasting of solar power generation for large-scale photovoltaic plants. Renew Energy 2020;150:797–807. doi:10.1016/j.renene.2019.12.131.

[66] Liu L, Liu D, Sun Q, Li H, Wennersten R. Forecasting Power Output of Photovoltaic System Using A BP Network Method. Energy Procedia 2017;142:780–6. doi:10.1016/j.egypro.2017.12.126.

[67] Gari da Silva Fonseca Jr J, Oozeki T, Takashima T, Koshimizu G, Uchida Y, Ogimoto K. Use of support vector regression and numerically predicted cloudiness to forecast power output of a photovoltaic power plant in Kitakyushu, Japan. Prog PHOTOVOLTAICS Res Appl 2012;20:874–82. doi:10.1002/pip.1152.

[68] Cheng HY, Yu CC, Lin SJ. Bi-model short-term solar irradiance prediction using support vector regressors. Energy 2014;70:121–7. doi:10.1016/j.energy.2014.03.096.

[69] Sharma N, Sharma P, Irwin D, Shenoy P. Predicting Solar Generation from Weather Forecasts Using Machine Learning. 2011 IEEE Int Conf Smart Grid Commun (SmartGridComm), Brussels 2011:528–33. doi:10.1109/SmartGridComm.2011.6102379.

[70] Sperati S, Alessandrini S, Pinson P, Kariniotakis G. The "Weather intelligence for renewable energies" benchmarking exercise on short-term forecasting of wind and solar power generation. Energies 2015;8:9594–619. doi:10.3390/en8099594.

[71] Saini LM, Aggarwal SK, Kumar A. Parameter optimisation using genetic algorithm for support vector machine-based price-forecasting model in National electricity market. IET Gener Transm Distrib 2010;4:36. doi:10.1049/iet-gtd.2008.0584.

[72] Hong W-C. Electric load forecasting by support vector model. Appl Math Model 2009;33:2444–54. doi:10.1016/j.apm.2008.07.010.

[73] Hong W-C. Chaotic particle swarm optimization algorithm in a support vector regression electric load forecasting model. Energy Convers Manag 2009;50:105–17. doi:10.1016/j.enconman.2008.08.031.

[74] VanDeventer W, Jamei E, Sidarth Thirunavukkarasu G, Seyedmahmoudian M, Kok Soon T, Horan B, et al. Short-term PV power forecasting using hybrid GASVM technique. Renew Energy 2019;140:367–79. doi:10.1016/j.renene.2019.02.087.

[75] Cuevas, Erik, Emilio Barocio Espejo ACE. Metaheuristics Algorithms in Power Systems. Springer Nature Switzerland AG: Springer International Publishing; 2019. doi:https://doi.org/10.1007/978-3-030-11593-7.

[76] Chicco G, Mazza A. Metaheuristic optimization of power and energy systems: underlying principles and main issues of the "rush to heuristics." Energies 2020;13:5097. doi:https://doi.org/10.3390/en13195097.

[77] Amiri R, Sardroud JM, Soto BG De. BIM-based Applications of Metaheuristic Algorithms to Support the Decision-making Process: Uses in the Planning of Construction Site Layout. Procedia Eng 2017;196:558–64. doi:10.1016/j.proeng.2017.08.030.

[78] Rasdi Rere LM, Fanany MI, Arymurthy AM. Metaheuristic Algorithms for Convolution Neural Network. Comput Intell Neurosci 2016;2016:1–13. doi:10.1155/2016/1537325.

[79] Yang X-S. Metaheuristic Optimization. Scholarpedia 2011;6:11472. doi:doi:10.4249/scholarpedia.11472.

[80] Lusis P, Rajab Khalilpour K, Andrew L, Liebman A. Short-term residential load forecasting: Impact of calendar effects and forecast granularity. Appl Energy 2017;205:654–69. doi:10.1016/j.apenergy.2017.07.114.

[81] Electric Power Research Institute, OpenDSS, Distribution System Simulator n.d. https://sourceforge.net/projects/electricdss/ (accessed October 21, 2020).

[82] Powerwall | Tesla n.d. https://www.tesla.com/powerwall (accessed September 27, 2020).

[83] Powerpack - Commercial & Utility Energy Storage Solutions | Tesla n.d. https://www.tesla.com/powerpack (accessed October 18, 2020).

[84] Cuevas E, Cienfuegos M, Zaldívar D, Pérez-Cisneros M. A swarm optimization algorithm inspired in the behavior of the social-spider. Expert Syst Appl 2013;40:6374–84. doi:10.1016/j.eswa.2013.05.041.

[85] Kennedy J, Eberhart R. Particle swarm optimization. Neural Networks, 1995 Proceedings, IEEE Int Conf 1995;4:1942–8. doi:10.1109/ICNN.1995.488968.

[86] Carneiro TC, Melo SP, Carvalho PCM, Plínio A, Braga S. Particle Swarm Optimization method for estimation of Weibull parameters: A case study for the Brazilian northeast region. Renew Energy 2016;86:751–9. doi:10.1016/j.renene.2015.08.060.

[87] Yang X-S, Deb S. Cuckoo Search via Levy Flights 2010. doi:10.1109/NABIC.2009.5393690.

[88] Yang X-S, Deb S. Engineering Optimisation by Cuckoo Search 2010:1–17. doi:10.1504/IJMMNO.2010.035430.

[89] Chang C-C, Lin C-J. Libsvm. ACM Trans Intell Syst Technol 2011;2:1–27. doi:10.1145/1961189.1961199.

[90] Faraji J, Abazari A, Babaei M, Muyeen SM, Benbouzid M. Day-ahead optimization of prosumer considering battery depreciation and weather prediction for renewable energy sources. Appl Sci 2020;10:1–22. doi:10.3390/APP10082774.

[91] Leva S, Dolara A, Grimaccia F, Mussetta M, Ogliari E. Analysis and validation of 24 hours ahead neural network forecasting of photovoltaic output power. Math Comput Simul 2017;131:88–100. doi:10.1016/j.matcom.2015.05.010.

[92] Tesfaye Eseye A, Zhang J, Zheng D. Short-term photovoltaic solar power forecasting using a hybrid Wavelet-PSO-SVM model based on SCADA and Meteorological information. Renew Energy 2017;118:357–67. doi:10.1016/j.renene.2017.11.011.

[93] Hastie T, Tibshirani R, Friedman J. The Elements of Statistical Learning. Math Intell 2001;27:83–85. doi:10.1198/jasa.2004.s339.

[94] Abuella M, Chowdhury B. Solar Power Forecasting Using Support Vector Regression n.d.

[95] Smola AJ, Sc Olkopf B. A tutorial on support vector regression. Stat Comput 2004;14:199–222.

[96] Wang J, Li L, Niu D, Tan Z. An annual load forecasting model based on support vector regression with differential evolution algorithm. Appl Energy 2012;94:65–70. doi:10.1016/j.apenergy.2012.01.010.

[97] Miraftabzadeh SM, Longo M, Foiadelli F. A-day-ahead photovoltaic power prediction based on long short term memory algorithm. SEST 2020 - 3rd Int Conf Smart Energy Syst Technol 2020:1–6. doi:10.1109/SEST48500.2020.9203481.

[98] Konstantinou M, Peratikou S, Charalambides AG. Solar Photovoltaic Forecasting of Power Output Using LSTM Networks. Atmosphere (Basel) 2021;12:124.

doi:10.3390/atmos12010124.

[99] Hsu C-W, Chang C-C, Lin C-J. A Practical Guide to Support Vector Classification n.d.

[100] Gómez JL, Martínez AO, Pastoriza FT, Garrido LF, Álvarez EG, García JAO. Photovoltaic power prediction using artificial neural networks and numerical weather data. Sustain 2020;12:1–19. doi:10.3390/su122410295.

[101] Renno C, Petito F, Gatto A. Artificial neural network models for predicting the solar radiation as input of a concentrating photovoltaic system. Energy Convers Manag 2015;106:999–1012. doi:10.1016/j.enconman.2015.10.033.

[102] Solar resource maps and GIS data | Solargis n.d. https://solargis.com/maps-and-gis-data/download/saudi-arabia (accessed October 3, 2020).

[103] Bright JM. Solcast: Validation of a satellite-derived solar irradiance dataset. Sol Energy 2019;189:435–49. doi:10.1016/j.solener.2019.07.086.

[104] Vestas V39 - 500,00 kW - Wind turbine n.d. https://en.wind-turbine-models.com/turbines/383-vestas-v39 (accessed June 29, 2020).

[105] Renewable Resource Atlas. Saudi Arab n.d. https://rratlas.kacare.gov.sa/RRMMPublicPortal/ (accessed October 10, 2018).